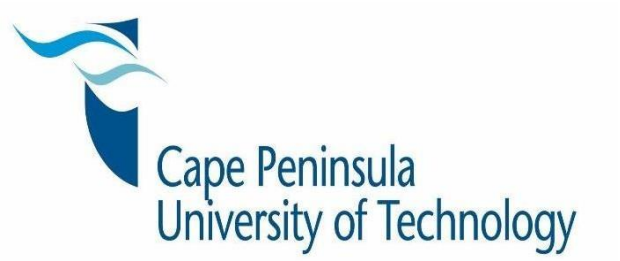

Characterization of Multi-Pass Friction Stir Processed AA1050 And AA6082 Dissimilar Joint

By

Oritonda Muribwathoho

Thesis submitted in fulfilment of the requirements for the degree.

Faculty: Engineering and Built Environment

Department: Mechanical Engineering

Degree and field: Master of Engineering in Mechanical Engineering

Supervisor: Dr Velaphi Msomi

Co-Supervisor: Mrs Sipokazi Mabuwa

Bellville

September 2021

DECLARATION

I Oritonda Muribwathoho, declare that the content of this thesis represents my own work unaided work, and that the thesis has not previously been submitted for academic examination towards the qualification. Furthermore, it represents my own opinions and not necessarily those of the Cape Peninsula University of Technology.

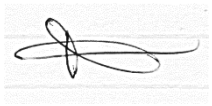

01/07/2021

…… …….

Signed Date

ABSTRACT

Due to their decreased weight, superior fatigue properties, high strength to weight ratio, good workability/formability, and corrosion resistance, aluminium-based metal matrix composites have emerged as appropriate materials for the automotive and aerospace industries. Recently, the joining of dissimilar metals has seen a lot of success in a variety of fields. Friction stir processing (FSP) has been used to create metal matrix composites of base metals such as aluminium, copper, iron, and nickel. Friction stir processing (FSP) is a new solid-state technology that modifies the microstructure of metals using the principles of friction stir welding. It improves strength and ductility, increases corrosion and fatigue resistance, and enhances hardness and formability by removing casting defects and refining microstructures on a local level.

The influence of process factors on the microstructure was characterized after a single pass in the majority of FSP studies. Multiple passes of FSP, on the other hand, are another way to further change the microstructure of Al castings. The majority of the literature on multi-pass FSP focuses on plate processing rather than joint processing, according to the accessible literature. Only a few studies have been published on multi-pass friction stir processed joints. As a result, more research into multi-pass friction stir processing on dissimilar aluminium alloys is required.

The aim of this research is to determine the impact of a multi-pass friction stir processed joint of dissimilar aluminium alloys AA1050 and AA6082. The knowledge gained from this study will serve as a guide for related sectors in determining the expected outcome of using this technique on dissimilar aluminium alloys. Two aluminium alloys AA1050 and AA6082 plates were welded utilizing the friction stir welding process prior to the joint's analysis. After that, the welded joints were friction stir processed using the same parameters as the FSW. The friction stir processed joints were then cut with a water jet cutting machine and prepared for various analyses. This involved the macrostructure, microstructure analysis, tensile tests, bending tests, hardness tests, and SEM. These tests were carried out to see how the multi-pass FSP will affect the previously friction stir welded joints.

The described specimens were cut from several points on the plates, such as the plate's beginning, middle, and end. The following symbol was used to represent the cut positions on the processed plates to symbolize their positioning (S for the start, M for the middle and E for the end of the plate). There were twelve generated specimens for each plate. Different tests were done on the cut specimen. On the basis of the test findings, conclusions were drawn. The microstructural analysis revealed that as the number of passes increased, the grain sizes decreased, and the distribution of grain sizes became more uniform across the processed zone, regardless of material position. The grain structure of the multi-pass friction stir processed 1050/6082 and 6082/1050 FSPed joints was refined from 19.84 µm to 5.381 µm for the 1050/6082 and from 13.12 µm to 1.744 µm for the 6082/1050 FSPed joints. The joint with 6082 on the advancing side exhibited significantly finer grains (1.744 µm) than the joint with AA1050 on the advancing side (5.381 µm). As the number of passes increased, the grain sizes decreased and the distribution of grain sizes became more uniform across the processed zone, regardless of material position.

The ultimate tensile strength (UTS) increased as the number of FSP passes increased when AA1050 was put on the advancing side. When AA6082 was positioned on the advancing side, the UTS varied across specimens taken from different locations of the FSPed joints. The maximum ultimate tensile strength was 86.1 MPa for the AA1050/AA6082 and 79.3 MPa for the AA6082/AA1050. When compared to both base materials, the percentage elongation of all joints was determined to be greater. The SEM fractographs of the fractured surface for the AA1050/AA6082 FSPed joints indicated ductile trans-granular failure features and the AA6082/AA1050 was characterised by ductile trans-granular failure and brittle failure features. The Vickers microhardness of AA1050/AA6082 FSPed joints increased towards AA6082, whereas the Vickers microhardness of AA6082/AA1050 FSPed joints decreased towards AA 1050 regardless of the number of passes. With AA1050 on the advancing side, the stir zone achieved a maximum hardness of 65.54 HV and when AA6082 was on the advancing side, the stir zone achieved a maximum hardness of 61.06 HV.

The deflection for the processed joints was detected in various regions of the joints, with some of the joints showing cracks and others being crack-free. There was no particular trend in Ultimate Flexural Strength that was observed during analysis. For AA1050/AA6082 FSPed joints, the average UFS of the root was found to be greater than that of the face, with the maximum UFS attained at 381.34 MPa for the root and 359.37 MPa for the face while for the AA6082/AA1050 processed joints, the average UFS of the root was higher than that of the face, with the maximum UFS obtained at 353.75 MPa for the root and 258.75 MPa for the face.

The data has revealed that multi-pass friction stir processing has an effect on joint mechanical properties irrespective of material positioning. This may be observed in the AA1050/AA6082 and AA6082/AA1050 FSPed dissimilar joints. As a result, it can be concluded that multi-pass friction stir processing improves mechanical properties significantly.

LIST OF PAPERS

Thesis includes the following supplements

Supplement 1

Muribwathoho, O., Mabuwa, S., Msomi, V. Review on Multi-pass Friction Stir Processing of Aluminium Alloys. *Preprints*. **2020**

Supplement 2

Muribwathoho, O., Mabuwa, S., Msomi, V., Motshwanedi, S.S. Impact of multi-pass friction stir processing on microhardness of AA1050/AA6082 dissimilar joint. *MaterialsToday: Proceedings, 46*, **2021**, pp.651-657.

Supplement 3

Muribwathoho, O., Msomi, V., Mabuwa, S. and Merdji, A. The mechanical properties of AA6082/AA1050 dissimilar joints subjected to multi-pass friction stir processing. *Engineering Research Express*, *3*(3), **2021**, p.035012.

ACKNOWLEDGEMENTS

First and foremost, I want to thank the almighty God for bringing me this far; I could not have done it on my own.

My sincere gratitude to the following people who made the completion of the study possible:

My supervisor, Dr Velaphi Msomi, for his tireless guidance, motivation, encouragement, support, commitment and patience throughout the entire thesis process. His ideas, suggestions and guidance inspired me to continue with the research. He was more like a father to me who never gives up on their child. Thank you.

I wish to thank my Co- supervisor Mrs Siphokazi Mabuwa who encouraged me to go on and motivated me to make this work complete and for assisting me throughout my research. She has been more than just a supervisor to me, and she kept on inspiring me and wished me nothing but success. Thank you for having faith in me.

To my mother, Ms Stella Mutavhatsindi, for raising me and all the foundation she laid on me, support, guidance, love, kindness and encouragement to further my studies. Thank you so much. Not forgetting Mrs Avhatakali Ramaano who always encouraged me, supported me and reminding me the importance of education. Thank you so much.

My siblings Rilinde and Hudivhaene Muribwathoho, thank you for your support, encouragement, motivations, kindness and always believing in me. You truly are a blessing to me, and I love you so much. I would also love to thank all my relatives, extended family and friends who encouraged me to further my studies.

I wish to thank all the participants in the research for their diligent response and sacrifices they made to participate in my study.

Lastly, I would like to thank Mr Moni for the supporting and giving me access to use the CPUT Mechanical engineering department lab for doing all the practical's and also Miranda Waldron of the University of Cape Town from the SEM department for use of the SEM equipment.

The financial assistance of Thuthuka grant towards this research is acknowledged. Opinions expressed in the thesis and the conclusions arrived at those of the author and are not necessarily to be attributed to the National Research Foundation.

DEDICATION

I dedicate this study to my late uncle Tshimangadzo Touch Mutavhatsindi. He was supportive and always believed in me and pushed me to do more. My achievements will always be attributed to the inspiration he put while he was still living. I also dedicate this study to my grandmother Nyadzanga Mutavhatsindi. She has always been my pillar of strength and played an important role in my life. I am where I am because of her endless support.

TABLE OF CONTENTS

Contents

LIST OF FIGURES

LIST OF TABLES

GLOSARY

Terms/Acronyms/Abbreviations	Definition/Explanation
AA	Aluminium Alloy
Al	Aluminium
ARB	Accumulative Roll Being
AS	Advancing Side
ASTM	American Society for Testing and Materials
B	Beginning
BM	Base Material
CMP	Continuous Multi-pass
CPUT	Cape Peninsula University of Technology
Cu	Copper
ECAP/E	Equal Channel Angular Pressing/Extrusion
FSP	Friction Stir Processing
FSPED	Friction Stir Processed
FSW	Friction Stir Welding
FSWED	Friction Stir welded
HAGB	High Angle Grain Boundaries
HAZ	Heat Affected Zone
HPT	High Torsion Torque
IMP	Intermittent Multi Pass
Li	Lithium
M	Middle
MFS	Maximum Flexural Strength

Mg	Magnesium
mm	Millimeter
mm/min	Millimeter per minute
MP-FSP	Multi-pass Friction stir Processing
NZ	Nugget Zone
rpm	Revolutions per minute
S	Start
RS	Retreating Side
SEM	Scanning Electron Microscope
Si	Silicon
SPD	Severe Plastic Deformation
SZ	Stir Zone
UFG	Ultrafine Grain
UFS	Ultimate Flexural Strength
UTS	Ultimate Tensile Strength
TMAZ	Thermo-Mechanically Affected Zone
Zn	Zinc

CHAPTER ONE
INTRODUCTION

1.1 Introduction of study

Different industries are now concentrating on reducing the weight of their products. Lightweight materials such as aluminium have become increasingly relevant. Aluminium alloys have become more common over time because of their wide variety of uses. Automobile bodybuilding, marine shipbuilding, aerospace, food packaging, and a variety of other structural uses are only a few examples [1-3]. Aluminium alloys are widely used due to their appealing properties, which include a high strength-to-weight ratio, simplicity of fabrication, increased ductility and a pleasing appearance [4-7]. Instead of using similar alloys to manufacture different components, most companies are opting for dissimilar alloys [8]. The alloying elements used in the production of different aluminium alloys decide their mechanical and thermal properties [6,7]. Material improvements, on the other hand, are undeniably important for bettering the material's results and extending the component's life cycle [9]. Friction stir processing is one of the materials enhancing techniques.

FSP operates in the same way as FSW, but instead of joining materials, it modifies them [10,11]. Friction stir processing (FSP) is a solid-state microstructural modification technique that produces high-specific strength by using friction heat and stirring action [12–23]. This method is based on the friction stir welding (FSW) theory [24]. The fundamental principle of FSP is incredibly straightforward. A rotating tool with a pin and shoulder is inserted into a single piece of material and traversed in the expected direction to cover the region of interest, resulting in substantial microstructural modifications in the processed zone because of intense plastic deformation, mixing, and thermal exposure. Microstructural refinement of cast aluminium alloys [25], homogenization of nanophase aluminium alloys metal matrix composites [12,26], and surface composites [16] are only a handful of the microstructural refinement of metallic materials applications that FSP's properties have supported.

The tool's main goals during the FSP process are to heat the material through internal friction induced by extreme plastic deformation and allow the material to flow locally [22, 27, 28]. The process heats the aluminium alloy to about 400-500 °C [22, 29], softens it, makes it malleable, and encourages movement from the tool's front to back and around the pin [22, 28]. During this phase, the material undergoes extreme plastic deformation at a high temperature, resulting in substantial grain refinement [12,30–33]. When it comes to material flow during the FSP operation, pin geometry is a crucial element. Threads push the material down the pin, and pin geometry moves it up and away from it until it reaches the bottom [22, 28]. The pin flutes [28] encourage and enhance the material flow movement. This dynamic pattern of material flow generates a variety of heat dissipation zones and mechanical properties [34]. Figure 1 depicts the FSP's operating principle.

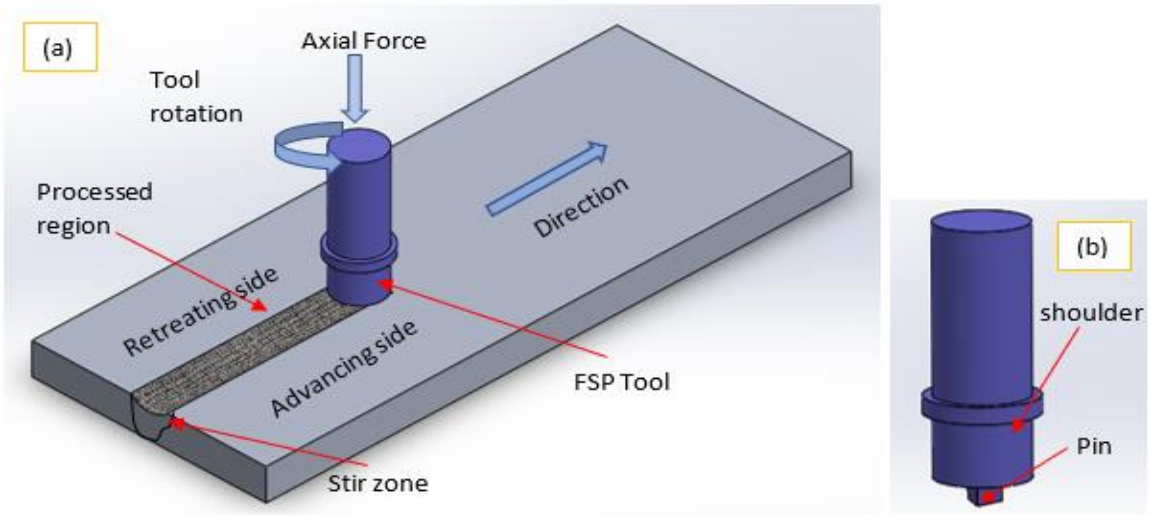

Figure 1:(a) Friction stir processing schematic illustration and (b) FSP Tool.

Tool geometry, rotational rate (ω-rpm) in a clockwise or counter-clockwise direction, and transverse speed (Vt -mm/min) are three significant process variables for FSP [27]. The shoulder and pin are the most important parts of tool geometry, and they are responsible for workpiece friction and plastic deformation, respectively [35]. To maximize forging action and allow adequate metal movement around the tool, the FSP tool is usually tilted at a 1- 3° angle during the process [36]. Additionally, the heated material is produced by the shoulder [22]. The shoulder holds the warm material in place [22]. A tunnel defect, i.e., a continuous pore along the traverse path, will develop if downward force or heat input is insufficient, or the flow of plasticized metal is inadequate [28, 37].

Because of the extreme plastic deformation produced and the generation of increased stirring heat caused by FSP, which significantly affect surface microstructure and properties, grain refinement and uniform distribution of the reinforcement particles (ceramic particles and precipitates) are achieved [34]. Friction stir processing (FSP) has been used to create metal matrix composites from a range of base metals, including aluminium, copper, iron, and nickel. FSP improves strength and ductility, increases corrosion and fatigue resistance, and increases stiffness and formability by removing locally casting defects and refining microstructures. In the automobile and aerospace industry, it is a promising process in which new materials are engineered to improve wear, creep, and fatigue tolerance. This approach improves the microstructural properties of powder metal artifacts while also incorporating wrought microstructure into a cast component.

Microstructural modifications, corrosion resistance improvement, mechanical properties modification, achieving superplasticity in materials, casting defects repair, composite manufacturing, and the production of special alloys have all been done with FSP due to its properties [34,38]. The most common applications are localized modification and microstructure control in thin surface layers of processed metallic components for property enhancement [34]. By application of FSP, microstructural changes such as cast microstructure break-up, grain refinement, homogenization of precipitates, and elimination of casting defects are expected [39]. As a result, FSP is believed to be one of the foremost effective methods for improving mechanical properties, particularly fatigue properties. In most FSP experiments, the influence of process parameters on the microstructure was measured after a single pass.

Multiple passes FSP, on the other hand, are another way to improve the microstructure of Al castings. The utilization of multi-pass FSP can result in many benefits including tensile properties, microstructure, microhardness, and wear properties according to the few studies that have been done [40]. There is a lot of literature on multi-pass FSP, it has been discovered that most studies focused on processed plate rather than processed joint. There are just a few works reporting on joints. As a result, further research into multi-pass friction stir processing is needed for dissimilar aluminium alloy.

The dissimilar alloys AA1050-H14 and AA6082-T6 were selected to be utilized for this study. Aluminium alloy 1050-H14 is a common grade of aluminium used in regular sheet metal work and is applied within the place where moderate strength is required. It is extremely ductile, extremely reflective finish, and is additionally known for its outstanding corrosion resistance [1]. Containers, lamp reflectors, chemical process plant equipment, pyrotechnic powder, architectural flashings, lamp reflectors, and cable sheathing are all popular uses for aluminium alloy 1050-H14 in industries e.g., food companies [41]. Aluminium alloy 6082-T6 (AA6082) on the other hand is a combination of aluminium (Al), magnesium (Mg), and silicon (Si) alloys with adequate plasticity for extrusions and has high relative strength. It is classified as a structural alloy with the highest strength of 6000 series alloys. In plate form, 6082 is the alloy most widely used for machining. The higher strength of 6082 has seen it replace 6061 in several applications despite being a relatively new alloy. The addition of a large amount of manganese controls the grain structure that successively ends up in a stronger alloy. This alloy is mostly used in the production of high-speed due to its excellent weldability, formability, and machinability [42-44].

1.2 Problem Statement

In recent years, the automotive industry has shown interest in polymer/metal systems to reduce fuel consumption and carbon emissions [45]. Aluminium-based metal matrix composites have emerged as a viable material for the automotive and aircraft industries due to their low weight, outstanding fatigue properties, high strength-to-weight ratio, enhanced workability/formability, and corrosion resistance [46-48]. Refining and homogenizing the microstructure and form the sheet at high temperatures using advanced forming techniques such as superplastic forming is another way to increase formability. According to recent findings, ultrafine grain sheet metals have been shown to have superior better formability at relatively moderate temperatures. The development of grain refining techniques is urgently needed. In many Al alloys, FSP has been shown to increase superplasticity [14,18,49-52]. To overcome some of the challenges of conventional metal forming processes, new grain refinement and microstructural modification techniques based on severe plastic deformation (SPD) have recently been proposed [53,54]. Equal-channel angular pressing/ extrusion (ECAP/E), high-pressure torsion (HPT), accumulative roll-bonding (ARB), and friction stir processing (FSP) are some of the most well-known SPD techniques [53-55]. The FSP, among others, is the best when it comes to the processing of large plates or sheets of material. Several FSP studies have shown that single and multi-pass processing can induce superplastic properties in various materials [56-59]. The utilization of friction stir processing can result in microstructure refinement, improved wear resistance, and increased creep and fatigue strength. Multiple FSP passes, on the other hand, can be used as a technique for

improving the microstructure of aluminium castings. FSP using overlapping passes (known as multi-pass FSP) was recently discovered to exhibit comparable superplastic properties to single-pass FSP. Other papers [39, 60] have extensively discussed the effects of multi-pass FSP on the mechanical properties and microstructure of the modified region. The multi-pass friction stir processing technique is still being investigated for the processing of dissimilar aluminium alloys that are wide apart from one another. This study aims to see how multi-pass friction stir processed (FSPed) joints affect the friction stir welded (FSWed) dissimilar aluminium joints of AA6082/AA1050 and AA1050/AA6082.

1.3 Research background

FSP was first studied and used as a technique for near-surface modification and enhancement techniques. Friction stir processing (FSP) is believed to have great potential in the field of superplasticity. The application of FSP has appeal in locally refining casting heterogeneities [20,35,61-63]. FSP has resulted in improvement in the mechanical properties of various aluminium and magnesium alloys [63-64]. FSP may be used in manufacturing processes for microstructural refinement, densification, and homogeneity of the processed region, as well as defect removal [20, 22, 65]. Mishra and Ma [22] looked at the FSP technique and concluded that it can be used to strengthen the properties of cast alloys. Mechanical properties such as wear resistance, fatigue, tensile strength, hardness, and corrosion have improved on processed surfaces [19,66].

It is undeniable that FSP removes casting defects and produces fully equiaxed and recrystallized grains, some literature argues that the grains' mechanical properties degraded after FSP. In the FSPed region material softening is considered to be the cause of this. Multiple passes of the FSP have been shown to improve mechanical properties such as hardness, tensile strength, and ductility [67]. The multi-pass FSP's homogeneous processed area was credited with this improvement. Yang et al. [68] investigated the microstructure and mechanical properties of Al3Ti/A356 using four-pass FSP with 100 percent overlap. They discovered that grain size was reduced significantly from the base material to the fourth pass, and that grain refining increased yield strength, tensile strength, and ductility following each subsequent pass. Regardless of the number of FSP moves, the mechanical properties of the FSPed material were found to be highly dependent on a material workpiece and processing parameters for FSP.

FSP is known to refine the course aluminium and resulting in recrystallized (equiaxed) grains. El-Rayes and El-Danaf [69] investigated the effects of multi-pass FSP on the properties of thick 6082-T651 AA plates. They found out that a single-pass friction stir processing caused dynamic recrystallization of the stir zone, resulting in grains being equiaxed, but that multiple passes resulted in a decrease in hardness and tensile strength. Hardness was said to be reduced due to SZ softening, which occurred as the number of passes increased. Following FSP passes, the softening was influenced by the larger grain size. The drop in tensile strength was also proposed to be due to the over-aging effect of subsequent passes on prior passes. Gan et al. [70] looked at how the hardness and microstructure of rolled pure aluminium changed after friction stir processing, they found a decrease in material hardness despite reaching equiaxed and fully recrystallized grains. A local softening of the material in the FSPed zone was discovered, it was determined that precipitate dissolution during FSP was

responsible for the reduction in hardness. Weglowski [71] published a paper on the hardness reduction of Al Si9Mg aluminium alloy after a single FSP pass.

Ma et al. [14], Charit and Mishra [72], Johannes et al. [73], Johannes et al. [74], Liu and Ma [75] have shown that FSP can result in a significant reduction in grain size and a high level of second phase particle refinement. The high-temperature mechanical performance and, in particular, the fatigue properties of cast Al-Si alloys should be enhanced by refining the microstructure [60]. There is a strong correlation between the number of grain boundaries and the number of FSP passes, according to Paidar et al. [76]. As the number of passes increased, the hardness of the FSPed area increased. An increase in microhardness value was observed and is attributed to smaller grain sizes. Multi-pass FSP decreases cluster size and ensures uniform reinforcement particle distribution, reducing the matrix grain size. Krishna and Satyanarayana [77] found that as the number of passes increased, yield strength, tensile strength, stiffness, and elongation all decreased. Following FSP passes, grain sizes and silicon flakes were reduced. Precipitate deterioration and limited re-precipitation caused by FSP's thermal cycles caused the mechanical properties to deteriorate.

According to the literature [39,62,78-80], FSP improves mechanical properties and significantly refines microstructure. FSP produces microstructure with fine grains with large grain boundary misorientations and high angle grain boundaries, according to Johannes et al. [74], both of which are critical for improved mechanical properties, as summarized by Mishra and Ma [22]. On the Al-5083 aluminium alloy sheet, Chen et al. [81] used a three-pass FSP with 100 % overlap and witnessed that grain refinement due to recrystallization in the first pass, but no identifiable difference in grain size after subsequent overlapping passes. The tensile strength, hardness, and yield strength at the stir zone (SZ) of the multi-pass FSPed samples were lower than the base material, with no major increases with subsequent multiple passes. Salman [82] observed that after one pass FSP on the microstructure and mechanical properties of Al-Zn-Mg-Cu alloy, the results suggest significant grain refining, removal of casting defects, and increases in the aluminium alloy's hardness, tensile strength, and ductility. Several tests, however, have shown that mechanical properties have deteriorated as a result of the FSP process.

In several experiments, FSP has been shown to enhance material mechanical properties. Hashim et al. [83] improved the hardness and tensile strength of 2024-T3 aluminium alloy using a single-pass FSP. As a result of substantial grain refining, there was a 77 percent decrease in grain size. The microstructural evolution of aluminium cast alloys during single-pass FSP was studied by Sun and Apelian [84] the researchers found high grain refinement and enhanced mechanical properties. The effect of friction stir processing on the microstructure and mechanical properties of aluminium was investigated by Yadav and Bauri [65]. The effect of friction stir processing on the mechanical properties of cast aluminium alloys A319 and A356 was investigated by Santella et al. [20]. After friction stir processing, both alloys' ultimate tensile strength, ductility, and fatigue increased. Karthikeyan et al. [85] discovered that the alloy had lower hardness in the FSP region in all of the conditions examined, however, UTS improved by about 30% as compared to the base metal in the investigation of the impact of FSP on the mechanical properties of cast 2285 aluminium alloy.

Casting pores may be eliminated with FSP. According to Rahsepar and Jarahimoghadam [86], using multi-pass FSP on Zr-reinforced Al metal matrix composites improved densification, uniform distribution, and refinement of reinforcements in the Al matrix. Barmouz and Givi [87] revealed that as the number of FSP cycles/passes increases, interfacial bonding and densification intensify, resulting in improved particle-matrix refinement and a reduction in the number of pores in the substrate composite. Barmouz and Givi [87] conducted multi-pass with even step (two, four, and up to eight-pass) FSP with 100 percent overlap on in situ fabricated Cu/SiC composite by FSP to investigate the impact of multi-pass on mechanical properties including tensile, hardness, and microstructure. According to the researchers the composite tensile properties, such as ductility and ultimate tensile strength were improved by multi-pass. The researchers attribute the change to lower porosity levels and improved bonding between SiC particles and the copper matrix. A356 Commercial alloy was produced by incorporating inorganic salt K2TiF6 powder to create a six-vol. percent Al3Ti/A356 compost, which was then further processed with multi-pass friction stir technology. According to Yang et al. [68], the microstructure and mechanical properties were enhanced. Multi-pass FSP improved Al3Ti distribution and dispersion and Si particle, decreased grain sizes, optimized metal matrix grains, and removed cavities and porosity, according to the writers. As a result, specimens' elongation and strength steadily improved.

Using multi-pass FSP, Ma et al. [60] investigated the microstructure and tensile properties of a cast aluminium-silicon alloy A356. According to the research, due to thermal cycle overaging, the strength of previously processed zones in multi-pass processed material is lower than that of the subsequently processed zones. Ma et al. [60] used five-pass FSP (with 50% overlap) on cast Al-Si–Mg A356 alloy and observed that overlapping FSP had little effect on the size and distribution of the Si particles. The Si particles that were broken by FSP were distributed evenly across the multiple-pass FSP processed regions. The transitional zones between two FSP pass had significantly lower strength and ductility than the nugget zones in the FSP condition. Furthermore, because of overaging from the FSP thermal cycles, the strength of the previously processed zones in the multiple-pass material was lower than that of the subsequently processed zones. After multiple passes of T6 heat treatment, the tensile properties of the 5-pass FSP A356 samples were similar to those of the single-pass FSP sample.

Mahoney et al. [88] described FSP as a thermo-mechanical method for inducing fine-grained microstructure in dense sections of AA 7050-T651 using a high strain rate (>10-3) and noted that the process involved strain strengthening and material induced dynamic recrystallization. The highest strain rate was obtained with single-pass friction stir processing for alloy AA7075 using multi-pass FSP [74]. Microstructure and mechanical properties of in situ nanosized TiB2/Al–Mg–Si composites processed by friction stir processing were investigated by Ma et al. [89]. The original unprocessed composite had a grain size of 50–100 m, according to the researchers, with synthesized nanosized TiB2 particles nearly agglomerating to micrometric clusters at grain limits. In the nugget region, FSP revealed fine and equiaxed recrystallized grains (1–5 m in average grain size). The original clusters were broken up, and nanosized TiB2 particles were evenly dispersed across the matrix, serving as dislocation pins. Guo et al. [90] created Al-based nanocomposites with FSP and studied how incorporating nano-Al2O3 particles influenced grain structure and mechanical properties. They discovered that

the pinning effect of Al2O3 particles delayed grain growth after recrystallization during FSP, resulting in a greater grain size reduction.

On the joints, the FSP approach was used with nanoparticles incorporated. The effect of FSP on the tensile properties of the AA8011/AA6061 dissimilar joint was investigated by Palani et al. [91]. After nanoparticles were added, the similar processed AA6061 joint had 98.58 percent tensile strength, compared to 90.08 percent for the AA8011/AA6061 dissimilar joint. Palani et al. [92] studied the influence of FSP parameters on the mechanical properties of AA8011-AA5083 similar and dissimilar joints. When the processing was done, Al2O3 and SiC nanoparticles were used. The addition of nanoparticles to the processed AA8011-AA5083 dissimilar joint improved the strength and hardness of the joint.

The microstructure can be refined using FSP. Kumar et al. [93] investigated the microstructure and mechanical behaviour of an ultrafine-grained Al-Mg-Sc alloy that had been friction stir processed. FSP resulted in substantial grain refining in twin-roll cast alloys, according to the researchers (80 percent of the grain size was less than 1m). They also mentioned that grain refining during the FSP was largely responsible for the increase in yield strength. Cui et al. [94] used Friction stir processing variables and in Situ passes to study the effects on the tensile properties and microstructure of Al-Si-Mg casting. In terms of microstructure modification, they found that the two-pass FSP sample outperformed the single-pass sample in multi-pass FSP. In situ passes and FSP parameters were used. The refinement of grain size is greatly improved by multi-pass FSP. Rao et.al [95] looked at the effect of overlap multi-pass FSP on a hyper eutectic Al–30Si alloy and discovered that increasing the number of FSP passes decreased corrosion rate due to reduced grain and silicon particle sizes as well as increased microstructure inhomogeneity.

Asadi et al. [96] investigated the effect of increasing the amount of FSP passes on the microstructure of the stir zone and the distribution of SiC nanoparticles in FSPed specimens without nanoparticles and found that increasing the number of FSP passes had no measurable impact on the stirring zone. The distribution of nanoparticles in FSPed samples containing SiC nanoparticles was observed to be influenced by the number of passes, which resulted in improved mechanical properties and microstructural evolutions of the stir zone as the number of passes were increased. Nano-sized SiC and Al2O3 particles were applied to as-cast AZ91 magnesium alloy using FSP [96]. Increasing the Friction Stir Processing pass number improved homogeneity and particle distribution, according to the researchers. The SiC particles were dispersed in the metal matrix by stirring the materials after each FSP pass. The SiC particles in the metal matrix were scattered by stirring the materials in each FSP pass. The results showed that even when the FSP pass numbers were the same, the mean average grain size for SiC samples was smaller than for Al2O3 samples. The more refined grains of the AZ91 matrix, SiC particles appeared to be distributed separately.

1.4 Research Objectives

This study aims to investigate the impact of the multi-pass FSPed joint between dissimilar aluminium alloys AA1050 as well as the AA6082. This aim will be achieved through the following objectives:

- The two dissimilar aluminium alloys will be joined using the FSW technique before FSP considering different material positioning.
- The FSWed joints will be processed using a maximum of four FSP passes.
- Evaluate the mechanical properties by performing tests on the processed plate. Tensile test, microhardness test, fracture morphology, and microstructural analysis are some of the tests that will be carried out.
- The impact of applying the FSP multi-passes will be studied through the tests performed including tensile tests, bending tests, microhardness, microstructural analysis, and fracture surface morphology.
- The effect of the material positioning on the multi-passes will also be determined.

1.5 Outline of the Dissertation

The following is the outline of the dissertation:

Chapter 1 – Introduction

This chapter provides a brief introduction, including the problem statement and the background of the study. Study aims and objectives, as well as related literature and the dissertation outline, are included.

Chapter 2 – Literature Review

This chapter explains detailed literature. It also covers other topics related to FSW and FSP, such as the FSW and FSP working principle, multi-pass friction stir processing, and process parameters and their importance in the process.

Chapter 3 – Experimental setup and performances

This chapter describes the equipment used for the FSW, FSP, and analysis of specimens, as well as the processing preparation and performances. This chapter analyses further into the mechanical and microstructural of the joints itself.

Chapter 4 –Test Results and Discussions

This chapter discusses the results obtained during the analysis of the joints.

Chapter 5 – Conclusions and recommendations

This chapter concludes based on results that were achieved in this study and provides recommendations for future work.

CHAPTER TWO
LITERATURE REVIEW

2.1 Introduction

This chapter presents the work that has been done so far on the multi-pass friction stir processing of the aluminium alloys. The main areas being considered include the impact of multi-pass FSP on the microstructure, tensile properties, bending strength, and hardness of the joints. A summary will be made highlighting the gap upon which this study will be filling.

2.2 Review on Multi-pass friction stir processing

The effect of process parameters on the microstructure was defined in the majority of FSP experiments after one pass. Multi-pass FSP, on the other hand, is a microstructure improvement technique for aluminium castings. There have been a few experiments reported on the microstructure evolution of multi-pass FSP, fatigue resistance improvement, and super-plasticity FSP [60,97,56].

Several FSP studies have shown that single and multi-pass processing can induce superplastic properties in different materials [56-59]. FSP using overlapping passes (known as multi-pass FSP) was recently discovered to exhibit comparable superplastic properties to single-pass FSP. The multi-FSP technique has been used in various applications as presented in the literature. Improvement in the corrosion resistance [98], mechanical properties [60], microstructure grain refinement [99], production of superplastic materials [100], reduction of the porosity of castings [60], or production of special alloys [57] is just a few instances included.

Different materials, such as cast [39,101] and wrought [99, 56] aluminium alloys, copper [58], magnesium alloys [56], titanium [102], and many others, can be subjected to the multi-run FSP technology, according to studies. Other papers [39, 60] have widely reported the effects of FSP multi-run on the modified area's mechanical properties and microstructure.

2.2.1 Microstructure

El-Rayes and El-Danaf [69] investigated the effect on mechanical and microstructural properties of AA6082 using an FSP multi-pass technique. The number of passes is more dominant than the traverse speed dials on the SZ's DRX of grain size. They discovered that the SZ-grain size increased as the number of FSP passes increased. On a 6 mm thick AA6082-T651 alloy, El-Rayes and El-Danaf [69] used a three-pass FSP with 100 percent overlap. When the number of FSP passes increased, the stir zone grain size increased, resulting in fraction high angle boundaries. Furthermore, as the number of FSP passes increased, more heat was accumulated, resulting in a decrease in the stir zone tensile strength. Both Johannes et al. [74] and Mishra et al. [16] believe that high angle boundaries are critical for improving mechanical properties.

Su et al. [103] investigated the microstructural changes that occurred as the number of passes increased when 7075 aluminium alloy was subjected to multiple FSP passes to assess the effects of FSP on large-area bulk UFG aluminium alloys. A single FSP pass, as well as a total

of four FSP passes, were used. The results shows the grain size of the microstructure was refined to a sub-micrometer scale of 250 nm. Using multiple FSP passes, the researchers were able to achieve ultra-fine grain microstructure. A three-pass FSP with 100 percent overlap was used to modify the microstructure and mechanical properties of the AA5083 alloy [77]. According to single-pass FSP, the stir zone underwent dynamic recrystallization, yielding equiaxed grain with high angle boundaries (HAGB). A linear relationship between rotational speed and grain size was discovered. It was discovered that the multi-pass FSP had no impact. When subjected to multiple pass FSP, the findings show there was no substantial effect on microstructural grain size at the stir zone.

Aktarer et.al [104] studied the impact of the multi-pass FSP on the Al-Si-9Mg cast aluminium alloy. The findings of the microstructural analysis revealed multi-pass resulted in reduced grain size while increasing homogeneity of microstructure. The uniform distribution of second phase particles was discovered by comparing the microstructure of the processed material to that of the cast condition. The processed zone porosity was reduced. In contrast to a single pass FSP, multi-pass FSP was used on the Al-Cu-Mg (AA2024) when loooking at the crystallographic texture evolution and microstructure [105]. The microstructure of the stir zone showed features that confirmed particle-stimulated nucleation caused by dynamic recrystallization. Furthermore, due to geometrical coalescence, the stir zone was discovered to have larger grains. All passes of FSP had consistent stir zone texture and microstructure, indicating that FSP should be used to produce a bulk volume of fine-grained materials.

Akinlabi et al. [67] investigated the impact of multi-pass friction stir processing on the mechanical properties of AA6061-T6, discovering that the single-pass FSP had a non-homogeneous processed zone, resulting in irregular grain growth, while the multi-pass FSP on the fifth pass had an entirely homogeneous processed zone due to accumulative plastic strain. A conclusion was made that the number of FSP passes has a substantial impact on the homogeneity of the processed region. Chen et al. [81] investigated the microstructure and mechanical properties of Al-5083 alloy after multi-pass friction stir processing. They performed a three-pass FSP on an AA 5083 sheet with 100 percent overlap and found that the first pass resulted in improved grain size because of recrystallization, but that subsequent overlapping passes resulted in no significant difference in grain size. As opposed to the base material, all of the multi-pass FSPed samples had tensile strength, lower hardness, and yield strength in the stir zone, with no major improvements with subsequent multiple passes.

Johannes and Mishra [56] investigated the formation of superplastic 7075 aluminium using multiple passes of friction stir processing. Multi-pass FSP was used to create a superplastic fine-grained microstructure in the AA7075 alloy**.** Multiple passes were seen to be efficient in producing large areas of superplastic 7075 Al material with insignificant microstructural discrepancies and grain sizes ranging from 3.6 μm to 5.4 μm. Ma et al. [106] looked at the Superplastic behaviour of micro-regions in a 7075Al alloy that was friction stir processed on a two-pass. The findings revealed that multi-pass FSP produced similar grain refinement in the microstructure of 7075 Al and that two-pass FSP samples with a 50% overlap have greater super-plasticity than single-pass FSP samples. This was due to the single-pass FSP sample's grain growth rate being faster than the two-pass FSP samples at a testing temperature of 480 °C.

Friction stir processing of AA7039 Alloy was investigated by Sinhmar et al [107]. Grain coarsening was observed after multiple FSP passes, according to their findings. The strain is associated with multiple mechanisms operating at different stages of the microstructure evolution after each successive multiple FSP pass. At each pass, the material goes through a strain rate and a thermal cycle. The existence of precipitates in the second phase is responsible for the significant-high strength in the base material. Al-Fadhalah et al. [99] investigated the impact of overlapping (26, 50, and 75 percent) between consecutive FSP passes on the microstructure, microtexture, and mechanical properties of the AA6063 Al alloy. They found that increasing the percentage of overlapping causes only a slight change in grain size in the overlapping region but results in an increased fraction of sub-grain boundaries forming in the TMAZ.

El-Rayes and El-Danaf [69] looked at the effect of multiple passes by FSP on the mechanical properties of AA6082. According to the authors, increasing the number of FSP passes causes dynamic recrystallization and heat accumulation in the stir zone, resulting in more equiaxed grains with high angle grain boundaries. In multi-pass processing, the relationship between hardness and grain size is opposite, with an increase in SZ-grain size as the number of passes increases. When opposed to the one-pass FSP sample, Cui et al. [94] found that the two-pass FSP sample has a clear benefit in microstructure modification. For the AA7022-T6 alloy, Nascimento et al. [108] recorded that one-pass FSP decreased grain size from 160 μm to an average grain size of 7.1 μm, which remained constant regardless of the number of passes and overlap ratios tested.

Mabuwa and Msomi [109] compared the mechanical properties of FSWed dissimilar aluminium joints processed by normal multiple-pass friction stir processing and submerged multiple-pass friction stir processing. Under different operating conditions, multiple-pass friction stir processing was used on friction stir welded dissimilar aluminium alloy joints AA8011-AA6082. Room temperature and underwater friction stir processing were used as processing conditions. As per the microstructural results, the grain structure of the multiple-pass submerged friction stir processed joints was 67.72 percent finer than that of the multiple-pass normal friction stir processed joints. Mabuwa and Msomi [110] investigated the Fatigue Behaviour of the 8011-H14 aluminium alloy and 6082-T651 aluminium alloy dissimilar joints that had undergone multi-pass friction stir processing. The multi-pass FSP produced microstructural grain sizes that were exceptionally fine. Regardless of material positioning, the microstructural analysis results as the increases in the passes of FSP passes resulted in grain size reduction. The multi-pass AA6082-AA8011 joint had a better grain structure than the multi-pass AA8011-AA6082 joint.

Muribwathoho et al. [111] explored the effect of multi-pass friction stir processing on the microhardness of 1050 aluminium alloy/6082 aluminium alloy dissimilar joints. The friction stir welding (FSW) technique was used to create a dissimilar joint using aluminium plates AA1050 and AA6082. After that, multi-pass friction stir processing was used to process the produced dissimilar joint. Microstructural analysis revealed that grain sizes reduced as the number of FSP passes increased. Nascimento et al. [108] investigated the microstructural modification and ductility enhancement of FSP-modified surfaces in aluminium alloys. In single and multiple passes, the effects of in-surface and in-volume friction stir processing of AA5083 and AA7022

aluminium alloys are investigated. FSP is a method that is very efficient in decreasing grain size from 160 μm of AA7022-T6 and 106 μm of AA5083-O to an average grain size of around 7.1 μm and 5.9 μm, respectively.

2.2.2 Tensile Properties

Johannes and Mishra [56] studied the development of superplastic 7075 aluminium using several passes of friction stir processing. A four-pass and a single pass FSP were applied to the AA7075 plate under similar conditions. A single pass of FSP for the AA7075 alloy yielded the maximum strain rate after multiple passes. The multi-pass FSP revealed at different strain rates larger areas of super plasticity. Furthermore, the single-pass FSP had a larger elongation. Grain boundary sliding was discovered to be the predominant mechanism for superplastic deformation in the multi-pass FSP. The two-pass FSP has a greater elongation, according to Ma et al. [106]. Brown et al. [112] performed a 100 percent overlap five-pass on 7050-T7451 alloy and discovered that the accumulated decrease from pass 1 to 5 had only a small impact on tensile strength and that the microstructure in the SZ did not change during the subsequent passes.

Senthilkumar et al. [113] analysed the microstructure and mechanical properties of the AA6082 using process parameters such as rotational tool speed and FSP pass number. As rotational speed increased, so did the amount of heat produce. As the number of FSP passes increased, tunnel voids decreased. Because of dissolution hardening caused by the heat encountered by the processed surface, an increase in the number of FSP passes resulted in a decrease in UTS at the stir region. UTS of the stir zone increased as the tool rotational speed improved, but the ductility of the joint decreased. El-Rayes and El-Danaf [69] investigated the effects of FSP multi-pass on the properties of commercial thick 6082-T651 aluminium alloy plates. They discovered that a single-pass FSP induced dynamic recrystallization of the stir field, resulting in grains equiaxed, but that multiple passes resulted in a tensile strength decrease. The over-aging effect of subsequent passes on the previous passes also contributed to the decrease in tensile strength.

Palani et al. [91] looked into the effect of FSP on the tensile properties of the AA8011-AA6061 dissimilar joint. With nanoparticles incorporated, technique of FSP was used on the joints, the AA6061 processed similar joint had 98.58 percent tensile strength with nanoparticles, while AA8011-AA6061 dissimilar joint had 90.08 percent tensile strength excluding nanoparticles. Shankar et al [114] looked at how machining changed the properties of aluminium 6061-T6 as it was subjected to large plastic strains. They discovered that precipitation-treatable aluminium alloys, such as peak-aged Al6061-T6, have a perfect precipitate distribution that guarantees the material's maximum strength. Ravikumar et al [115] researched the mechanical properties characterization of aluminium 6061-T6 after FSW and found a similar high strength. As the UTS decreases, the yield strength appears to decrease uniformly. After the first FSP pass, there was precipitate dissolution, leading to softening in the SZ and a decrease in pre-existing dislocations, which resulted in a significant reduction in the tensile properties.

Age-hardened aluminium alloys, according to Al-Fadhalah et al [99], are highly dependent on distributions and precipitate size instead of grain size. This can be seen in the values of tensile on the pass two and three, where grain size, UTS, and yield strength all decreased relative to

the anticipated increment in values based on the Hall-Petch relation [116]. These decreases in Ultimate tensile strength and yield strength may be attributed to the overaging effect that succeeding passes had on the preceding one [69]. According to El-Rayes and El-Danaf.[69], as the number of passes increases, the hardening phase dissolves, softening and lowering Ultimate tensile strength at the SZ but increasing hardness because of the forming of second phase particles.

Meenia et al. [117] studied the microstructure and mechanical properties when the hypeutectic Al-Si alloy was exposed to multi-pass FSP. Three passes were used in total. The three-pass FSP had the most refined grain structure and provided the maximum ductility as compared to the single-pass FSP. The tensile strength followed the same trend. Furthermore, using the multi-pass FSP on the same alloy has shown an increase in elongation and tensile strength [43]. Rao et al. [118] explored the impact of a two-pass with 100 percent overlapping FSP on the hyper eutectic Al–30Si alloy. The tensile strengths of the multi-pass friction stir processed specimens are considerably greater than those of the cast aluminium alloy. Both Pradeep et al. [119] and Nakata et al. [97] discovered that multi-pass produced a higher tensile strength than the base material.

Baruch et al. [40] investigated the overlap multi-pass FSP on die-cast Al-Si-3Cu aluminium alloy. According to the results, the tensile strength rose from 121 to 273 MPa. When the number of passes increased, the microstructural grains became more refined, resulting in an improvement. Simultaneously, fracture strain was found to have increased from 1.8 to 10%. Changes in the size, shape, morphology, and distribution of eutectic silicon ions, as well as the removal of porosities, are the primary causes of increases in tensile strength and ductility due to friction stir processing. Ramesh et al. [120] performed a twelve-pass FSP on the AA5086 –O plates using two FSP approaches with a 50% overlap. The FSP methods used were intermittent multi-pass and continuous multi-pass. The mechanical properties of the AA5086 alloy were compared using these two methods. According to the results, specimens exposed to IMP FSP had better mechanical properties.

Mandal [121] looked at using multi-pass friction stir processing to modify the surface of an aluminium alloy (7xxx series). Aluminium plates were subjected to MP-FSP for 1 to 14 passes in the longitudinal path, with the process parameters of 1000 rpm rotational speed, 70 mm/min travel speed, and 15 KN axial force. In comparison to DP-FSP, the multi-pass specimen significantly improved tensile strength and ductility to 122.48 percent and 42.55 percent, respectively. This is used not only to refine the cast dendritic structure and remove segregation in the as-cast alloy but also to refine grains, such as Al3Sc distribution uniformity and hardening precipitates. The age-hardening effect with a fine dispersion of Al3Sc particles and stirring effects, however, has improved tensile properties.

Mabuwa and Msomi [109] compared the mechanical properties of FSWed dissimilar aluminium joints processed by submerged multiple-pass FSP and normal multiple-pass FSP. Friction stir welded dissimilar aluminium alloy joints AA8011-AA6082 were subjected to normal and submerged multi-pass friction stir processing. The ultimate tensile strength increased as grain size decreased, resulting in a UTS of 97.99 MPa for the submerged multiple-pass FSPed joint and a UTS of 94.19 MPa for the normal multi-pass FSPed joint. Tensile and grain size results were correlated with the percentage elongation results. The

obtained UTS was corresponded with grain size behaviour, leading to a UTS of 3.2 percent increase in the submerged multiple-pass joint than in the normal friction stir processed joints.

Muribwathoho et al [111] explored the effect of multi-pass friction stir processing on the microhardness of 1050 aluminium alloy/6082 aluminium alloy dissimilar joints. The friction stir welding (FSW) technique was used to create a dissimilar joint using aluminium plates AA1050 and AA6082. After that, the generated dissimilar FSWed joint was processed using the multi-pass FSP technique. The multi-pass ultimate tensile strength increased as elongation reduced, compared to a single pass with the same material positioning for AA1050-AA6082 joints. Mabuwa and Msomi [110] investigated the fatigue behaviour of 8011-H14 aluminium alloy and 6082-T651 aluminium alloy dissimilar joints that had been processed with multi-pass friction stir processing. Only the AA8011-AA6082 joints showed an increase in UTS because of the increase in FSP pass number, although a fluctuation between 91.1 and 92.3 MPa was observed for the AA6082-AA8011 joints. The multi-pass FSP increased UTS by 11.6 percent as opposed to the single-pass FSP, only for AA8011-AA6082 joints, while the two-pass FSP of AA6082-AA8011 increased ultimate tensile strength by 9%.

2.2.3 Hardness

By locally eliminating casting defects and refining microstructures, multi-pass FSP can improve corrosion resistance, but the hardness has different behaviour. There have been several experiments on multi-pass FSP on AA2219 aluminium alloy without the use of reinforcing particles [16,21,22]. In all processing parameters, they found that the stirred zone had lower hardness than the base metal. Surekha et al. [98] processed the 2219 aluminium alloy with FSP multi-pass and discovered that stir zone had less hardness than the base material. When aluminium alloy 2024 was exposed to multi-pass FSP, Ghanbari et al. [122] discovered that the hardness of the stir zone decreased as the amount of FSP increased. Several experiments [31,99,123,124,125] discovered that in terms of hardness they all had similar behaviour.

According to Paider et al. [126], the grain boundaries number has a clear connection with the number of passes of FSP. Based on results obtained the hardness of the SZ was observed to rise with the increase in FSP pass number. This phenomenon was prompted by a reduction in grain size. A three-pass FSP was compared to a single-pass FSP on mechanical properties of the 7B04-O aluminium alloy [127]. The findings showed a 40 HV increase as compared to the base metal. According to Moharrami et al. [128], the hardness of AA6082 alloy was increased from 178 HV to 270 HV after a six pass. Similarly, compared to the single-pass FSP, the multi-pass FSP improved the stiffness of the A390. When the number of FSP passes increased, so did the hardness. Mahmoud [129] investigated multi-pass FSP AA6063, found a significant reduction in the microhardness of FSPed samples (40–60 HV) as opposed to the BM sample. The multi-pass has shown to raise or decrease the hardness of the material but has little effect on the stir zone's hardness. Johannes et al. [56] discovered that hardness was constant in all passes after investigating the influence of FSP multi-pass FSP with 42 percent overlap between the passes on the AA7075 alloy. Khorrami et al. [111] related findings have been published.

The effect of overlapping direction in multi-pass friction stir processing was investigated by Gandra et al [130]. When overlapping by the advancing side (AS) or the retreating side (RS), structural and mechanical variations were found. The findings revealed that after the hardness test, the hardness of the processed layer remains relatively constant and does not differ between passes. Test in stiffness and bending was used to compare the multi-pass surface ductility to that of a single-pass FSP. Mechanical resistance and toughness under bending were also increased by 18 and 19 percent, respectively, according to the findings. The harness of material was observed to have an 8.5 percent increase as compared to one pass. Similar investigation observed that using multi-pass FSP increased hardness [107,131-135]. Muribwathoho et al [111] explored the effect of multi-pass friction stir processing on the microhardness of AA1050/AA6082 dissimilar joints. The friction stir welding (FSW) technique was used to create a dissimilar joint using aluminium plates AA1050 and AA6082. The produced dissimilar joint was then processed. The method used in this analysis was multi-pass friction stir processing. The number of FSP passes has a small impact on microhardness.

Palani et al. [92] investigated the mechanical properties of similar and dissimilar AA8011-AA5083 joints using FSP parameters. Al2O3, as well as SiC nanoparticles, were used in the processing. It was discovered that adding nanoparticles to the processed AA8011-AA5083 dissimilar joint enhanced the joint strength and hardness. According to Lu et al. [136], as the number of FSP passes increases, the Si particle size decreases, and the microhardness increases. The improved distribution of Si particles in the processed material, as found by Tutunchilar et al. [79], is the most important consideration for increasing strength, elongation, and hardness. Nascimento et al. [108] investigated the FSP of an AA5083-O aluminium alloy in bulk and surface processing, obtaining a uniform hardness increase within the processed surface using both single and multi-pass methods.

El-Rayes and El-Danaf [69] looked at how multi-pass FSP affected the properties of dense 6082-T651 AA plates. They discovered that a single-pass FSP induced dynamic recrystallization of the stir area, resulting in equiaxed grains, but that after repeated passes, the hardness decreased. The softening SZ that followed the rise in the FSP number of passes was said to be the cause of the hardness reduction. Following FSP passes, the softening was attributed to a larger grain size. The mechanical properties of FSWed dissimilar aluminium joints processed by normal multiple-pass friction stir processing and submerged multiple-pass friction stir processing were compared by Mabuwa and Msomi [109]. Under different operating conditions room temperature, multiple-pass friction stir processing, and underwater multiple-pass friction stir processing were used on dissimilar FSWed aluminium alloy joints AA8011-AA6082. The hardness of multiple-pass submerged friction stir processed joints was 65 HV, while the hardness of normal multiple-pass friction stir processed joints was 53 HV.

Mabuwa and Msomi [110] investigated the fatigue behaviour of the multi-pass friction stir processed aluminium alloy 8011-H14 and aluminium alloy 6082-T651 dissimilar joints. Using the friction stir welding technique, the AA8011-H14 and AA6082-T651 were used to create dissimilar joints. Multi-pass friction stir processing was used to process the generated dissimilar joint. The number of passes of friction stir processing has a slight impact on microhardness. The microhardness of the joints was found to be affected only slightly by the FSP pass number. Mirjavadi et al. [123], Moustafa [131], investigated the impact of multi-pass friction stir processing on the microstructure, mechanical, and wear properties of

AA5083/ZrO2 nanocomposites, as well as the impact of friction stir processing multiple passes on AA2024/Al2O3 nanocomposites materials mechanical properties. As the number of FSPs increased as per findings, grain refining occurred. Furthermore, as a result of the thermal expansion mismatch between these second-phase particles and the matrix, the density of dislocations increased, and the hardness values improved [137].

Mandal [121] investigated multi-pass FSP for surface modification of Aluminium alloy (7xxx series). Aluminium plates were subjected to MP-FSP for 1 to 14 passes in the longitudinal direction with the following process parameters: 1000 rpm rotational speed, 70 mm/min travel speed, and 15 KN axial force. The MP-FSP has improved the hardness of the alloys, according to the findings. Hardness was also improved by increasing the number of MP-FSP passes. In comparison to DP-FSP, the data reveal that the hardness has decreased by 4.84 percent. The microstructural refinement caused by fine precipitates and Al3Sc dispersoids may be related to this. This is used not only to refine the cast dendritic structure and remove segregation in the as-cast alloy but also for grain refinements, such as uniform Al3Sc distribution and hardening precipitates. Decomposition may have been primarily caused by the precipitation of coherent Al3Sc precipitates, but discontinuous precipitation caused some coarsening of these precipitates, according to the strength and hardness results. However, owing to the dynamic recrystallization of highly deformed grains during MP-FSP, SZ exhibits homogeneous and fine equiaxed grains.

2.2.4 Bending strength

In multi-pass friction stir processing, Gandra et al. [130] looked at the effect of overlapping direction. An 8 mm thick AA 5083-H111 alloy was tested. When overlapping in the advancing side (AS) and retreating side (RS) directions, structural and mechanical differences were observed. Under tensile and compressive loads, the maximum load needed for bending increased for all friction stir processed samples, but the best results were obtained for overlapping by the RS. Both overlapping methods reduced the toughness of the processed layer during bending under tensile loading. In multi-pass FSP the maximum bending load increased 18% when overlapping by RS. Because of the asymmetric nature of the material flow, the overlapping method has a significant impact on the processed surface characteristics.

Nascimento et. al. [108] investigated the microstructural modification and ductility enhancement of FSP on modified surfaces in aluminium alloys. The effects of single and multiple passes of in-surface and in-volume friction stir processing of AA5083 and AA7022 aluminium alloys were investigated in this analysis. In the AA7022-T6 sample, the findings showed a substantial increase in material formability due to an increase in ductility caused by grain size refinement, with the maximum bending angle increasing by a factor of 12 for the VFSP treatment and 4 for the SFSP treatment. In AA5083-O, VFSP treatment resulted in 2.5 times increase in maximum bending angle, while SFSP treatment resulted in 1.5 times increase in maximum bending angle.

2.3 Summary.

FSP has an undeniable track record as a tool for improving soft alloys, counting aluminium. According to the literature on the subject, the majority of the work on the multi-pass FSP concentrated on plate processing. In a searchable database, there is not much literature on FSWed joints which were FSPed using the multi-pass technique. This provides an opportunity to explore multi-pass friction stir processing of FSWed aluminium alloy joints which are dissimilar and similar. Since most industries choose to use dissimilar alloys in the production of different parts, it is critical to concentrate on the FSP multi-pass of the dissimilar joints. The majority of the works on multi-pass FSP concentrated on plate processing rather than joint processing, according to the available literature. Multi-pass friction stir processed joints are the subject of very few studies. As a result, further research into friction stir processing of dissimilar aluminium alloys using multiple pass is necessary.

CHAPTER THREE
EXPERIMENTAL SETUP AND PERFORMANCE

This chapter describes all the equipment used in the study's experiments, as well as a detailed description of each piece of equipment. This involves the friction stir welding technique that was used to create the welds, which were then friction stir processed using multi-pass FSP. This chapter describes the welding and processing conditions. This chapter also provides information on the experiments that were conducted on the processed joints.

3.1 Welding setup

The following machines were used to prepare welding performance:

- Guillotine cutting machine.
- Semi-automated milling machine

3.1.1 Guillotine cutting machine

A guillotine cutting machine is a machine that uses both foot and hand-powered techniques to cut sheet metal into ideal dimensions. Figure 3.1.1 shows an example of a guillotine cutting machine. Upper and lower blades, a shear table, and a gauging device are among the components of this system. The shear table is used to rest the material whilst it is being sheared. The gauging device is used to measure the material to be cut to the appropriate scale. The material is cut using the upper and lower blades.

The plates to be cut must first be marked for simple alignment before using the guillotine cutting system. The plates are then aligned with the shear master blade using the marks, and the cutting blade is lowered to begin cutting by pressing the foot pedal. The cut-off piece falls in the box provided.

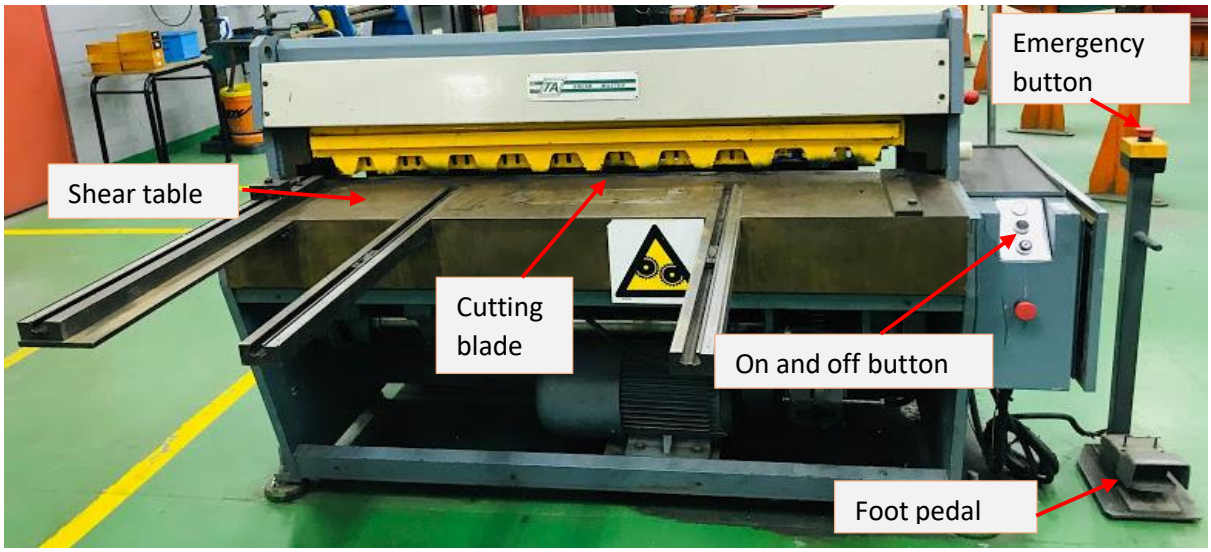

Figure 3.1.1: Guillotine cutting machine.

3.1.2 Semi-automated milling machine

A semi-automated milling machine was used to carry out the friction stir welding and friction stir processing technique (see figure 3.1.2(a)). To position the workpiece for FSW / FSP, a backplate with a clamping fixture was built and placed into the semi-automated milling machine bed. The FSW/FSP tool and clamps were designed and developed based on the literature. Figure 3.1.2 (b) displays the triangular threaded pin tool used for this study. The tool aims to create a weld along the workpieces' centerline. During welding, clamps were used to secure both the backing plate and the plate to be welded in place.

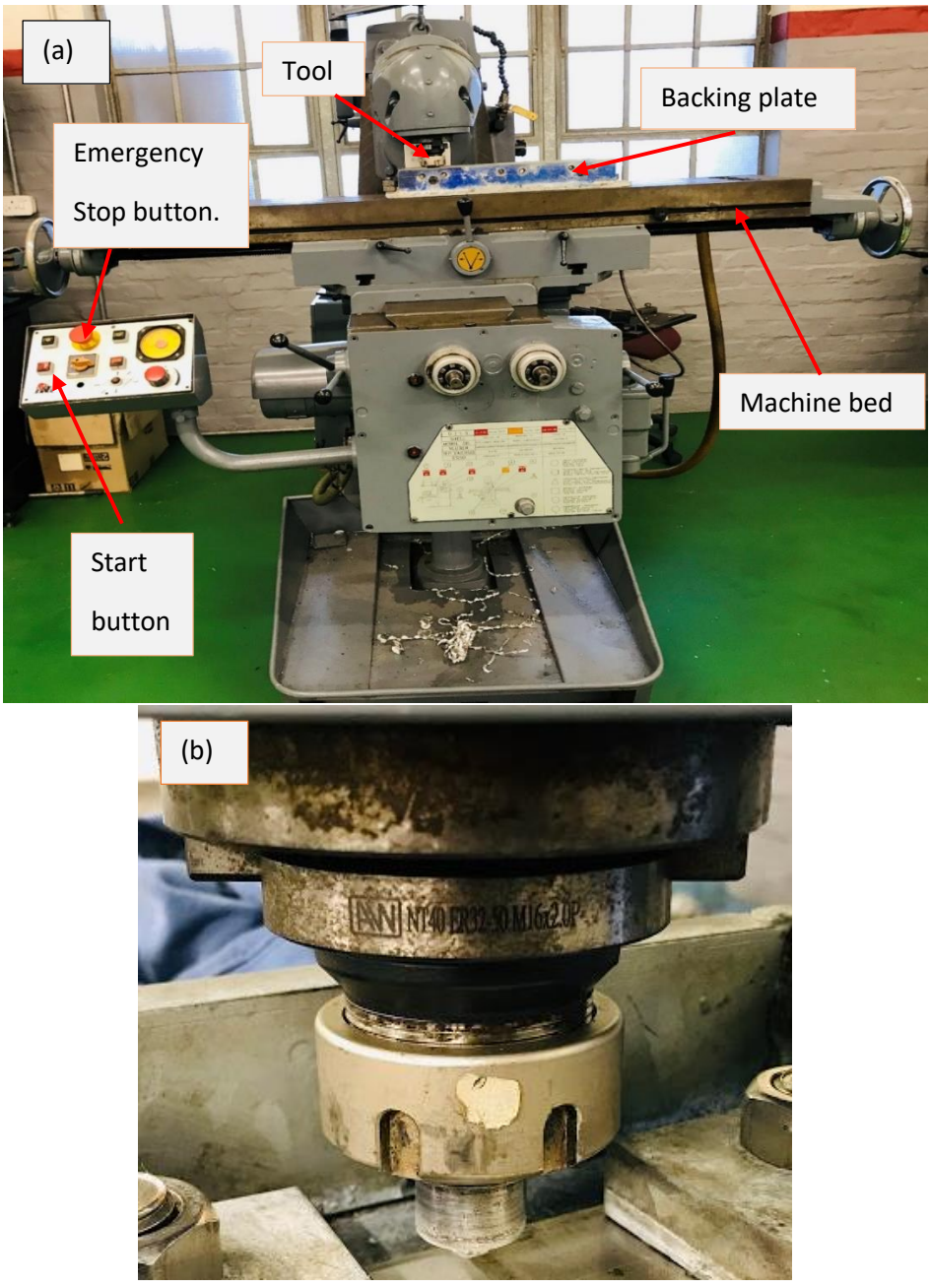

Figure 3.1.2: (a) Semi-automated milling machine, (b) FSW/FSP Tool.

3.2 Welding preparation and performance

3.2.1 Material selection

Two dissimilar aluminium alloy plates were selected for this study i.e. AA1050-H14 and AA6082-T651 dissimilar aluminium alloy with 6mm thickness. Table 3.2.1 shows the chemical compositions of two dissimilar aluminium alloy plates that were measured using Belec spectroscopy.

Table 3.2.1: Dissimilar aluminium alloys chemical composition.

	Si	**Fe**	**Cu**	**Mn**	**Mg**	**Ni**	**Zn**	**Ti**	**Pb**	**V**	**Co**	**Al**
AA1050	0.16	0.66	0.03	0.12	0.60	0.07	0.56	0.02	0.69	0.02	0.03	Bal
AA6082	0.33	0.43	0.02	0.35	1.09	0.05	0.32	0.01	0.39	0.00	0.01	Bal

3.2.2. cutting of the dissimilar aluminium alloy plates.

Eight sets of each dissimilar aluminium alloy were marked to match the FSW backplate in the appropriate dimensions. In preparation for the friction stir welding technique, a guillotine system was used to cut dissimilar AA1050 and AA6082 plates of 6 mm thickness into appropriate dimensions (52 mm X 260 mm). The measurements of the plate were selected to match the backing plate. Figure 3.2.2 (a) depicts the aluminium alloy plates before cutting with a guillotine cutting machine, while figure 3.2.2 (b) depicts plates after they have been cut.

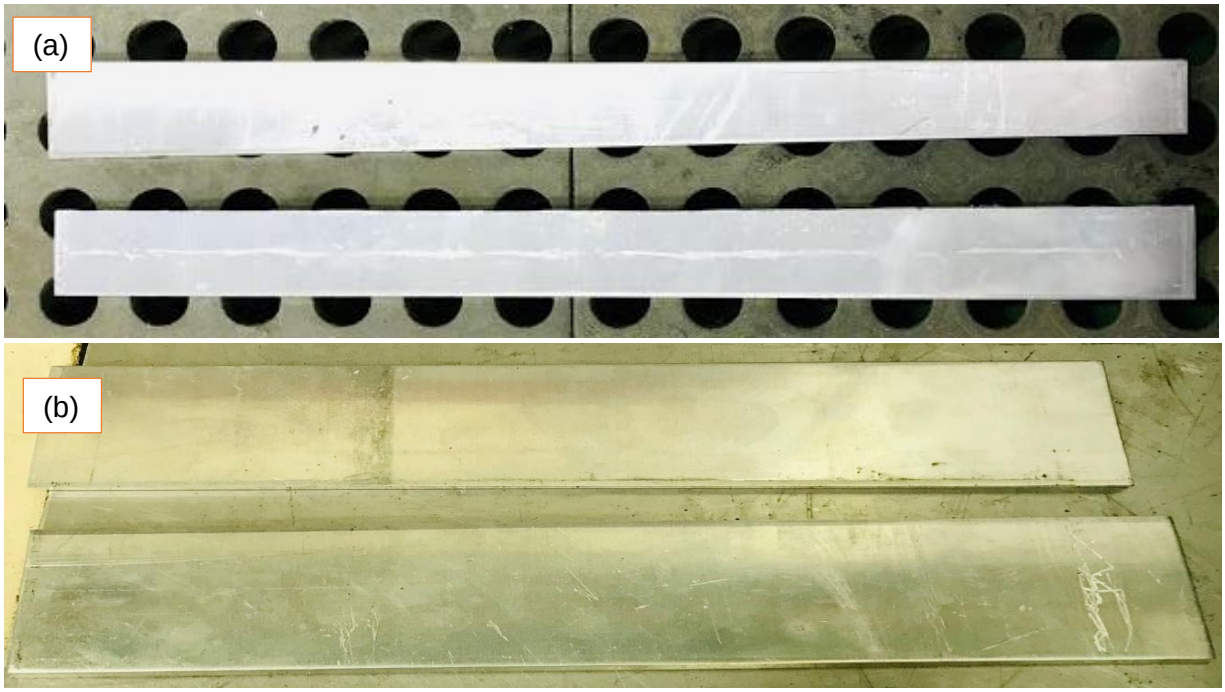

Figure 3.2.2: (a) Aluminium alloy plates before cutting, (b) Cut aluminium alloy plates to fit the FSW backplate ready for welding.

3.2.3. The material position of the aluminium plates.

Two material positions were selected for this study to compare the mechanical properties of the multi-pass friction stir processed joints. The advancing side of the first four plates was AA1050, while the retreating side was AA6082 (see figure 3.2.3 (a)). AA6082 was placed on the advanced side of the last four plates, while AA1050 was placed on the retreating side (see figure 3.2.3 (b)). It is worth noting that AA1050/AA6082 suggests that during FSW and FSP, AA1050 was on the advancing side. It is also worth noting that AA6082/AA1050 indicates that during FSW and FSP, AA6082 was on the advancing side.

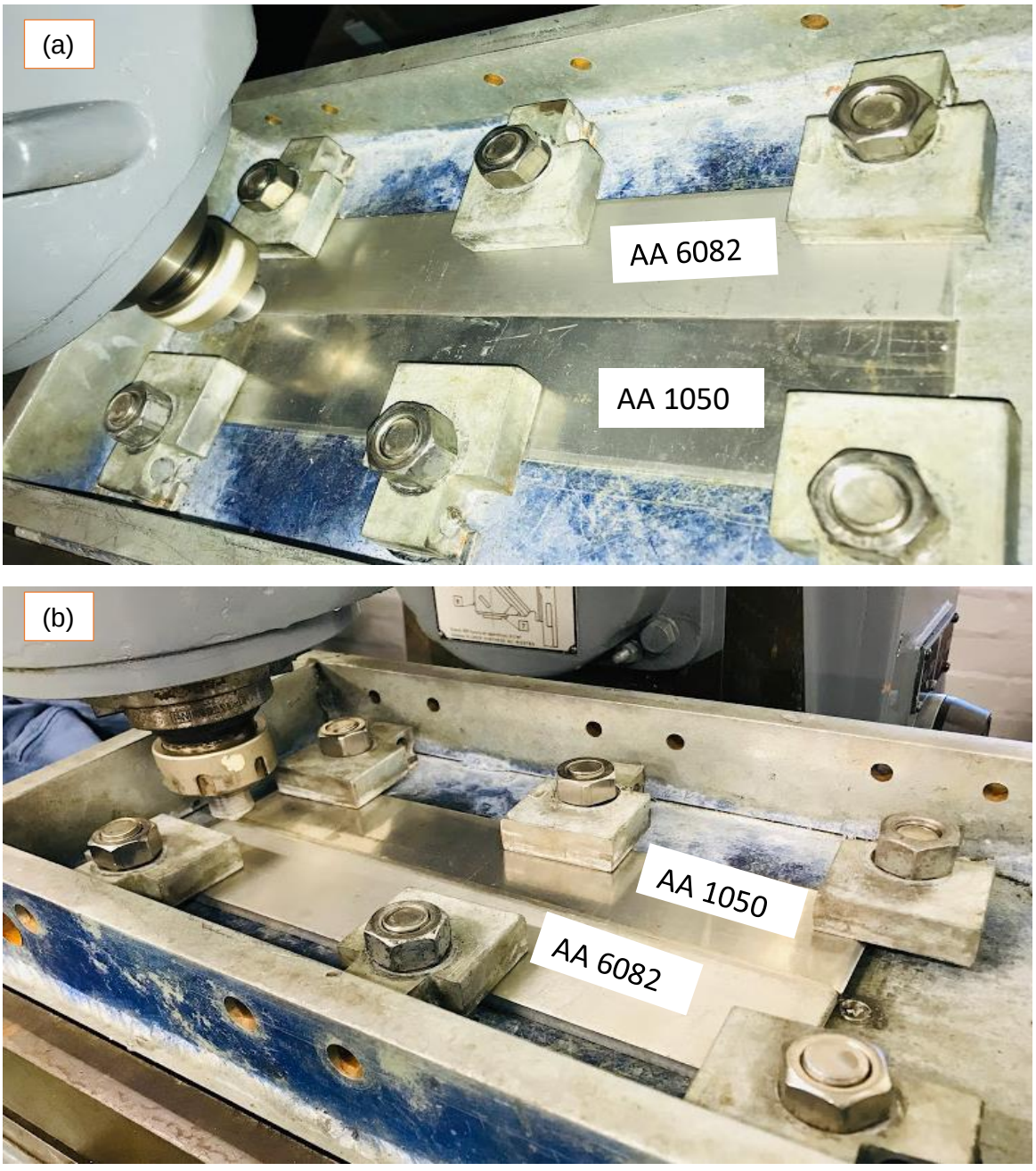

Figure 3.2.3: (a) AA1050/AA6082 dissimilar plates, (b) AA6082/AA1050 dissimilar plates.

3.2.4. Welding procedure.

The properly dimensioned plates were fitted to the backplate of a semi-automated milling machine which were locked suing clamps. Six clamps were used to lock the plates to the system backplate, ensuring that they do not separate while the rotating pin was in motion. After that, the plates were then welded using a high-speed steel tool using friction stir welding techniques. The high-speed steel tool was selected for its properties. The capacity to keep a high level of hardness at high temperatures. At room temperature, resistance to penetrating by a diamond-hard indenter. Capacity to absorb (impact). Grindability, metal-to-metal, and other types of testing are commonly used to get a relative grade for abrasion resistance [138]. AA6082/AA1050 dissimilar joints and AA1050/AA6082 dissimilar joints were created using the FSW. Table 3.2.4 displays the welding parameters used for FSW, such as welding speed, traverse speed, and rotational speed. The FSW's performance is represented in figure 3.2.4 (a). Figure 3.2.4 (b) shows a welded plate.

Table 3.2.4: Parameters for friction stir welding.

Rotational speed (rpm)	**Traverse speed (mm/min)**	**Tilt angle (^{0})**
1200	60	2

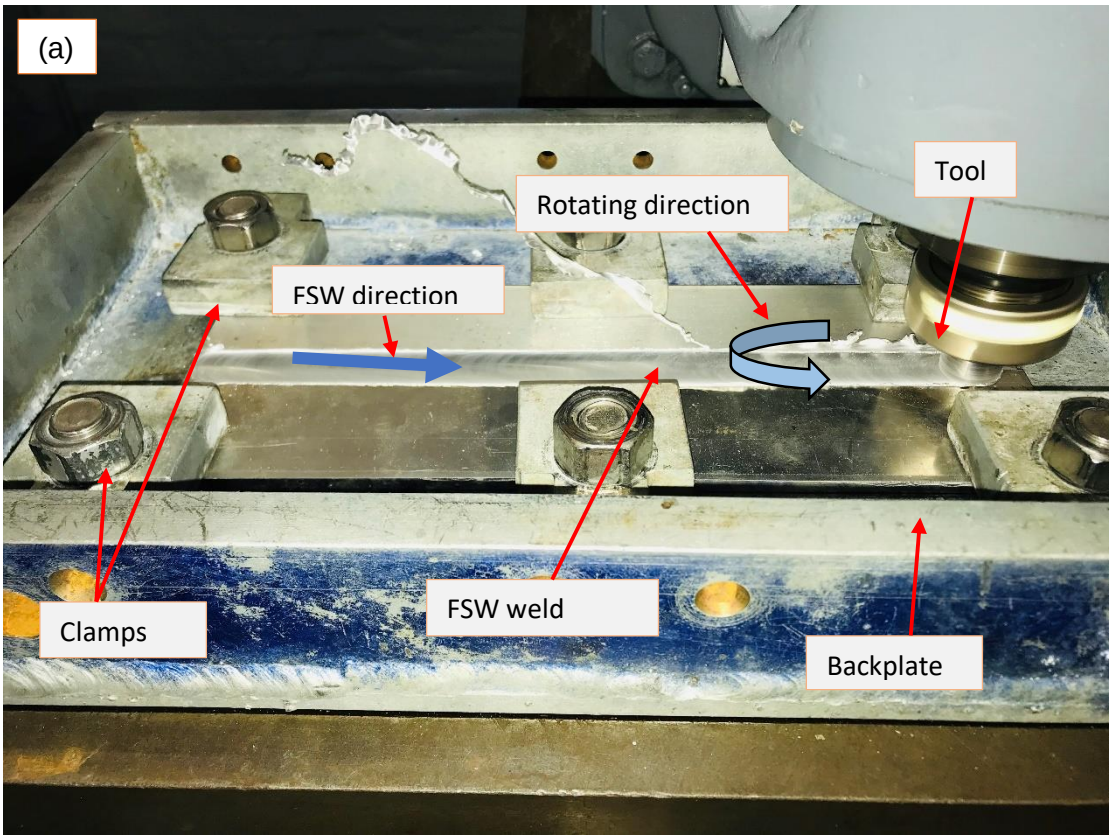

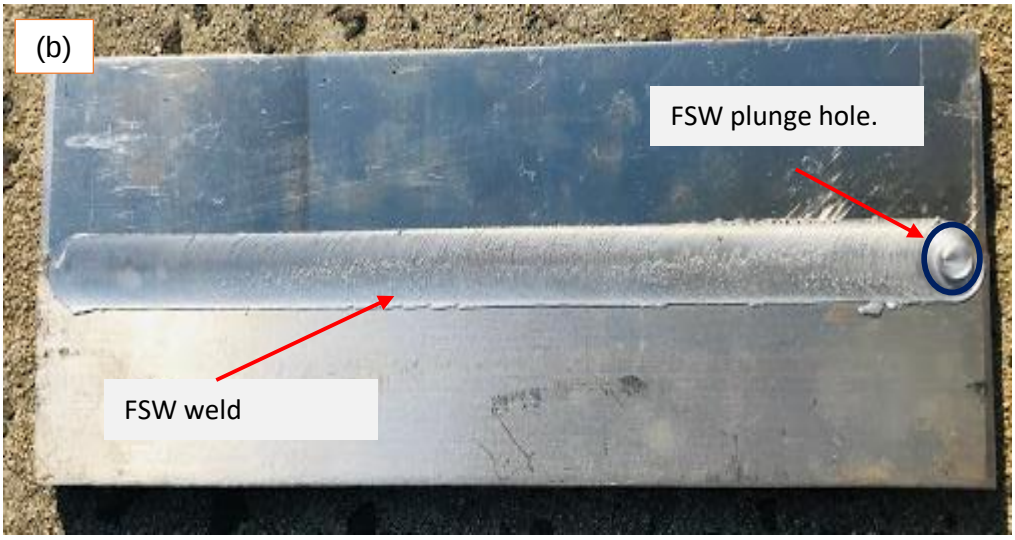

Figure 3.2.4: (a) The performance of the FSW, (b) FSWed plate.

The tool used for Friction Stir welding had a 20 mm shoulder diameter and a 7 mm pin diameter, the tool pin's profile was triangular threaded. The triangular threaded pin tool (see figure 3.1.2 (b) had a 1 mm pitch and a height of 5.8 mm. The tool design with proper dimension in mm is showed in Figure 3.2.4 (c). The tool was selected due to the fact that the SZ, in contrast to the Triangular threaded pins, has an onion ring design in which the reinforcements are mostly dispersed. This is owing to the sufficient heat input generated by these tools, which allows for the material flow required to produce the onion ring pattern [139].

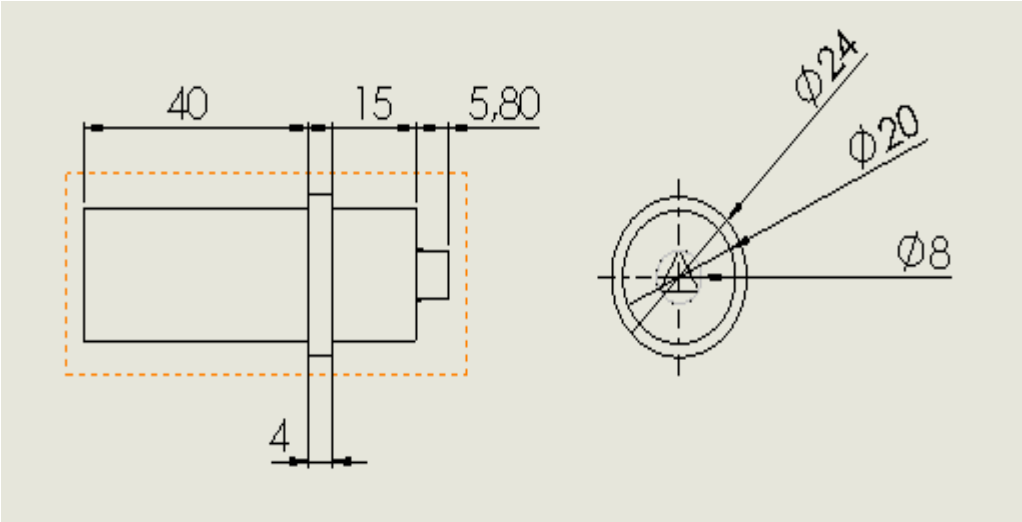

Figure 3.2.4: (c) Designed FSW/FSP tool AutoCAD version.

3.3 Multi-pass Friction Stir Processing performance.

The semi-automated milling machine was used to perform multi-pass friction stir processing on the friction stir welded joints. FSP parameters are the same as FSW parameters (refer to table 3.2.4). For each material positioning, the FSWed joints were subjected to one-pass (1P), two-pass (2P), three-pass (3P), and four-pass (4P) FSP, resulting in a total of four FSPed plates on each position (AA1050/AA6082 and AA6082/AA1050). All FSP passes had a 0% overlap. Figure 3.3 (a): depicts the FSP's performance. Figure 3.3 (b) – (e) displays the

processed joints for each pass while Figure 3.3:(f) shows the multi-pass FSPed plates. The tool created the holes when it unplugged at the end of the FSW and FSP processes. It is worth noting that there was one plunge hole at the end of the plate after welding, and an additional hole was developed after each FSP pass towards the end.

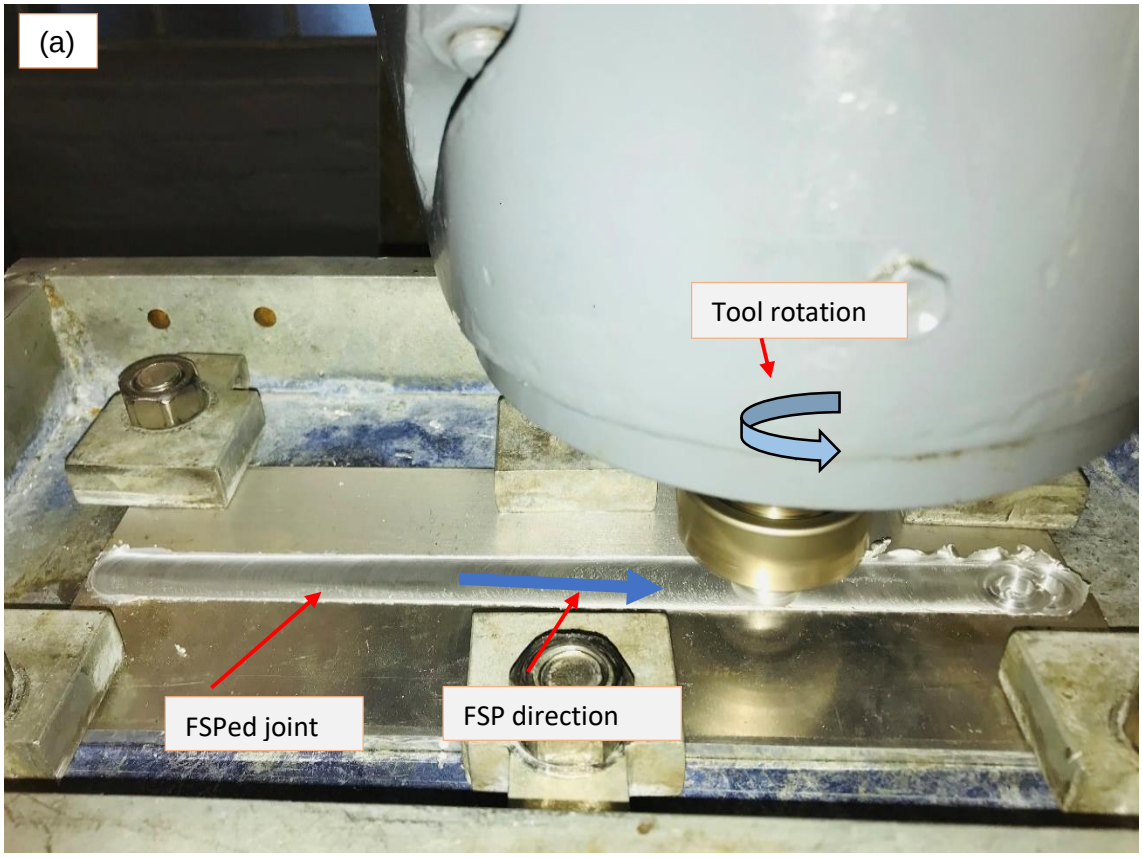

Figure 3.3: (a) FSP application on FSWed joint.

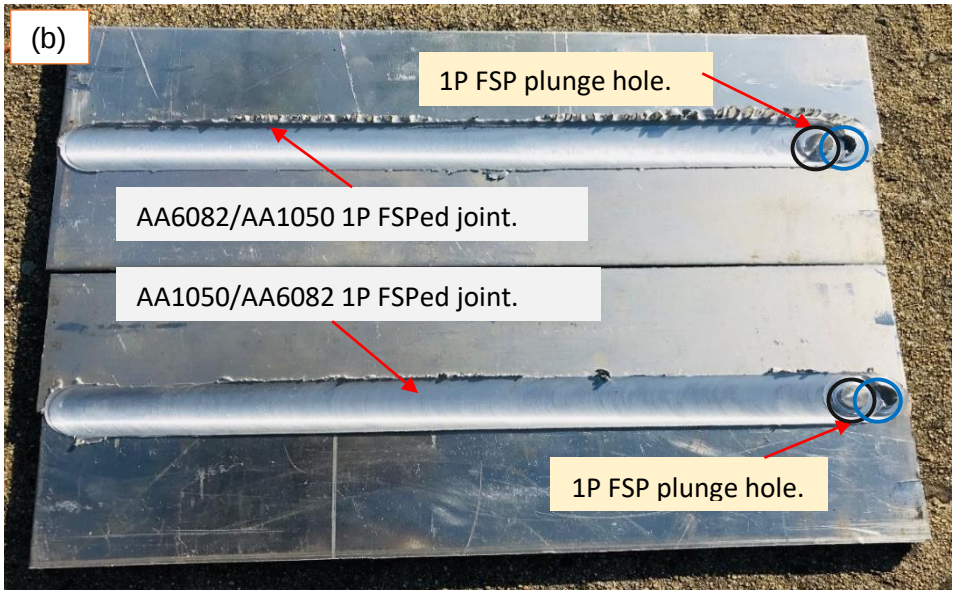

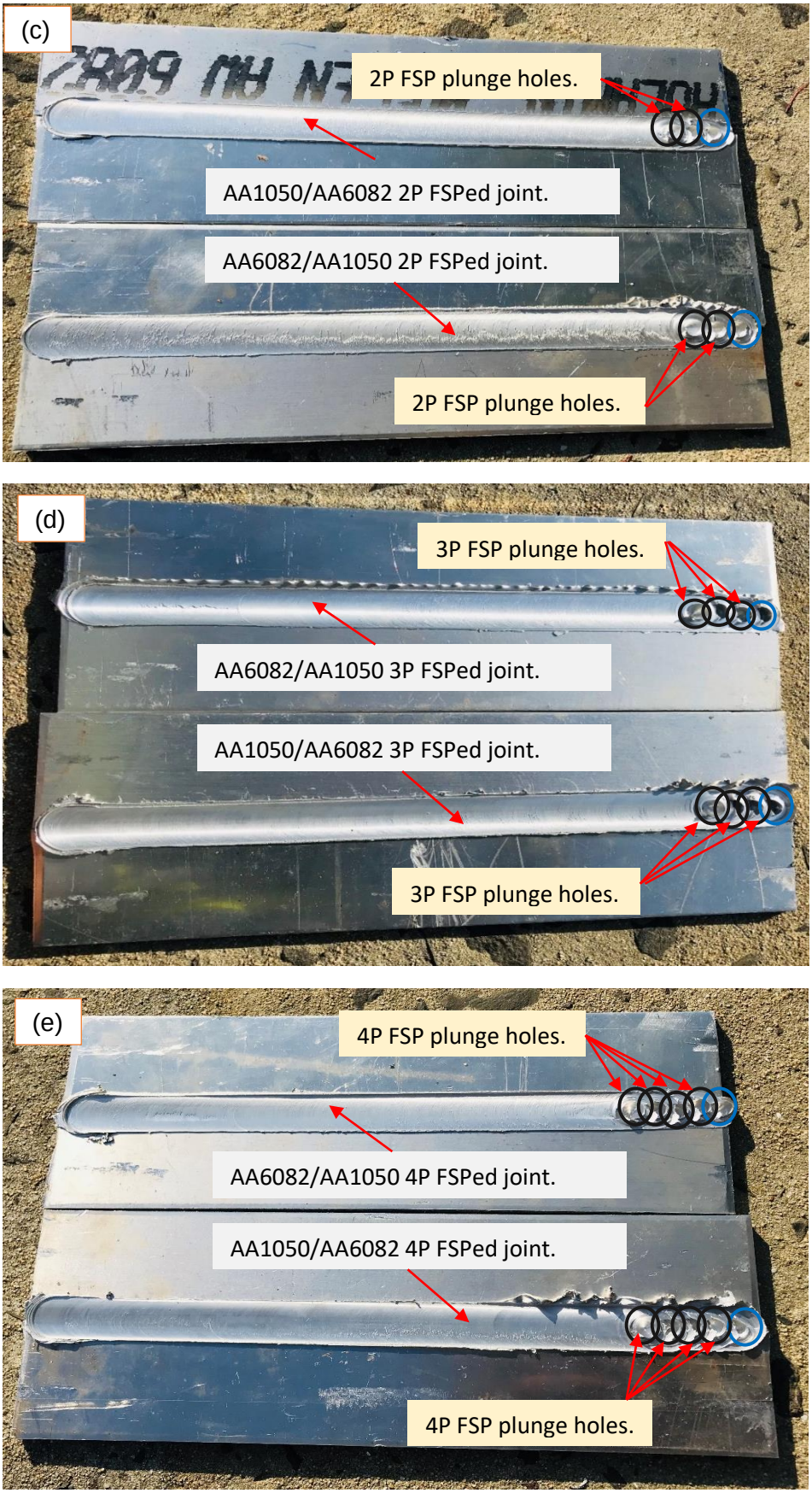

Figure 3.3: (b) 1 Pass FSPed plates, (c) 2 Pass FSPed plates, (d) 3 Pass FSPed plate, (e) 4 Pass FSPed plates.

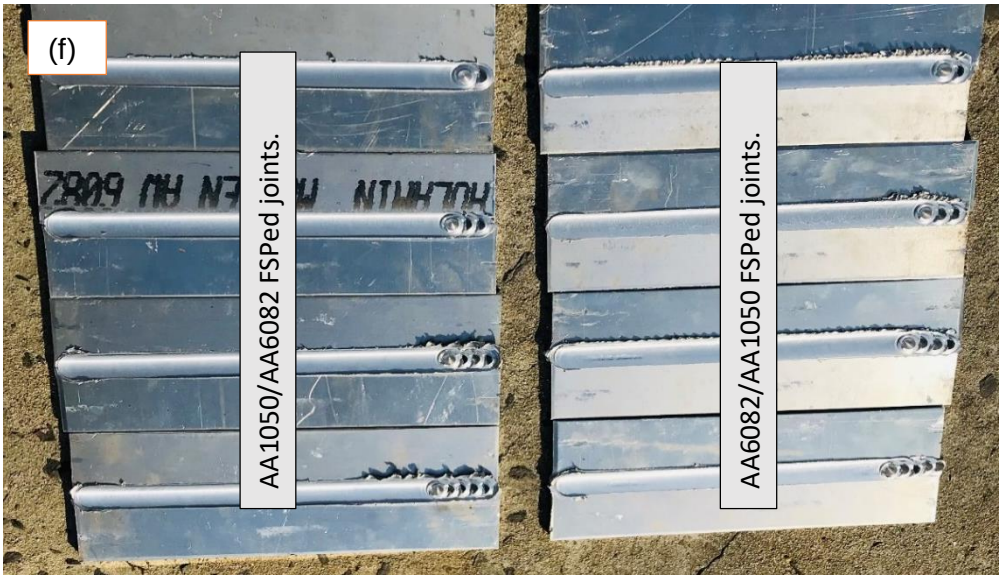

Figure 3.3: (f) Multi-pass FSPed plates.

3.4 Specimen Preparation

This section covers the preparation of the specimens.

3.4.1 Tensile Test Specimen Preparation

For the tensile specimen geometry, the ASTM-E8M-04 standard was used. The specimen in the form of a dog bone was created using AutoCAD design software. Fig 3.4.1 shows the specimen measurements in millimeters (mm).

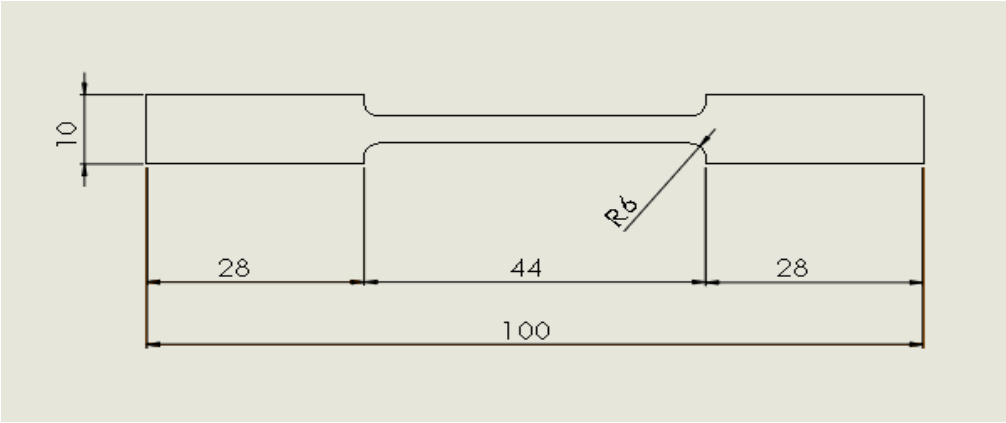

Figure 3.4.1: Tensile test specimen with overall dimensions in millimeters.

3.4.2 Microstructural/ Microhardness Test Specimen Preparation

AutoCAD design software was used to create the microstructure specimens. Fig 3.4.2 shows the specimen measurements in millimeters (mm).

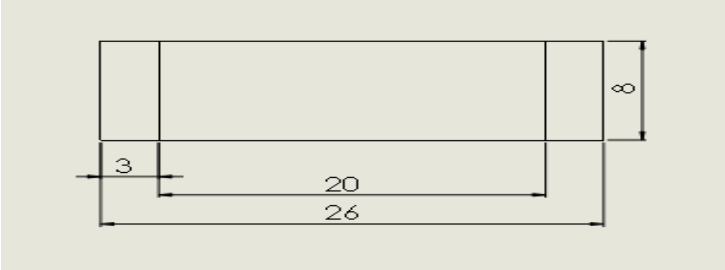

Figure 3.4.2: Microstructure and microhardness test specimen with overall dimensions millimeters.

3.4.3 Bending Test Specimen Preparation

The bending specimen design and geometry were created following the ASTM E290 standard. The bending specimen's dimensions are 20mm x 135mm x 6mm, as seen in Figure 3.4.3. The specimen measurements in millimeters (mm).

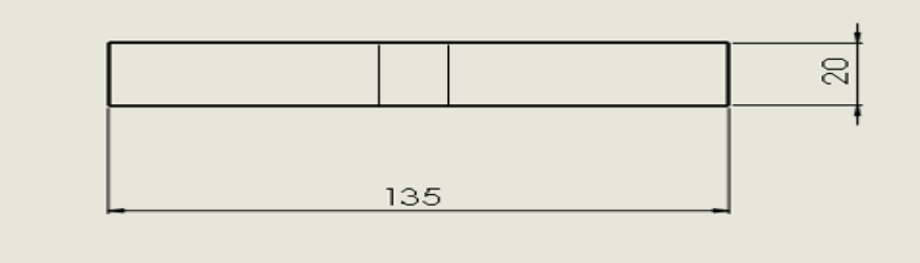

Figure 3.4.3: Bending test specimen with dimension in mm.

3.5 Cutting of plates

A waterjet cutting machine was used to cut the designed specimens. Water jet machining is a non-traditional machining technique that uses a high-velocity water jet to cut and machine soft and non-metallic materials. It is a cutting machine that uses cutting technology to cut a variety of metals. It is worth remembering that the waterjet was outsourced. The specimens were cut perpendicular to the FSPed joints. A sample of the FSPed plate after cutting is seen in Figure 3.5. The specimens were cut in a variety of locations (refer to figure 3.5). To denote the start, middle, and end of the friction stir processed joints, labels S, M, and E were used. Per the FSP pass, a total of 6 specimens were used.

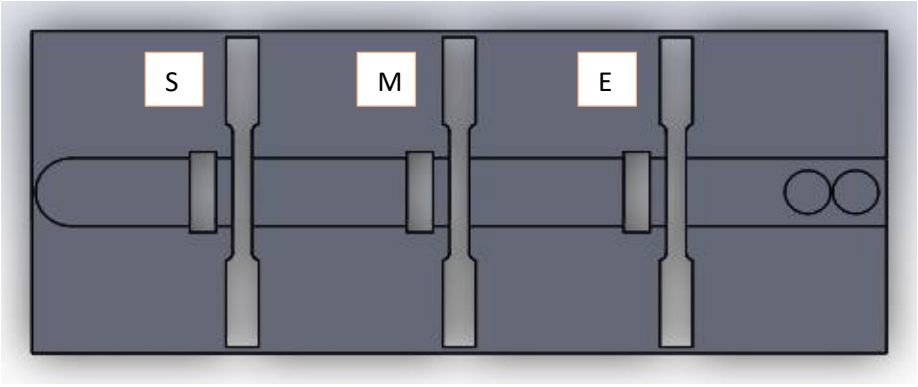

Figure 3.5: A friction stir-processed plate sample cut perpendicular to the joint.

3.6 Performance of microhardness/microstructural Specimen Preparation

The preparation of microhardness and microstructural specimens for testing is included in this section. The specimens used for hardness testing and microstructural analysis were the same size, so one specimen was used for all experiments.

3.6.1 Mounting press

Struers labopress-3 machine (see figure 3.6.1) was used to mount the cut cross-sectioned surfaces of the friction stir processed joints specimens. A Struers Labo-3 hot mounting press machine was used to encase the specimens in a cylinder with the black phenolic hot mounting resin whereby antistick stearate powder was applied to the lower and upper ram surfaces to prevent resin from sticking. Specimens were placed on the ram with the viewing surface facing down. The ram was pushed to its lowest point. The funnel was used to fill the cylinder with a suitable volume of resin of approximately 1 scoop. The upper ram was then mounted on the mounting cylinder, and the top closure was pushed down until it reaches its lower limit. Thereafter, the heating time, cooling time power, and heating temperature were set. The mounting was then operated by the set parameters until it is removed from the machine.

Figure 3.6.1: Mounting press machine

3.6.2 Polishing machine

To eliminate the surface damage caused during cutting, the mounted specimens were polished with a Struers LaboPol-5 polishing machine (shown in figure 3.6.2 (a)). The Struers LaboPol-5 polishing machine was used for grinding, lapping, and polishing microstructural and microhardness specimens with a variety of consumables. A preparation disk with the appropriate grit size was placed on the turnable during grinding, lapping, and polishing (see figure 3.6.2 (b)). Specimens were mounted on a specimen holder where running water was turned on for cooling, and the speed limit was set between 50 and 500 rpm. The specimen was polished until it is glossy. The Aka-poly used for polishing are shown in figure 3.6.2 (c)

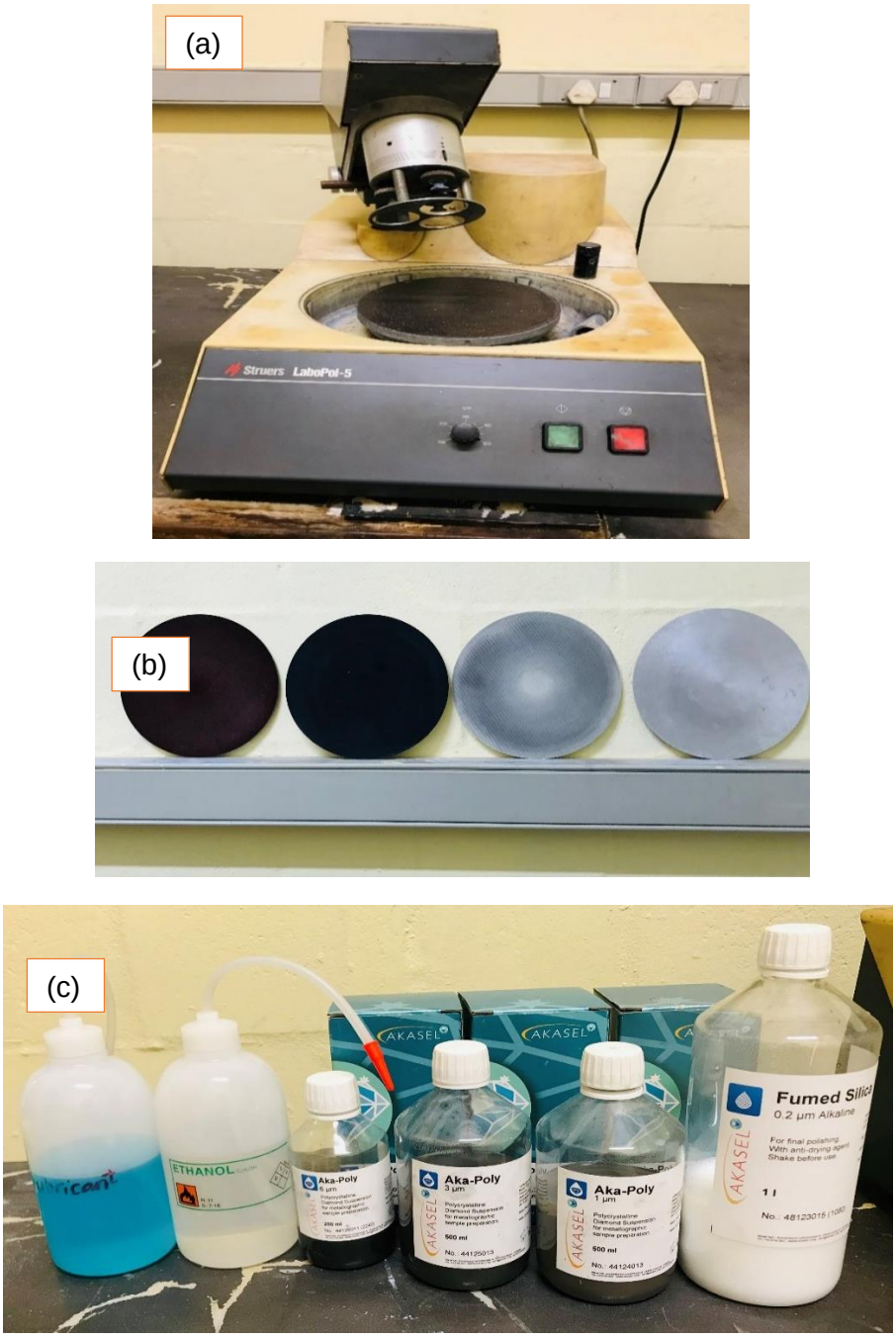

Figure 3.6.2: (a) Polishing machine, (b) Discs for polishing, (c) The Aka- poly used for polishing.

3.6.3 Etching of specimen

The specimen was prepared for etching after the cross-section surface of the friction stir treated joints were polished. Modified Keller's reagent and Weck's reagent are etchants used for microstructural analysis. The specimen were immersed for 15- 20 sec on Weck's reagent etchants and immersed for 10- 60 sec in the modified Keller's reagent etchants. The specimens were then removed from the etchants and washed with warm water, blow-dried. A hot hair dryer was used to dry from the specimen. During the etching process, it is very

important not to rub the surfaces. The solution for the modified Keller's reagent and Weck's reagent etchant are shown in table 3.6.3 (a) and table 3.6.3 (b), respectively.

Table 3.6.3: (a) Modified Keller's reagent etchant.

Solution	Quantiy
Distilled water ($\boldsymbol{H_2O}$)	87.5 ml
Hydrochloric acid ($\boldsymbol{HCl}$)	1.5 ml
Hydrofluoric acid ($\boldsymbol{HF}$)	1.0 ml
Nitric acid ($\boldsymbol{HNO_3}$)	10 ml

Table 3.6.3: (b) Weck's reagent etchant.

Solution	Quantity
Distilled water ($\boldsymbol{H_2O}$)	100 ml
Sodium hydroxide (**NaOH**)	1 g
Potassium permanganate (**$KmnO_4$**)	4 g

It should be remembered that the microhardness specimens were prepared in the same way as the microstructure specimens, with the exception that the microhardness specimens were not etched.

3.7 List of test equipment.

The list of pieces of equipment used for the testing purpose is covered in this section. For each piece of equipment, a clear description is given.

3.7.1 Hounsfield 50 K Testing Machine

The Hounsfield 50 k testing machine (see figure 3.7.1 (a)) was used to conduct tensile tests. The data obtained from this machine is used to determine material properties such as Young's modulus, tensile strength, and so on. During testing a specimen is loaded between two grips that are manually and automatically calibrated to apply force to the specimen and the force is applied to the opposite ends of the specimen until it breaks. To suit the grips, the material to be cut must be shaped into a precise shape. In most instances, the shape of a dog bone is used.

Figure 3.7.1: (a) Hounsfield 50 K testing machine (Used for Tensile test).

Bending experiments were also carried out on the Hounsfield 50 k testing machine. The data gathered by the machine is used to calculate the material's maximum stress at the time of failure of all FSPed joints. The Hounsfield testing machine with a 3-point bent fixture was used to bend the specimen during the bending test (see figure 3.7.1 (b)).

Figure 3.7.1: (b) Hounsfield 50 K testing machine (Used for the Bending test).

3.7.2 Motic AE200 Microscope

To determine the grain size of the FSPed joints, a microscope was used. A microscope is a device that magnifies objects that are too small to see through the naked eye. It creates an image that makes an object look larger. Micrographs are images of cells obtained using a microscope. The Motic AE2000 microscope (see figure 3.7.2) was used to conduct the microstructural metallographic analysis for this study.

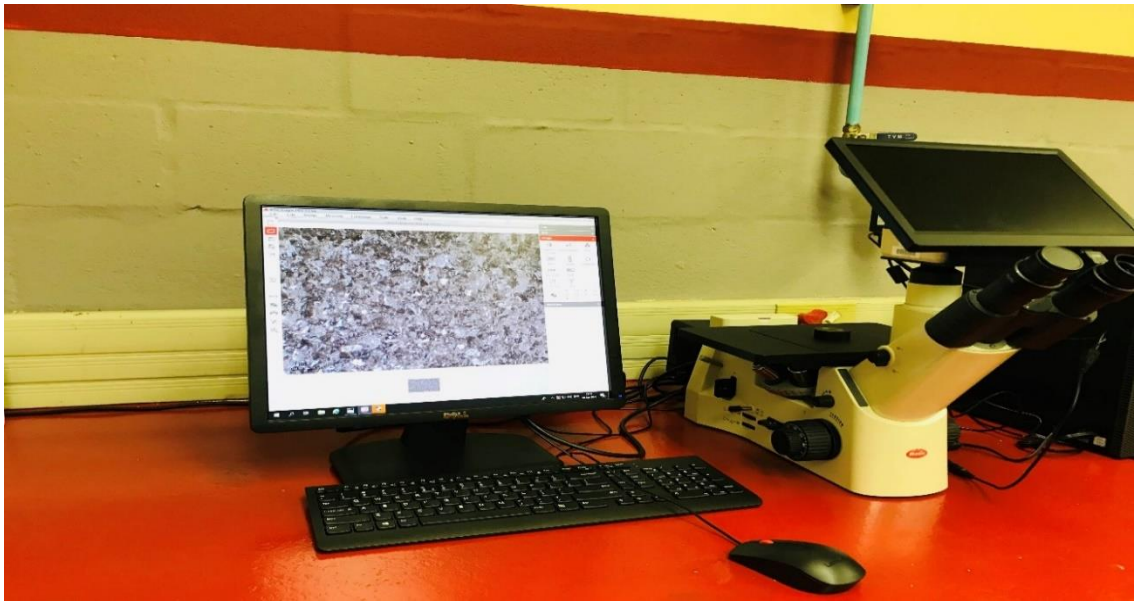

Figure 3.7.2: Motic AE200 Microscope.

3.7.3 Innova Test (Falcon 500)

The Vickers microhardness of the FSPed multi-pass joints was determined by a hardness test. The microhardness test were carried out on an Innova Test (Falcon 500) machine (see figure 3.7.3) following the ASTM E384-11 standard.

Figure 3.7.3: Innova Test (Falcon 500).

3.7.4 Scanning electron microscope (SEM)

A scanning electron microscope (SEM) is a method for examining topographies of specimens at exceptionally high magnifications. Die/package cracks and fracture surfaces, bond failures, physical detect on the die or package surface are often inspected using SEM inspection. It should be noted that (SEM) was outsourced.

3.8 Mechanical Tests

This section describes the mechanical test that were carried out. Different test analyses were conducted to compare the variations in multi-pass FSPed joints for AA1050/AA6082 joints and AA6082/AA1050 joints. Tensile testing, SEM, microhardness tests, bending tests, and microstructure tests were performed on the prepared specimens. For each pass, three specimens were tested: at the start, middle, and end of the plate.

3.8.1Tensile Test

The ultimate tensile strength, yield strength, percent elongation, strain, and Young's modulus of all multi-pass processed joints were examined. Tensile tests were conducted using a computer-operated Hounsfield 50K type of tensile testing machine, as seen in figure 3.8.1 (a). The dog bone-shaped specimens were used. Table 3.8.1 shows the tensile test parameters that were used for the FSPed joints. The ASTM-E8M-04 tensile testing standard was used in this study. The test were conducted to measure the ultimate tensile strength of all the AA1050/AA6082 FSPed joints and AA6082/AA1050 FSPed joints.

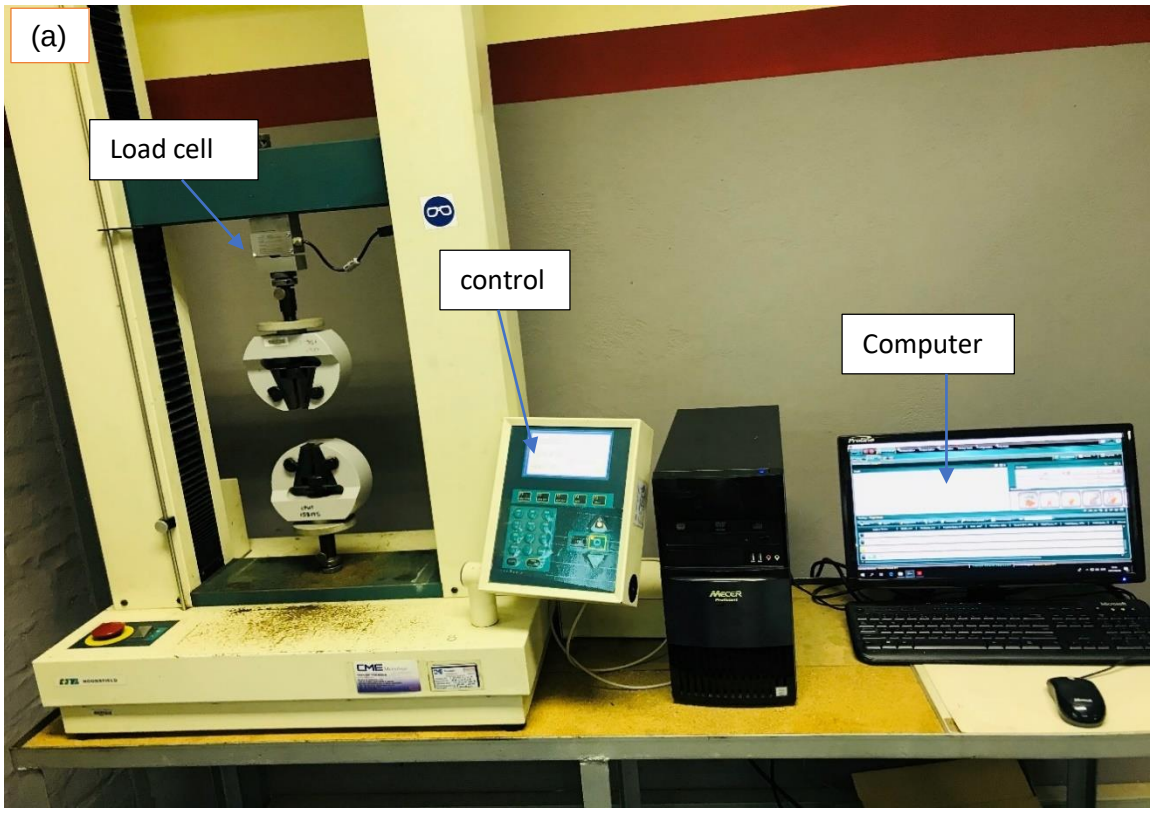

Figure 3.8.1 (a) Hounsfield 50K tensile testing machine apparatus.

Table 3.8.1: Tensile test parameters.

Speed (mm/min)	Extension range (mm)	Load range (kN)	Load cell (kN)
1	0-10	0-10	50

To conduct the test, the computer was first switched on. The measurements of the specimens (thickness and gauge length) were measured and recorded before their installation on the machine to help determine the engineering stress and engineering strain. For gripping, the specimen was placed in the grips (see figure 3.8.1 (b)). To prevent sliding during the test, the screws were tightened. The tensile test was then performed until the specimen broke (see figure 3.8.1 (c)). The experiments were carried out one by one on each specimen. The data for the test were logged using the Horizon software and exported from the computer for further analysis. The data logged included the applied tensile load (N) and position (mm), which were later used to determine stress and strain. The force versus position graph was developed as the test was being performed, see figure 3.8.1 (d) for an illustration of results obtained after running the tensile test. The percentage elongation and the yield strength were all determined. The information was logged and analyzed to provide the findings presented in the following chapter.

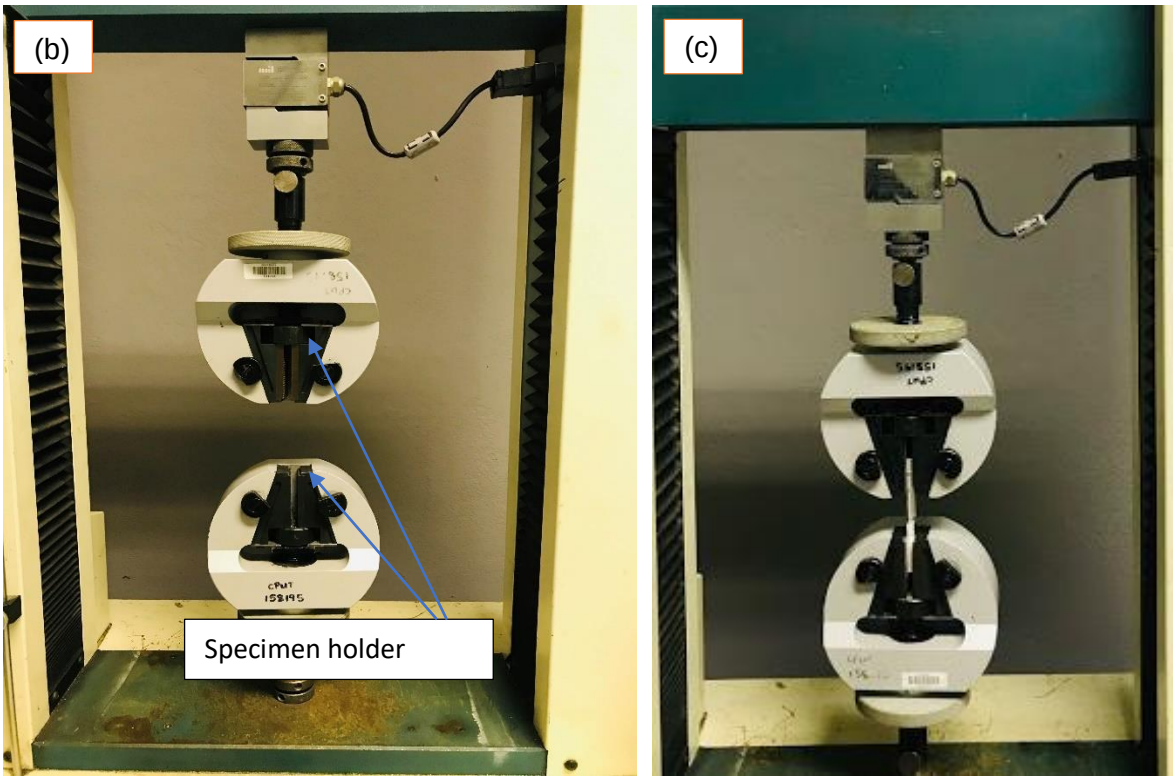

Figure 3.8.1: (b) Hounsfield 50K tensile testing grips for holding the specimen, (c) completed tensile testing on the specimen.

(d)

Cape Peninsula University of Technology

Method Name: Generic Tensile - Force vs. Position Output Name:

Width mm	Thickness mm	Area mm²	Ultimate Force N	Ultimate Stress MPa	Break Distance mm
6,00	6,00	36,0	2530	70,3	7,67

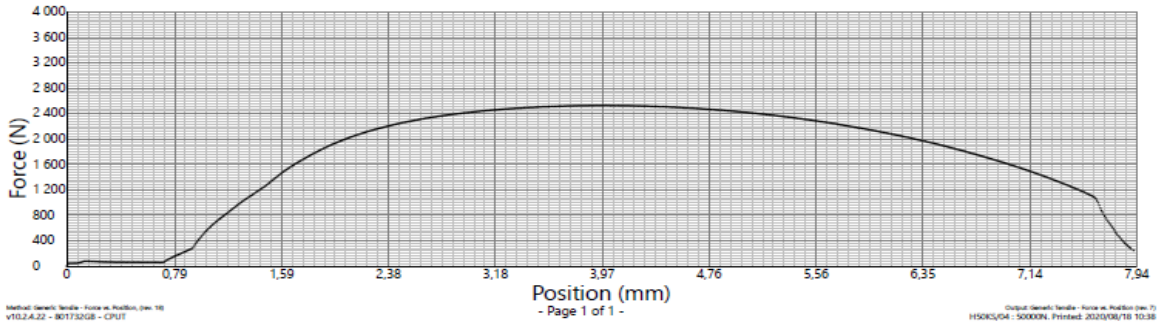

Figure 3.8.1: (d) Graph of force versus position obtained after the tensile test of a specimen.

The tensile stress is calculated using the formula below.:

$$\sigma = \frac{F}{A} \tag{1}$$

Where A is the cross-sectional area, F is the force, and σ is the tensile stress.

To calculate strain, the following equation was used:

$$\varepsilon = \frac{\Delta L}{L_o} = \frac{Final\ length - Initial\ length}{Original\ lenghth} \tag{2}$$

where ΔL is the change in length and L_o is the initial length.

To calculate percent elongation, the following equation was used:

$$\%\,E = \frac{\Delta L}{L_o} \times 100 \tag{3}$$

3.8.2 Microhardness Tests

The Innova Test (Falcon 500) was used to determine the Vickers microhardness of the FSPed joint as seen in figure 3.8.2. The test were conducted to measure the Vickers microhardness

of all the AA1050/AA6082 FSPed joints and AA6082/AA1050 FSPed joints. To carry out the hardness test, the machine was first set and put in a condition appropriate to start the testing. After initialization, the specimen were then placed on the specimen bed and focused using the objectives 10 and 20. Once the specimen was focused, a test pattern was selected. For this study, a 3-line pattern was used whereby the distance between the line is 2 mm and the distance between the points is 1mm. When the pattern setting was done, snapshots of what the specimens looked like were then taken using the inbuilt camera, whereby the captured images can also be used for microstructure. The machine automatically generated the data which was used in producing graphs that are presented in the next chapter.

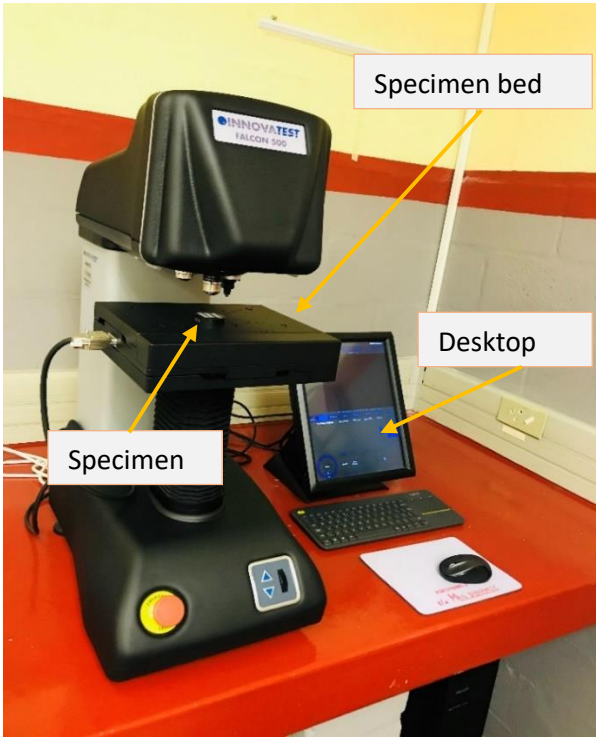

Figure 3.8.2: InnovaTest (Falcon 500) testing machine with the specimen.

3.8.3 Microstructural Tests

Microstructural analysis were performed to determine the grain size of the FSPed joints. The Motic AE2000 microscope (see figure 3.8.3) was used to conduct the microstructural metallographic analysis. The tests were conducted to determine the microstructural analysis of all the AA1050/AA6082 FSPed joints and AA6082/AA1050 FSPed joints. To conduct the test, the etched specimens were placed on the specimen bed with the FSPed joints facing up for examination to analyze the microstructure of the specimens. The software was opened, which is the Motic Image Plus and the scale setting was defined. To observe different features of the microstructure, different magnifications were used, such as 5,10,20,26,40,50, etc. The grain sizes were then determined, and images were taken after achieving an estimated focus using the built-in camera. During the process, it is very important to make sure that the stamp and the scale of the objective lens are visible for further data processing using the ImageJ software. The average grain size was calculated using the ImageJ software and the ASTM E112-12 standard was used.

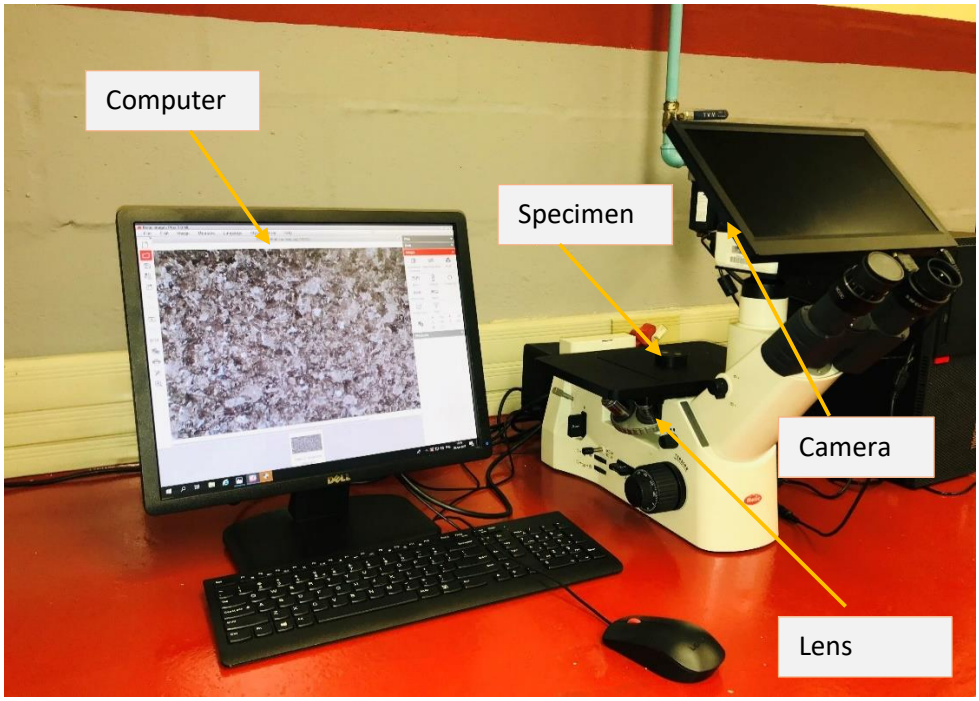

Figure 3.8.3: Microstructural apparatus.

3.8.4 Bending Test.

The bending tests which are sometimes referred to as flexural testing were carried out to assess the maximum stress of all AA1050/AA6082 FSPed joints and the maximum stress of AA6082/AA1050 FSPed joints as they broke. The Hounsfield testing machine was used to conduct bending tests on the bending specimen, as seen in figure 3.8.4 (a). The testing machine having a 3- point support features and rolling support as illustrated in figure 3.8.4 (b) The bending test parameters were identical to the tensile test parameters (see table 3.8.4 below). The data was logged in the same way as tensile test data was logged. The Porizon software was used to record the test results, which were then exported from the machine for further research.

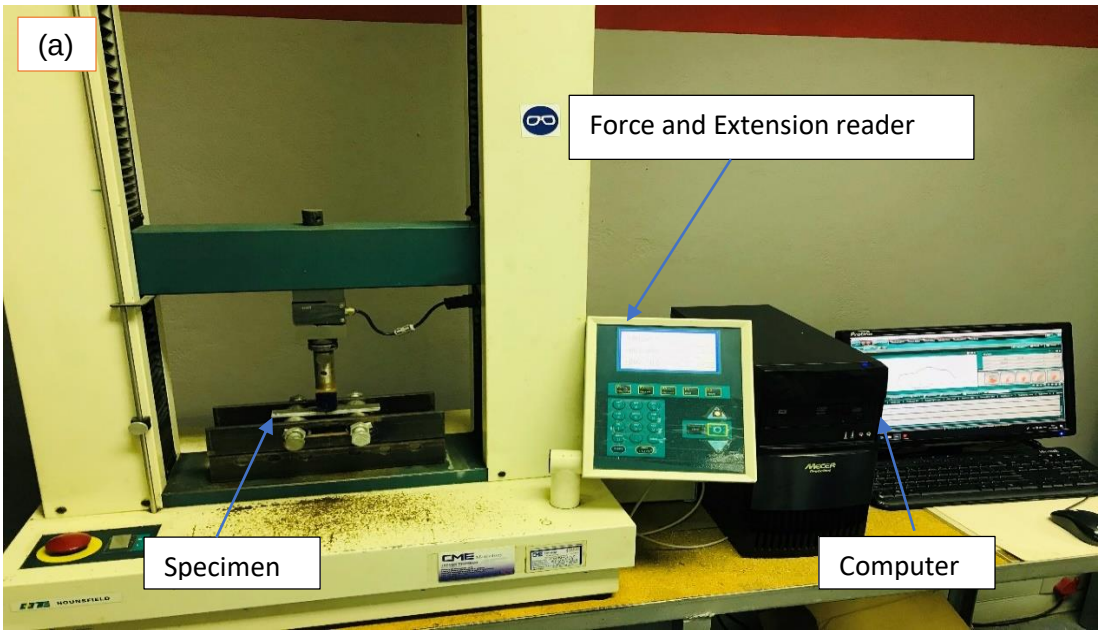

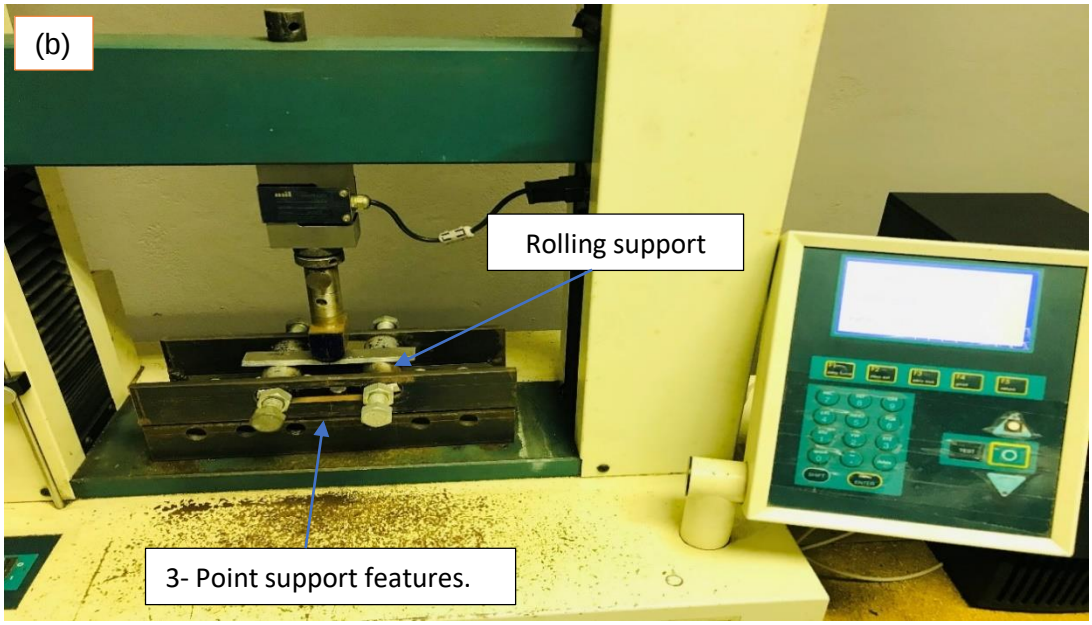

Figure 3.8.4: (a) Hounsfield 50K bending testing machine apparatus, (b) Demonstration of 3-Point support features and rolling support.

Table 3.8.4: Bending test parameters.

Speed (mm/min)	Extension range (mm)	Load range (kN)	Load cell (kN)
1	0-10	0-10	50

Before the bending test, the specimens were then cut from various positions of the processed plates. The Guillotine cutting unit was used to cut the specimens. Rectangular-shaped specimens were cut perpendicular to the processed joint. As seen in Figure 3.8.4 (c), some plates were used for the face test (the side of the plate that was processed) and others for the root test (which is underneath the welded side).

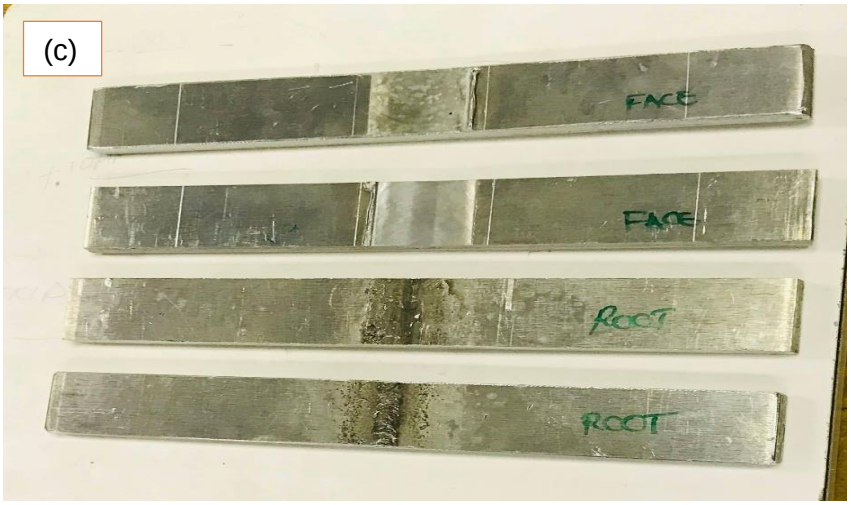

Figure 3.8.4: (c) Sample of a bending specimen.

The second step in the bending test was to measure the specimen to ensure that the dimensions were correct. For alignment with the center of the indenter, a center mark line was drawn on the center of the joint. The test were carried out one by one on each specimen. The specimen were flat mounted on the rolling supports, and then aligned with the loading pin center using the center mark line as seen in figure 3.8.4 (d). The loading pin was then lowered until it reached the top surface of the specimen. Following that, the machine was zeroed before the start of the Test. 0.5 mm extension increments were used to record the force. The data was logged from the beginning until the failure of the specimen. The results from the produced data are presented in the next chapter.

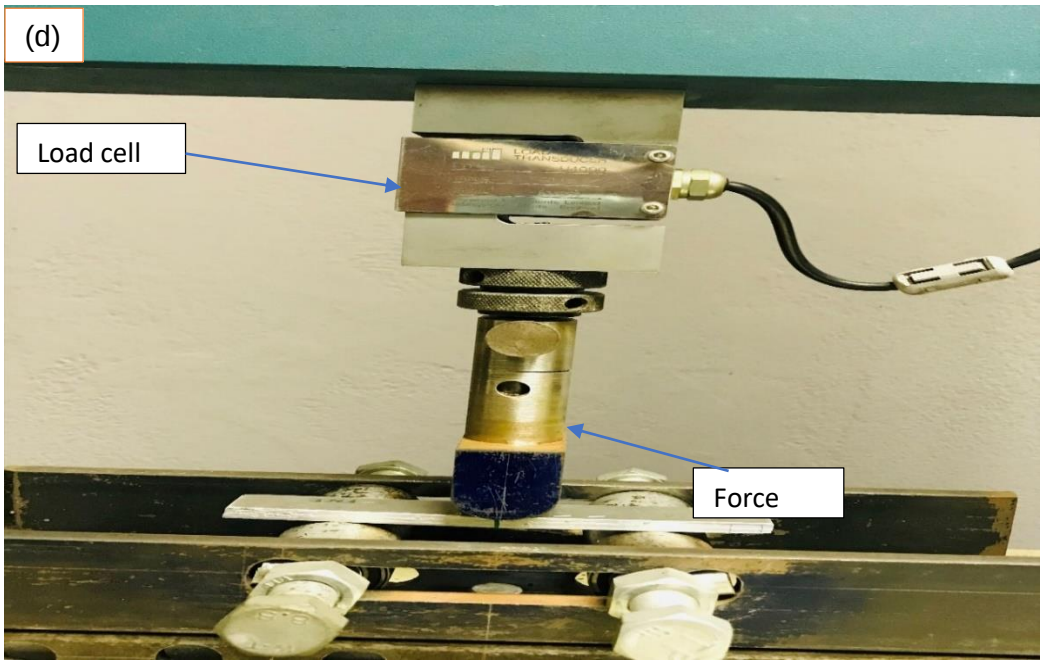

Figure 3.8.4: (d) Specimen alignment using the centerline.

The formulas used to determine the flexural strength was:

$$\sigma_F = \frac{3FL}{2bd^2} \quad (4)$$

where F is the force, b is the width of the specimen, L is the length, and d is the thickness.

The formulas used to determine the flexural strain was:

$$\varepsilon_F = \frac{\Delta L}{L_o} \quad (5)$$

where ΔL is the change in length and L_o is the initial length.

3.8.5 Scanning electron microscope (SEM) analysis technique

The post-tensile test cut-off specimen were used for the SEM tests. The fractured surfaces from the post-tensile test were cut to compatible size for the SEM machine. Fractured surfaces were then examined to learn more about the nature of the fracture. The following is the general SEM procedure: The samples are held in place by a sample holder, which must be electrically connected to prevent the electron beam from "charging" the sample and distorting the image. A double-sided conductive tape is used to achieve this. To produce an image and examine the specimen, a focused beam is scanned over across the specimen. In the following sections, the findings of all the tests performed are discussed.

CHAPTER FOUR
RESULTS AND DISCUSSIONS

This chapter explains into details of the results collected from the numerous tests conducted in Chapter 3. Macrostructure, microstructure, tensile testing, hardness testing, bending testing, and scanning electron microscopy (SEM) data were all obtained.

4.1 Macrostructure Tests

4.1.1 AA1050/AA6082 FSPed joints results

The friction stir processed FSWed joints AA1050/AA6082 macrographs are shown in Figure 4.1.1 (a)-(l) with AA1050 on the advancing side. Figure 4.1.1 (a) - (c) depicts the macrostructure of a single pass FSPed joint from the beginning to end of the specimen. The macrostructure for the two-pass FSPed joint is shown in Figure 4.1.1 (d)–(f) from start to the end of specimen Figure 4.1.1 (g) - (i) depicts the macrostructure of a three-pass FSPed joint from start to end of the specimen. The macrostructure for the four-pass FSPed joint is shown in Figure 4.1.1 (j)–(l) from the beginning to the end of the specimen.

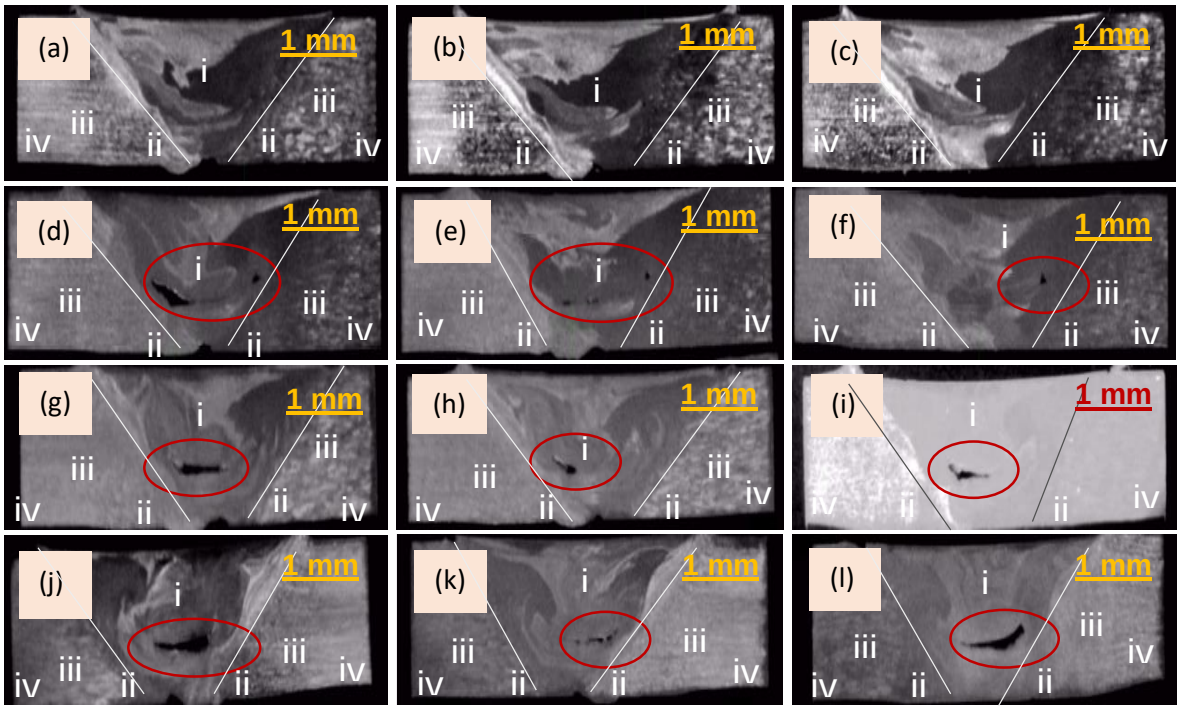

Figure 4.1.1: Macrostructure (macrographs), (AA1050-AA6082); 1P FSPed (a) S, (b) M, (c) E; 2P FSPed (d) S, (e) M, (f) E; 3P FSPed (g) S, (h) M, (i) E; 4P FSPed (j) S, (k) M and (l) E.

The macrographs displayed in Figure 4.1.1 revealed the four distinct microstrure zones namely stir zone, which is the dynamic recrystallization zone, thermo-mechanically affected zone (TMAZ) on both sides of the stir zone, heat affected zone (HAZ), and non-affected base metal (BM) of AA1050 and AA6082 are among the zones. The SZ is represented by i, the TMAZ on both sides of the stir zone are represented by ii, the HAZ on the advancing side also for the retreating side is represented with iii. The AA1050 and AA6082 non-affected BM are

presented with iv. The ring pattern in SZ areas is seen in the multi-pass FSPed joints of the FSWed 1050/6082 in Figure 4.1.1 (a) –(l). The patterns such as onion rings are observed which are caused by materials flowing during the FSW/ FSP process [140]. Dynamic recrystallization happens in the SZ area, where the crystallization process switches from homogeneous to nonhomogeneous due to unexpected crystallization of sediments on dislocations [141,142]. On the surface of the FSPed joints shown in Figure 4.1.1 (a) -(c), there are no defects such as voids or cracks, as may be seen. The presence of a tunnel defect (void nugget) is shown in Figure 4.1.1 (d)-(l) by means of oval. Insufficient material flow, which is caused by insufficient heat input, is usually blamed for tunnel flaws [143], [144], [145], [146]. The remaining macrographs revealed structures with no onion rings with no flaws, indicating that the joint received appropriate heat input, resulting in adequate material flow [147], [148], [149].

4.1.2 AA6082/AA1050 FSPed joints results

The macrographs for the friction stir processed FSWed joints AA6082/AA1050 are shown in in Fig. 4.1.2 (a)-(l) with AA6082 on the advancing side. Figure 4.1.2 (a) - (c) depicts the macrostructure of a single pass FSPed joint from start to end of the specimen. The macrostructure for the two-pass FSPed joint is shown in Figure 4.1.2 (d)–(f) from start to the end of specimen Figure 4.1.2 (g) - (i) depicts the macrostructure of a three-pass FSPed joint from start to end of the specimen. The macrostructure for the four-pass FSPed joint is shown in Figure 4.1.2 (j)–(l) from start to end of the specimen.

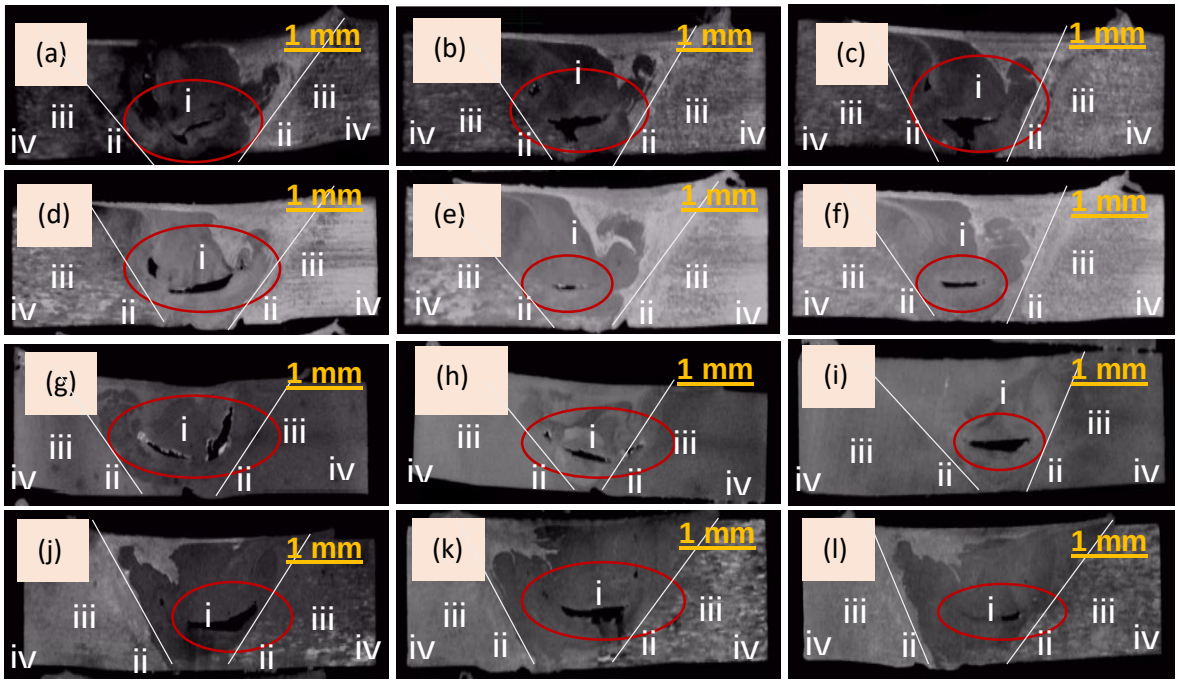

Figure 4.1.2: Macrodtructure (macrographs), (AA6082/AA1050); 1P FSPed (a) S (b) M, (c) E; 2P FSPed (d) S, (e) M, (f) E; 3P FSPed (g) S, (h) M, (i) E; 4P FSPed (j) S, (k) M and (l) E.

The macrostructures of 6082/1050 showed the SZ, HAZ, TMAZ, and non-affected BM of AA6082 and AA1050 on the FSPed cross-section of the multi-pass processed joints, as shown in Figure 4.1.2. The SZ is represented by i, the TMAZ on both sides of the stir zone are represented by ii, the HAZ on the advancing side also for the retreating side is represented with iii. The AA1050 and AA6082 non-affected BM are presented with iv. The stir zone appears

as a ring structure, similar to onion rings,as a result of the multi-pass FSP process, as depicted in Figure 4.1.2 (a) – (l) [150]. Figure 4.1.2 (a) – (l) illustrates the ring pattern in the SZ areas of the FSWed 6082/1050 joints during the FSP procedure. Materials flowing during the FSW/ FSP process cause onion patterns like onion rings [140,150]. The existence of tunnel defect (void nugget) is seen as shown by means of ovals in Figure 4.1.2 (a)- (l). The reason for these faults is unknown; however, the heat input caused by placing stronger material on the advancing side is assumed to be the cause [10, 151,152]. According to Dialami et al. [153], improper bonding, inter-material flow, and weld defects such as cavities, voids, flash, and wormhole are caused by irregular flow and undesired heat input, which can be either excessive or inadequate.

4.2 Microstructure analysis Tests

4.2.1 AA1050/AA6082 FSPed joints results

Figure 4.2.1 (a) - (n) shows the SZ microstructure of the AA1050 BM, AA6082 BM 1P1050/6082, 2P1050/6082, 3P1050/ 6082, and 4P1050/ 6082. Figure 4.2.1 (a) shows a micrograph of the 1050 base material, figure 4.2.1 (b) shows a micrograph of the 6082 base materials whereas figure 4.2.1 (c), (d), and (e) show SZ micrographs of sampled specimens sampled from the beginning (S), middle (M), and finish (E) of the 1P1050/6082 joint. The microstructure of sampled specimens at the be S, M, and E of the 2P1050/6082 is shown in Figure 4.2.1 (f), (g), and (h). Figure 4.2.1 (i), (j), and (k) illustrate the microstructure of sampled specimens from the S, M, and E of the 3P1050/ 6082. The microstructure of specimens taken at the S, M, and E of the 4P1050/ 6082 is shown in Figure 4.2.1 (l), (m), and (n). Table 4.2.1 lists the mean grain sizes, standard deviations, minimum and maximum grain sizes for the base materials surfaces are shown in Figure 4.2.1 (a) and (b), as well as the multi-pass 1050/ 6082 FSPed joints surfaces shown in Figure 4.2.1 (c) – (n).

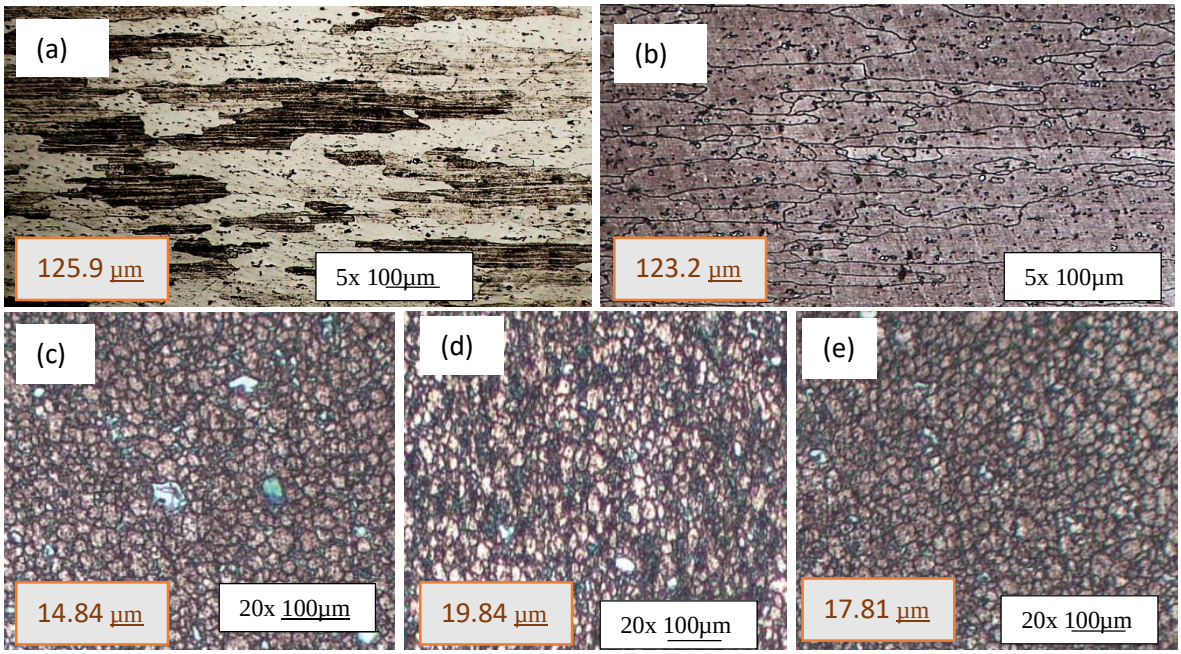

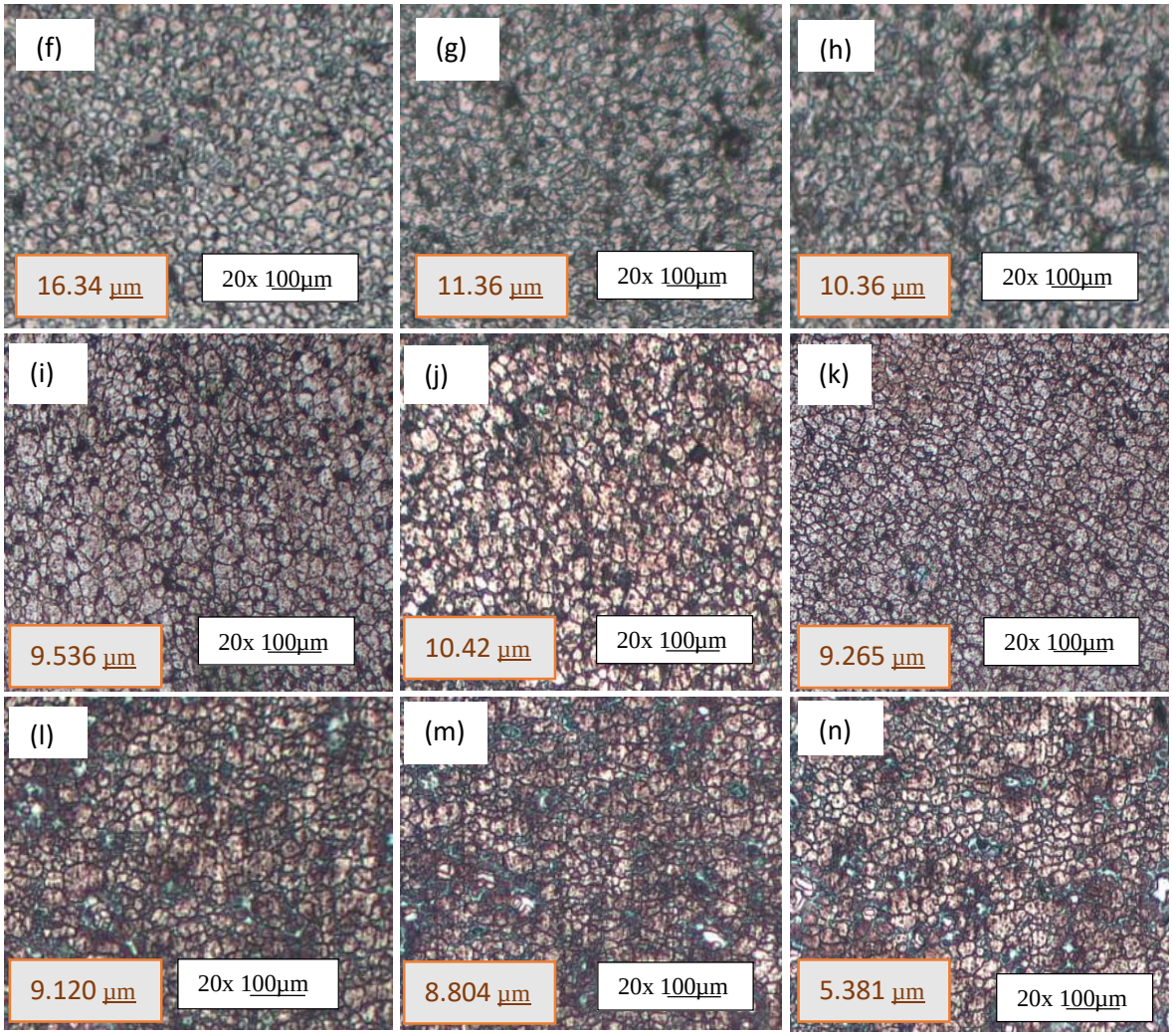

Figure 4.2.1: Micrographs; Base material (a) AA1050-H14;(b) AA6082-T651, 1050/6082 FSPed; 1P (b) S, (c) M, (d) E; 2P (e) S, (f) M, (g) E; 3P (h) S, (i) M, (j) E; 4P (k) S, (l) M and (m) E.

The minimums for 1P1050/6082 ranged from 7.499 to 11.32 µm, for 2P1050/6082 from 8.250 to 9.803 µm, for 3P1050/6082 from 6.510 to 8.100 µm, and for 4P1050/6082 from 2.56 to 6.250 µm. The maximum values for 1P1050/6082 ranged from 22.91 to 28.28 µm, for 2P1050/6082 from 20.20 to 21.88 µm, for 3P1050/6082 from 14.67 to 18.00 µm, and for 4P1050/6082 from 9.874 to 13.81 µm. The mean grain size of the 1P1050/6082 joint varied between 14.84 and 19.84 µm. The mean grain size for the 2P1050/6082 joint varied from 10.36 to 16.34 µm. The average grain size of the 3P1050/6082 joint varied from 9.265–10.42 µm. The mean grain size for the 4P1050/6082 joint varied from 5.381 to 9.120 µm. For 1P- 4P FSPed 1050/6082, the standard deviation ranged from 1.599 to 3.419 µm. The computed mean grain size for the processed joint was particularly close to the individual grain size found at the measured joints due to the low standard deviation. As the number of FSP passes increased, grain sizes were demonstrated to decrease. Grain size refinement was caused by the recrystallization and re-recrystallization that happened as the number of FSP passes increased experienced by the joint subjected to multi-pass FSP [15,95,154]. Furthermore, the extreme heat generated during processing contributes significantly to equiaxed grain sizes and homogeneity [19,99,155].

Table 4.2.1: Microstructure grain sizes analysis results for AA1050/AA6082.

	Mean Values (μm)	Standard deviation	Minimum	Maximum
Base Material				
AA1050-H14	125.9	16.53	94.43	160.5
AA6082-T651	123.2	22.94	77.25	184.8
1 Pass AA1050/AA6082				
S	14.84	3.419	7.499	22.98
M	19.84	3.225	11.32	28.28
E	17.81	3.179	10.98	22.91
2 Pass AA1050/AA6082				
S	16.34	3.038	9.803	21.88
M	13.36	2.903	8.727	20.39
E	10.36	2.749	8.250	20.20
3 Pass AA1050/AA6082				
S	9.536	2.578	8.100	18.00
M	10.42	2.344	7.452	16.91
E	9.265	2.301	6.510	14.67
4 Pass AA1050/AA6082				
S	9.120	2.245	6.250	13.80
M	8.804	1.971	6.250	13.75
E	5.381	1.599	2.560	9.874

4.2.2 AA6082/AA1050 FSPed joints results

Figure 4.2.2 (a) - (l) shows SZ microstructure of the 1P6082/ 1050, 2P6082/1050, 3P6082/1050, and 4P6082/1050. Figure 4 (a), (b), and (c) show SZ micrographs of specimens sampled from the beginning (S), middle (M), and end (E) of the 1P6082/1050 joint. The microstructure of specimens sampled at the S, M, and E of the 2P6082/1050 is shown in Figure 4.2.2 (d), (e), and (f). Figure 4.2.2 (g), (h), and (i) illustrate the microstructure of specimens sampled from the S, M, and E of the 3P6082/1050. The microstructure of specimens taken at the S, M, and E of the 4P6082/1050 is shown in Figure 4.2.2 (j), (k), and (l). Table 4.2.2 lists the mean grain sizes, standard deviations, minimum and maximum grain sizes for the the multi-pass 6082/1050 FSPed joints surfaces shown in Figure 4.2.2 (a) – (l).

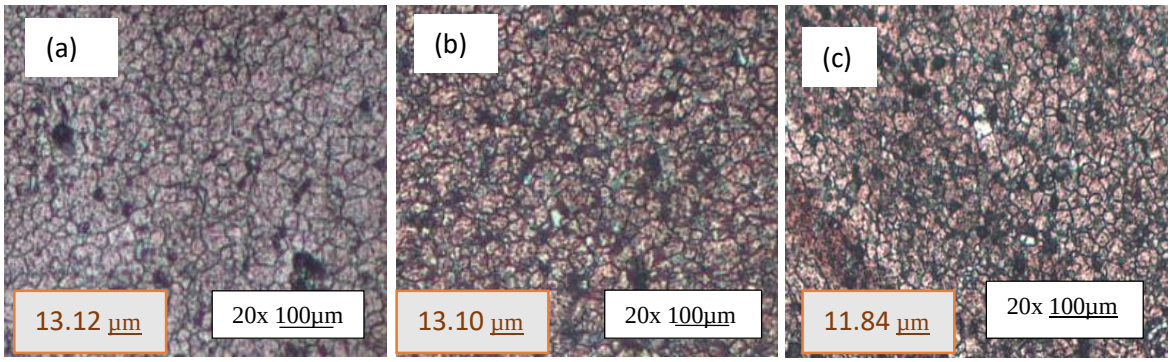

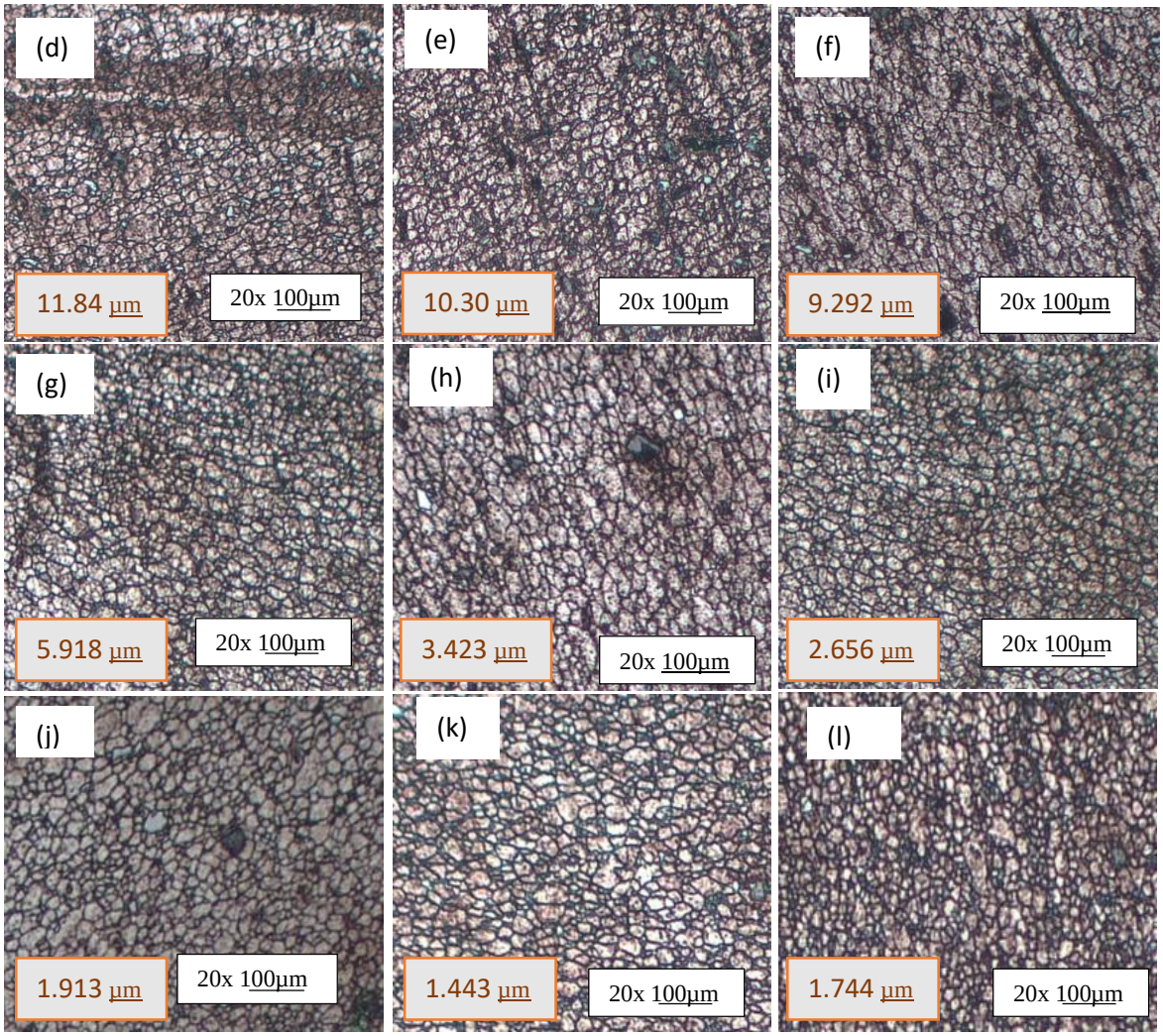

Figure 4.2.2: Micrograph; Base material (a) AA6082-T651; (b) AA1050-H14,6082/1050 FSPed; 1P (c) S, (d) M, (e) E; 2P (f) S, (g) M, (h) E; 3P (i) S, (j) M, (k) E; 4P (l) S, (m) M and (n) E.

The minimum values for 1P6082/1050 ranged from 7.476 – 8.534 µm, 7.803 – 6.250 µm for 2P6082/1050, 3.000 –1.839 µm for 3P6082/1050, and 1.913 –1.274 µm for 4P6082/1050. The maximum values ranged from 17.24 -17.44 µm for 1P6082/1050, 12.87 -16.58 µm for 2P6082/1050, 3.267 – 7.433 µm for 3P6082/1050, and 2.297 -2.479 µm for 4P6082/1050. The mean grain size of the 1P6082/1050 joint varied between 11.84 and 13.12 µm. The mean grain size varied from 9.292 µm to 11.34 µm for the 2P6082/1050 joint. The 3P6082/1050 joint has a mean grain size range of 2.656 µm to 5.198 µm. The mean grain size for the 4P6082/1050 joint varied from 1.744 µm to 1.193 µm. For 1P- 4P FSPed 6082/1050, the standard deviation ranged from 0.320 to 2.300 µm. As the number of passes was increased, the computed mean grain size for the processed joint reduced, as did the standard deviations. It was also discovered that repeating the FSP process and increasing the proper nucleation sites resulted in more grains being formed and the room for grain development becoming constrained, resulting in smaller grain sizes as the number of FSP passes increased [156]. The joint subjected to multi-pass FSP experienced repeated dynamic recrystallization, resulting in a reduction in grain size as the number of FSP passes increased [19, 69,99,155] The high temperature and deformation rate induced by pin stirring action create this behavior [151, 157].

Table 4.2.2: Microstructure grain sizes analysis for AA6082/AA1050

	Mean Values (µm)	Standard deviation	Minimum	Maximum
1 Pass AA6082/AA1050				
S	13.12	2.300	7.476	17.44
M	13.10	2.118	8.537	17.44
E	11.84	1.902	8.534	17.24
2 Pass AA6082/AA1050				
S	11.34	1.689	7.803	16.58
M	10.30	1.656	6.727	13.45
E	9.292	1.510	6.250	12.87
3 Pass AA6082/AA1050				
S	5.198	0.989	3.000	7.433
M	3.423	0.725	2.020	4.765
E	2.656	0.691	1.839	3.267
4 Pass AA6082/AA1050				
S	1.913	0.351	1.913	2.479
M	1.443	0.335	1.235	2.469
E	1.744	0,320	1.274	2.297

4.2.3 Comparative between the multi-pass FSP AA1050/AA6082 and AA6082/AA1050 FSPed joints results.

The AA1050 BM had a mean value of 125.9 µm, whereas the AA6082 BM had a mean value of 123.2 µm, as shown in tables 4.2.1 and 4.2.2. The standard deviation of the AA1050 base material was 16.43, whereas the standard deviation of the AA6082 base material was 22.94. The minimum and maximum values found for the AA1050 base material are 99.43 and 160.5, respectively. For the AA6082 base material, the minimum and maximum results were 75.25 and 184.8, respectively. It's worth noting that when the passes number were increased, the mean grain sizes decreased. Grain size refinement occurred as a result of recrystallization and re-recrystallization when the number of FSP passes increased [19,155]. Increased FSP passes on the 1050/6082 and 6082/1050 surfaces resulted in equiaxed grains with high angle grain boundaries as a result of dynamic recrystallization in the stir zone, which accords with El-Rayes and El-Danaf [69].

4.3 Tensile Tests

The findings from the tensile testing machine are shown in this section. The related specimens' tensile stress (UTS) and % elongation were calculated using the data acquired in this section, and the related calculations are presented in Appendix F.

4.3.1 AA1050/AA6082 FSPed joints tensile test results

Figure 4.3.1 (a) - (d) shows fractured specimens for the multi-pass FSPed joints post tensile

testing. Figure 4.3.1 (a) depicts the post-tensile specimen for a 1P1050/6082 FSPed joint, 4.3.1 (b) depicts the post-tensile specimen for a 2P1050/6082 FSPed joint, 4.3.1 (c) depicts the post-tensile specimen for a 3P1050/6082 FSPed joint, and 4.3.1 (d) depicts the post-tensile specimen for a 4P1050/6082 FSPed joint. The fracture position varies with the specimens, as shown in the post-tensile specimens. Table 4.3.1 displays the failure positions for all multi-pass FSPed joints. It was revealed that no matter how many FSP passes were performed, all specimens continuously failed outside the joint. The heat-affected zone is where the fracture occurs. Because of the grain coarsening that is usually linked with this region, HAZ is known to be the weakest of the regions identified in the FSP joint [158-160].

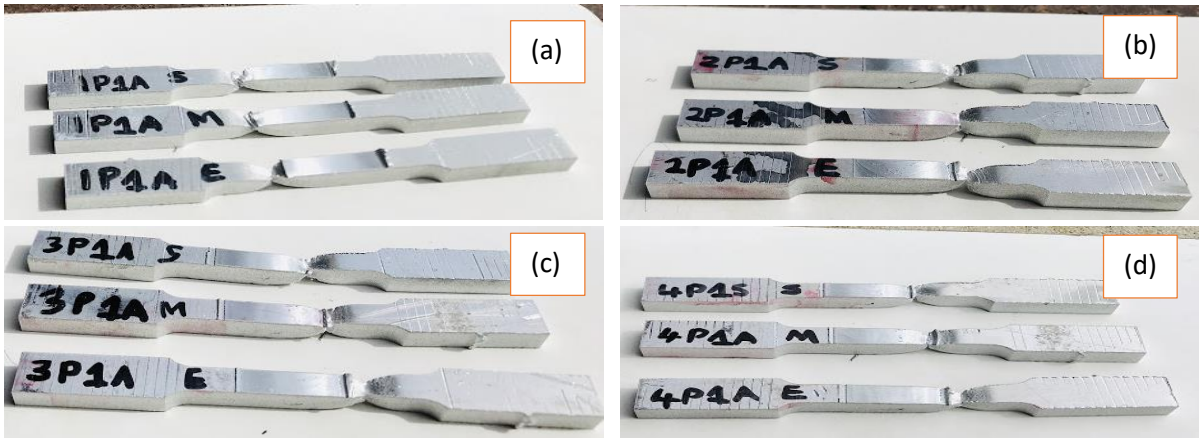

Figure 4.3.1: Post tensile specimens (FSPed); (a) 1P1050/6082; (b) 2P1050/6082 (c) 3P1050/6082 and (d) 4P1050/6082.

The stress-strain curves for each specimen are presented in Figure 4.3.1 (e)-(h), and their relative tensile properties are included in Table 4.3.1. Figure 4.3.1 (e) shows the stress-strain curve for the 1P1050/6082, figure 4.3.1 (f) shows the stress-stain curve for the 2P1050/6082, figure 4.3.1 (g) shows the stress-strain curve for the 3P1050/6082, and figure 4.3.1 (h) shows the stress-stain curve for the 4P1050/6082. Table 4.3.2 contains the base material properties for AA1050-H14.

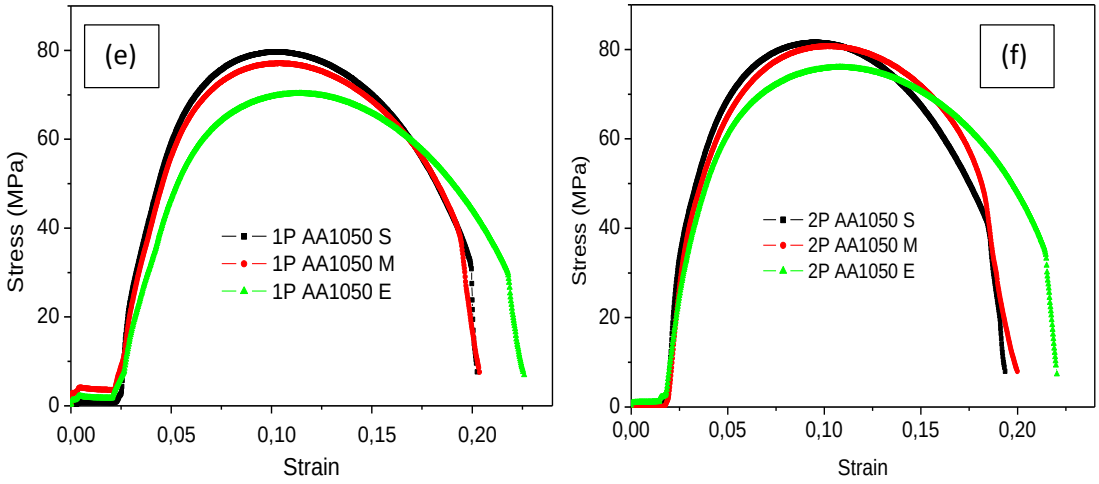

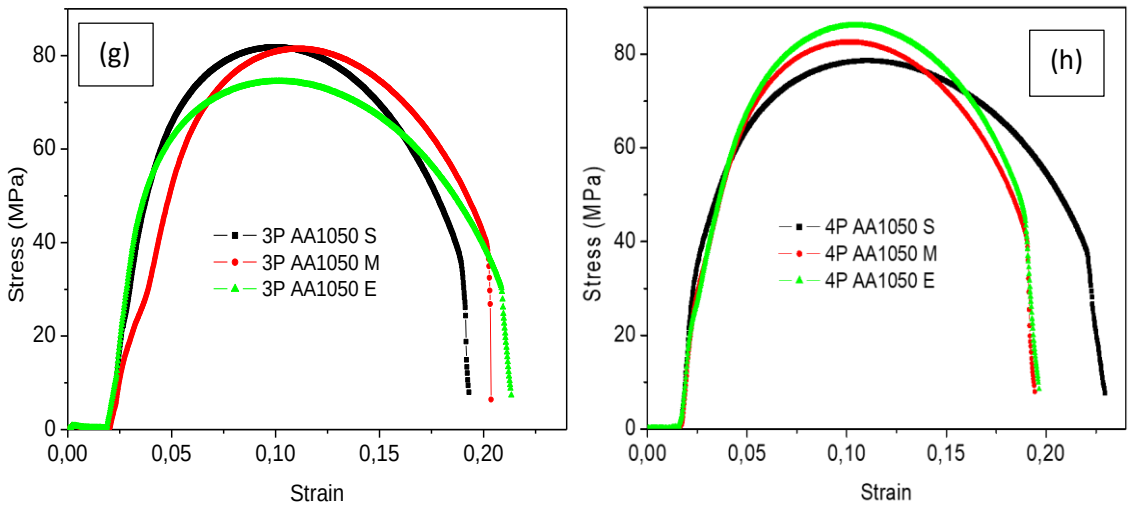

Figure 4.3.1: Stress Strain curves; (FSPed) (e) 1P1050/6082; (f) 2P1050/6082; (g) 3P1050/6082 and (h) 4P1050/6082.

The 1P1050/6082 joint yielded the highest ultimate tensile strength (UTS) of 79.7 MPa at the joint's S on the sampled specimen with a percentage elongation of 19.99 percent. The maximum UTS for the 1P joint was 75.9% when compared to the AA1050 BM and 28.5% when compared to the AA6082 BM. For the 2P1050/6082 joint, the highest UTS of 81.6 MPa was achieved from a specimen sampled at the joint's S with a percentage elongation of 18.65 percent. The maximum UTS for the 2P joint was 77.7% when compared to the AA1050 BM and 29.1% when compared to the AA6082 BM. For the 3P1050/6082 joint, the maximum UTS of 81.8 MPa was achieved from a specimen sampled at the joint's S with a percentage elongation of 18.97 percent. The maximum UTS for the 3P joint was 77.9% when compared to the AA1050 BM and 29.2% when compared to the AA6082 BM. For the 4P1050/6082 joint, the highest UTS of 86.1 MPa was achieved from a specimen sampled at the joint's E with a percentage elongation of 18.97 percent. The highest UTS for the 4P joint was 82 % when compared to the AA1050 BM and 30.75 % when compared to the AA6082 BM. In comparison to both base materials, the percentage elongation of the 1P – 4P joint was greater than 100%. The ultimate tensile strength (UTS) of the 1P, 2P, and 3P FSPed joints was found to be decreasing from the beginning to the end of the joint, accompanied by an increase in the percentage elongation from the beginning to the end. The variation in grain size discovered during microstructural analysis is to blame for the reduction in UTS along the 1Pass, 2Pass, and 3Pass 1050/6082 FSPed joints [52,60]. The UTS of the 4Pass 1050/6082 FSPed joints was found to increase from the beginning to the end of the joint, whereas the percentage elongation decreased from the S to the E. The reduction in grain size at the 4P FSPed 1050/6082 junction is responsible for this phenomenon [10,161].

Table 4.3.1: Tensile test results

Joint type & sampling position	**Ultimate Tensile Stress (MPa)**	**Percentage elongation (%)**	**Fracture Position**
AA1050			
The base material	105	6	
1P Joint			

S	79.7	19.97	HAZ
M	77.1	19.65	HAZ
E	70.3	21.88	HAZ
2P Joint			
S	81.6	18.65	HAZ
M	80.7	19.99	HAZ
E	76.0	21.48	HAZ
3P Joint			
S	81.8	18.97	HAZ
M	81.5	20.22	HAZ
E	74.5	20.88	HAZ
4P Joint			
S	78.6	22.22	HAZ
M	82.6	19.05	HAZ
E	86.1	18.97	HAZ

4.3.2 AA6082/AA1050 FSPed joints results

Figure 4.3.2 (a) - (d) shows fractured specimens for the multi-pass FSPed joints post tensile testing. Figure 4.3.2 (a) depicts the post-tensile specimen for a 1P6082/1050 FSPed joint, 4.3.2 (b) depicts the post-tensile specimen for a 2P6082/1050 FSPed joint, 4.3.2 (c) depicts the post-tensile specimen for a 3P6082/1050 FSPed joint, and 4.3.2 (d) depicts the post-tensile specimen for a 4P6082/1050 FSPed joint. The fracture position varies with the specimens, as shown in the post-tensile specimen. Table 4.3.2 lists all of the failure positions for all of the multi-pass FSPed joints. The location of failure varied by specimen for the 6082/1050FSPed joints; unlike the 1050/6082 FSPed joints, failure did not occur solely outside the joint. Some of the specimens failed on the weaker material's outside of the joint. The same behavior was found in [159,162,163]. This trend indicates that a stronger material, in our instance the AA6082 alloy, controlled the joint. Some specimens failed at the joint's center. Inadequate heat production was the cause of the behavior [143], [144].

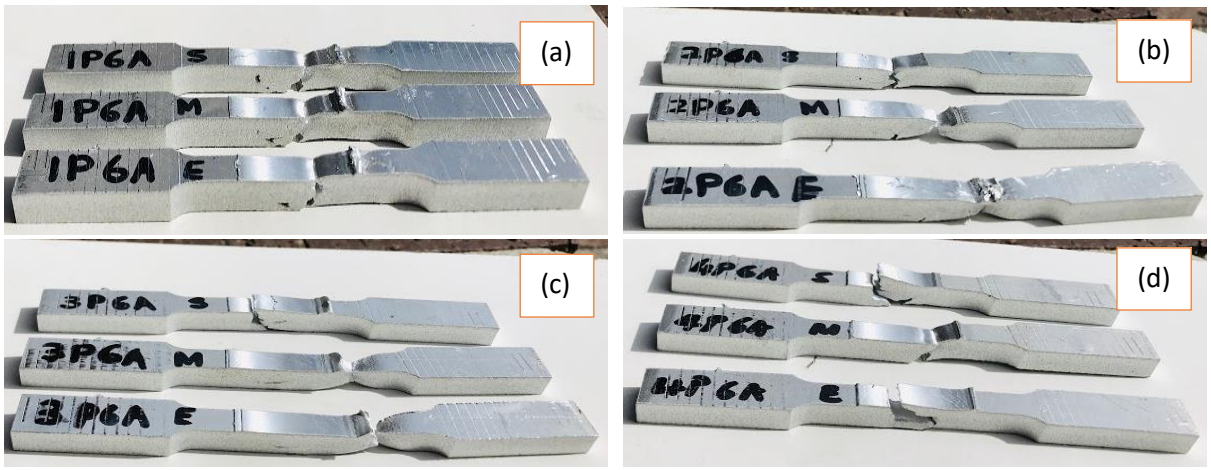

Figure 4.3.2: Post tensile specimens (FSPed); (a) 1P6082/ AA1050; (b) 2P6082/1050 (c) 3P6082/1050 and (d) 4P6082/1050.

The stress-strain curves for each specimen are presented in Figure 4.3.2 (e)-(h), and their relative tensile properties are included in Table 4.3.2. Figure 4.3.2 (e) shows the stress-strain curve for the 1P6082/1050, figure 4.3.2 (f) shows the stress-stain curve for the 2P6082/1050, figure 4.3.2 (g) shows the stress-strain curve for the 3P6082/1050, and figure 4.3.2 (h) shows the stress-stain curve for the 4P6082/1050. Table 4.3.2 contains the base material properties for AA6082-T651.

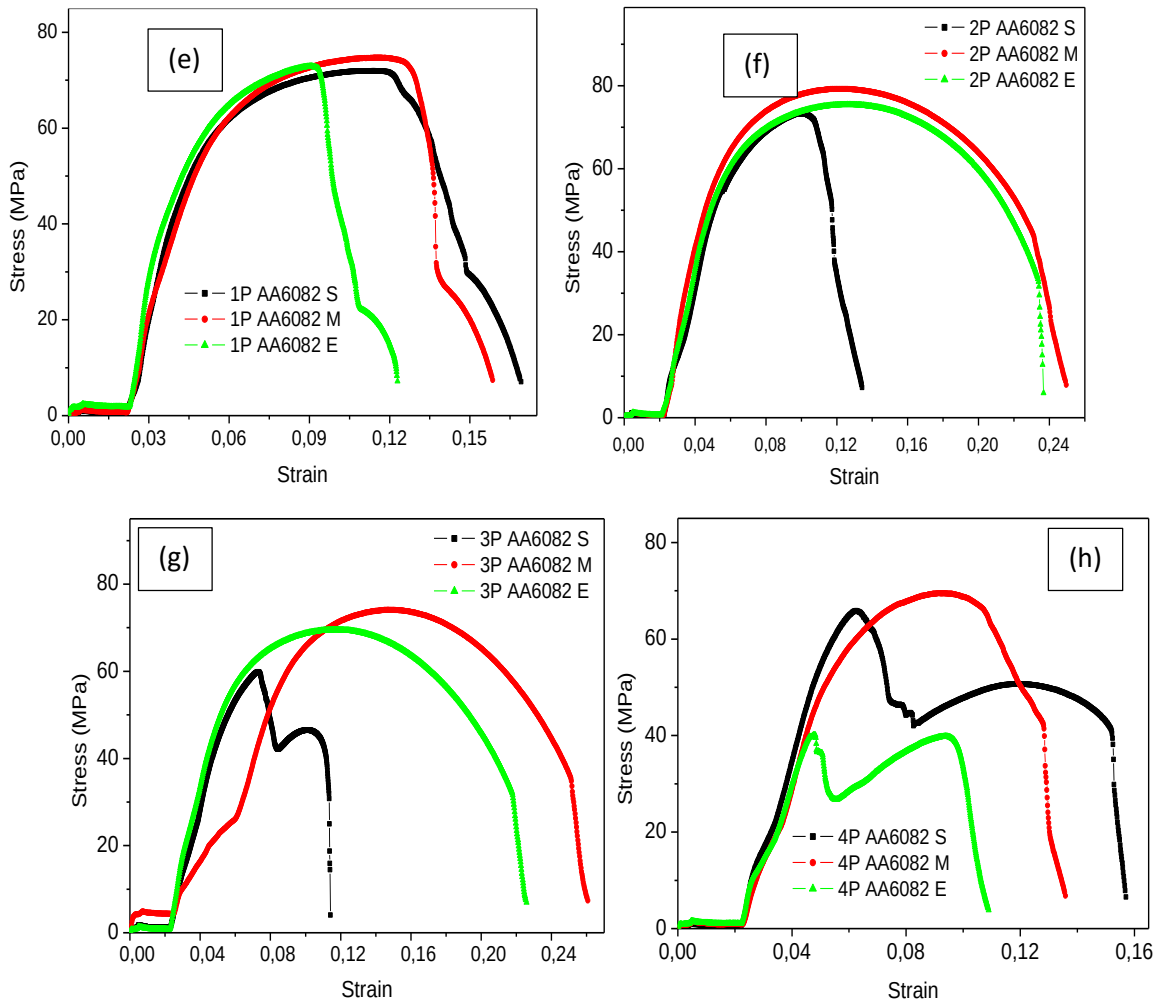

Figure 4.3.2: Stress Strain curves; (FSPed) (e) 1P6082/1050; (f) 2P6082/1050; (g) 3P6082/1050 and (h) 4P6082/1050.

For the 1P6082/1050 joint, the highest UTS of 74.7 MPa was achieved from a specimen sampled at the joint's M with a percentage elongation of 15.86 percent. The highest UTS for the 1P joint was 71.1 percent when compared to the AA1050 BM and 26.7 percent when compared to the AA6082 BM. For the 2P6082/1050 joint, the highest UTS of 79.3 MPa was achieved from a specimen sampled at the joint's middle with a percentage elongation of 24.95 percent. The highest UTS for the 2P joint was 75.5 percent when compared to the AA1050 BM and 28.3 percent when compared to the AA6082 BM. For the 3P6082/1050 joint, the highest UTS of 69.5 MPa was achieved from a specimen sampled at the joint's middle and end with a percentage elongation of 21.88 percent. The highest UTS for the 3P joint was 62.2 percent when compared to the AA1050 BM and 24.8 percent when compared to the AA6082 BM. For the 4P6082/1050 joint, the highest UTS of 69.5 MPa was achieved from a specimen sampled at the joint's middle with a percentage elongation of 21.86 percent. The highest UTS

for the 4P joint was 62.2 percent when compared to the AA1050 BM and 24.8 percent when compared to the AA6082 BM. The ultimate tensile strength (UTS) of the 1P, 2P, and 4P FSPed joints was seen to fluctuate from the S to the E of the joint, however, the 3P UTS was seen to increasing from the beginning to the end of the joint. From the start to the end of the joint, the percentage elongation of the 1P and 4P was noted to be decreasing. From the beginning to the end of the joint, the percentage elongation for the 2P was seen to fluctuate. From the beginning to the end of the joint, the 3P percent elongation increased. All the UTS for 1P, 2P, 3P, and 4P6082/1050 joints were lower than those for the base metals, a trend that was previously noted in the literature [164]. When compared to the UTS for both BM, the UTS for 1P - 4P was lower. In comparison to both BM, the % elongation of the 1P – 4P joint was greater than 100%. The root of this phenomena is assumed to be the microstructural arrangement, which was driven mostly by material positioning. [10,159,165].

Table 4.3.2: Tensile test results

Joint type & sampling position	Ultimate Tensile Stress (MPa)	Percentage elongation (%)	Fracture Position
AA6082			
The base material	280	10	
1P Joint			
S	71.9	16.91	SZ
M	74.7	15.86	SZ
E	72.9	12.26	SZ
2P Joint			
S	73.3	13.43	SZ
M	79.3	24.95	HAZ
E	75.5	23.39	HAZ
3P Joint			
S	59.8	11.35	HAZ
M	69.5	21.88	HAZ
E	69.5	21.88	HAZ
4P Joint			
S	65.8	15.23	SZ
M	69.5	12.86	HAZ
E	40.1	10.18	SZ

4.3.3 Comparative between the multi-pass FSP AA1050/AA6082 and AA6082/AA1050 FSPed joints results.

Figure 4.3.3 (a) - (f) shows the stress-strain curves for different material locations in multi-pass FSPed specimens. Figure 4.3.3 (a) depicts the stress-strain curve for the 1P, 2P, 3P, and 4P of the 1050/6082 FSPed joint at the S position, whereas figure 4.3.3 (b) depicts the stress-stain curve for the same position for the 1P, 2P, 3P, and 4P of the 6082/1050 FSPed joint. Figure 4.3.3 (c) depicts the stress-strain curve for the 1P, 2P, 3P, and 4P of the AA1050/AA6082 FSPed joint in the M position, whereas figure 4.3.3 (d) depicts the stress-

stain curve for the same position for the 1P, 2P, 3P, and 4P of the 6082/1050 FSPed joint. Figure 4.3.3 (e) depicts the stress-strain curve for the 1P, 2P, 3P, and 4P of the AA1050/AA6082 FSPed joint at the E position, whereas figure 4.3.3 (f) depicts the stress-stain curve for the same position for the 1P, 2P, 3P, and 4P of the 6082/1050 FSPed joint.

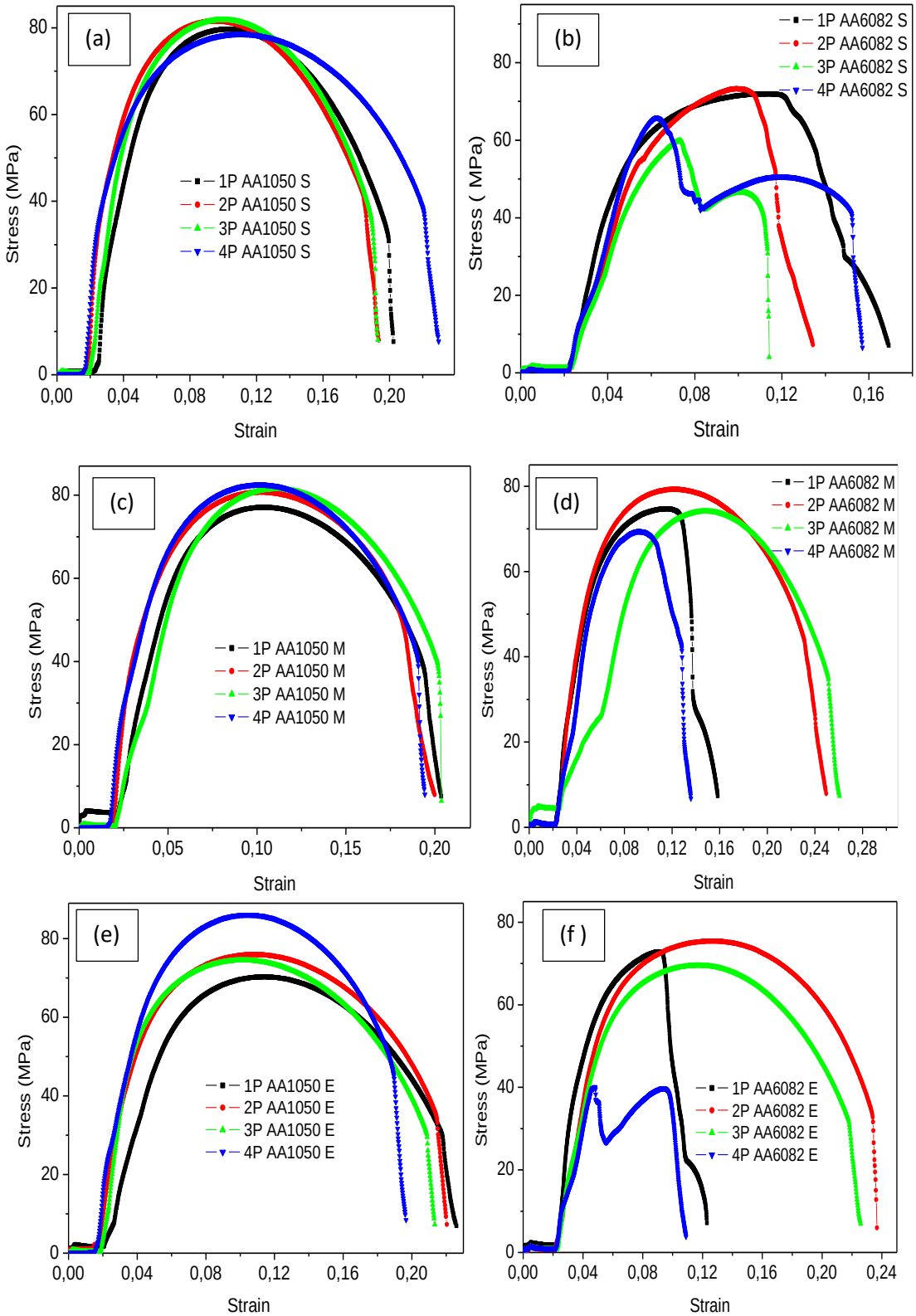

Figure 4.3.3: Stress Strain curves; (1P- 4P FSPed) (a) 1050/ 6082 S; (b) 6082/1050 S; (c) 1050/6082 M; (d) 6082/1050 M; (e) 1050/6082 E and (f) 6082/1050 E.

For the 1050/6082, the ultimate tensile strength (UTS) for the 1P – 3P FSPed joint increased from 79.7 MPa – 81.8 MPa at the start position and decreased to 78.6 MPa on the fourth pass, whereas the UTSfor the 6082/1050 fluctuated between 59.8 – 73.3 MPa with an increase in the passes number. The UTS of the 1P – 4P FSPed joint in the center position increased from 77.1 MPa to 82.6 MPa for the 1050/6082, whereas the UTS of the 6082/1050 fluctuated between 69.5 and 79.3 MPa as the passes increased. The 1050/6082 joint's UTS fluctuated between 70.3 and 86.1 MPa at the end position, while the 6082/1050 joint's UTS fluctuated between 40.1 and 75.5 MPa. The 1050/6082 joint's greatest ultimate tensile strength was 86.1 MPa on the fourth pass at the joint's end, whereas the 6082/1050 joint's highest ultimate tensile strength was 79.3 MPa on the second pass in the center. In comparison to the 1050/6082 FSPed joints, the stress-stress graph for the 6082/1050 FSPed joints exhibited a lot of variances. This is because the 1050/6082 joints had better material flow than the 6082/1050 joints, resulting in fewer faults in the 1050/6082 joints. The grain refinement seen during microstructural investigation is responsible for the variation in tensile properties. On general, grain morphology and alignment have a significant impact in a material's tensile characteristics [10, 166, 167]. .89+The percentage elongation for both 1P - 4P of 1050/6082 and 6082/1050 FSPed joints was larger than 100% relative to both AA1050-H14 and AA6082-T651 base materials, regardless of material position, whereby material location altered the microstructural arrangement. Guo et al [159] discovered a similar trend. When the AA1050 was positioned on the advancing side, it was revealed that as the number of passes increased, joint strength increased nonlinearly. According to literature, a similar pattern has been found [91,112, 126,168,169].

4.4 Scanning Electron Microscopy (SEM) Tests

The findings of the tensile test fractured surfaces, which were further analyzed using the SEM testing equipment, are presented in this section. In this section, the morphology of each specimen collected by SEM is illustrated at different magnification. Tensile testing is a method of determining the strength of a material. At low and high magnification, broken surfaces were studied.

4.4.1 AA1050/AA6082 FSPed joints results

To further understand the fracture mechanism, at low and high magnification the tensile test fractured surfaces were examined. Figure 4.4.1 shows the the fractured tensile specimens fractographs. The fractured surface morphology of the specimens taken from the S, M, and E of the 1P1050/6082 joint is shown in Figure 4.4.1 (a) – (c). The fractured surface morphology of the specimens taken from the S, M, and E of 2P1050/6082 is shown in Figure 4.4.1 (d) – (f). The fractured surface morphology of the specimens taken from the S, M, and E of 3P1050/6082 joint is shown in Figure 4.4.1 (g) – (l). The fractured surface morphology of the specimens taken from the S, M, and E of 4P1050/6082 is shown in Figure 4.4.1 (j) – (l). For the 1P - 4P 1050/6082 FSPed joints, there were dimples on the fractured surface, which characterized it., as shown in figure 4.4.1 (a) - (l). It was discovered that the dimple sizes reduces as the number of passes increases, and this effect is caused by improved tensile properties [170]. Dimples and microvoids were seen in the morphology of 1P up to the fourth pass of the 1050/6082 FSPed joints. The presence of dimples in conjunction with microvoids

indicates ductile failure mode [170-171]. There were ductile trans-granular failure characteristics in all of the joints [172].

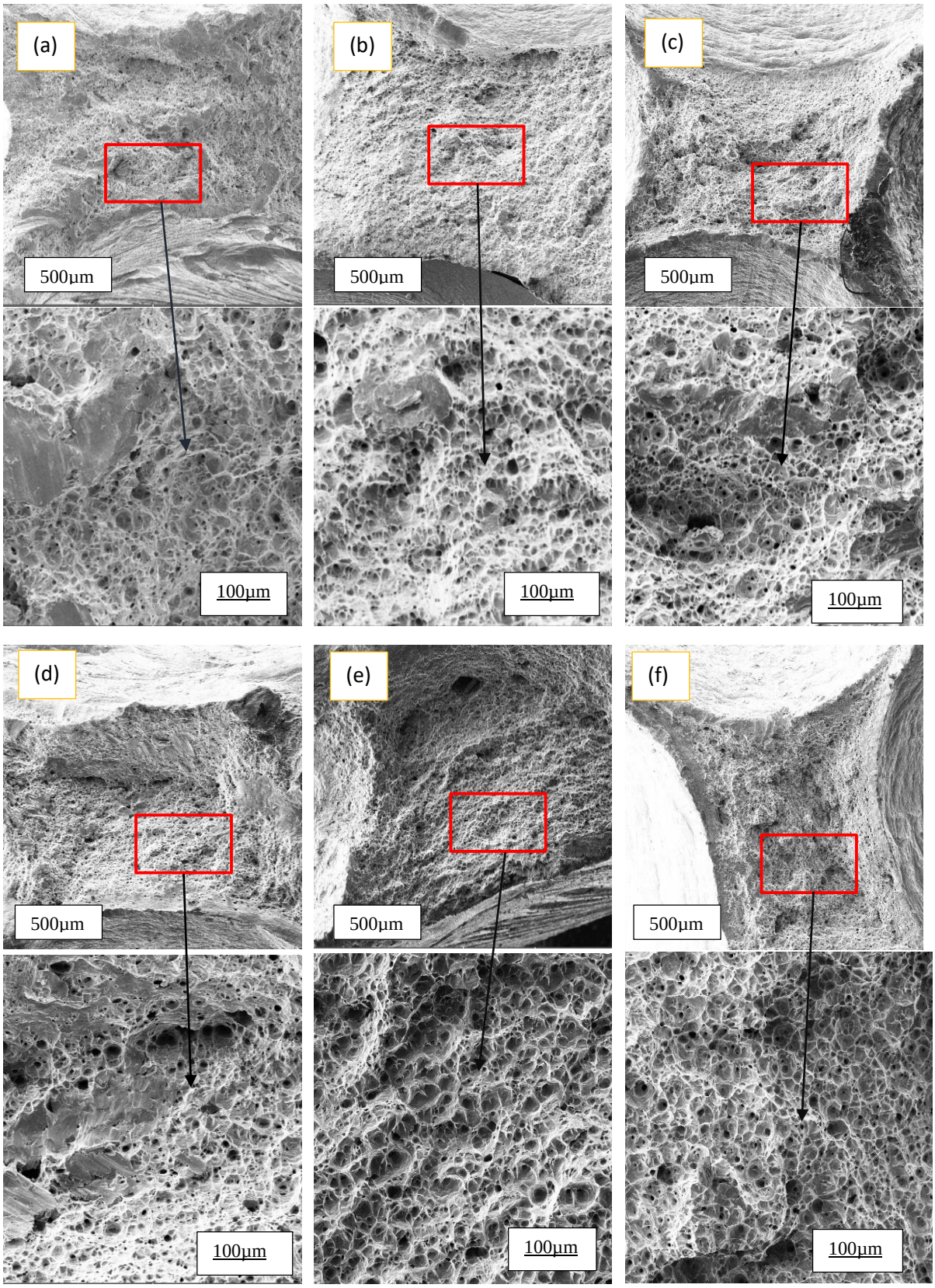

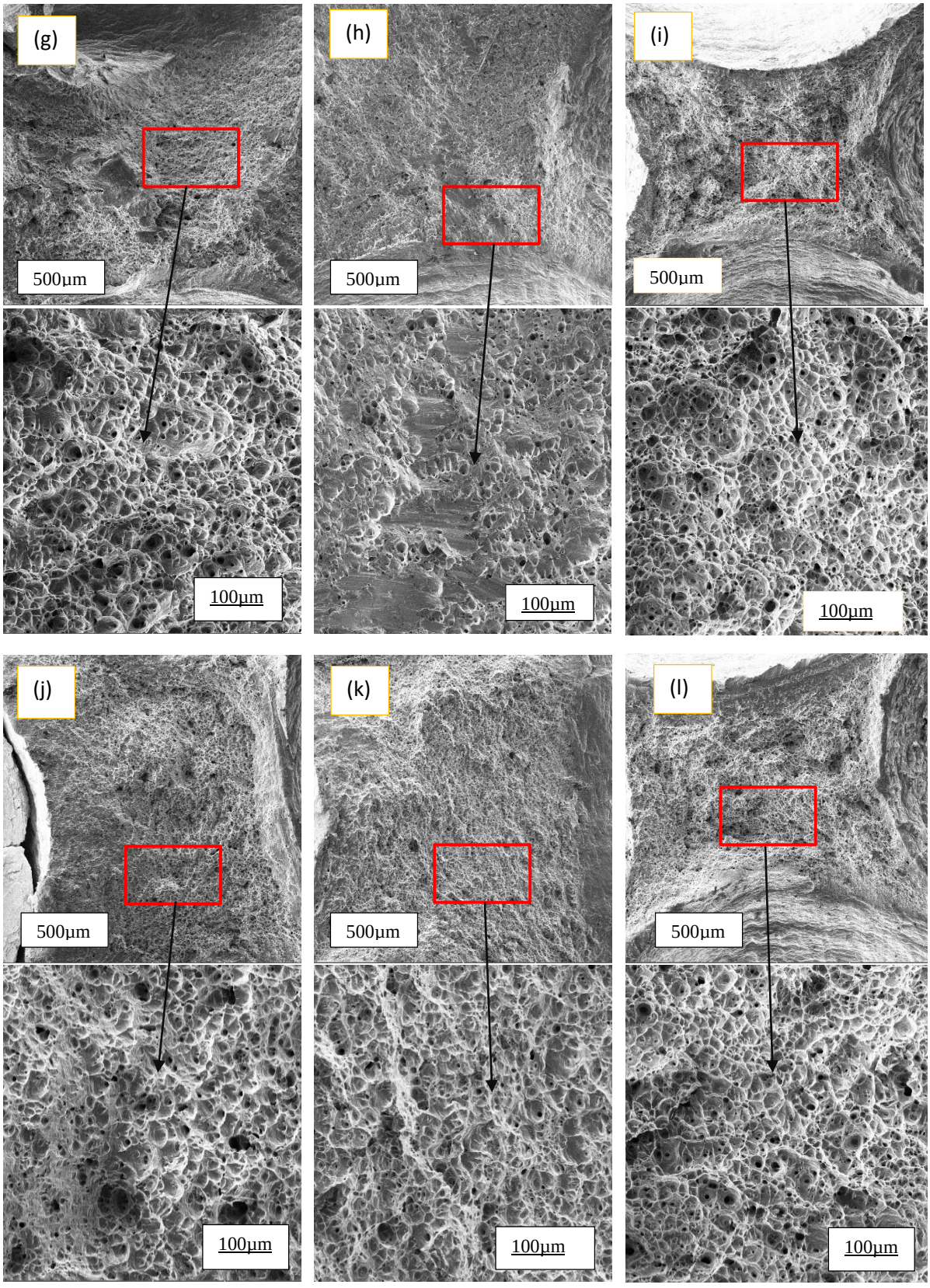

Figure 4.4.1: SEM tensile; 1P1050/6082 (a) S, (b) M. (c) E; 2P1050/6082 (d) S, (e) M, (f) E; 3P1050/6082 (g) S, (h) M, (i) E and 4P1050/6082 (j) S, (k) M, (l) E.

4.4.2 AA6082/AA1050 FSPed joints results

The tensile test fractured surfaces were studied at low and high magnification to better understand the fracture mechanism. Figure 4.4.2 shows the fractured tensile fractographs of the specimens. The fractured surface morphology of the specimens taken from the S, M, and E of 1P6082/1050 joint is shown in Figure 4.4.2 (a) – (c). The fractured surface morphology of the specimens taken from the S, M, and E of 2P6082/1050 is shown in Figure 4.4.2 (d) – (f). The fractured surface morphology of the specimens taken from the S, M, and E of 3P6082/1050 is shown in Figure 4.4.2 (g) – (i). The fractured surface morphology of the specimens taken from the S, M, and E of 4P6082/1050 is shown in Figure 4.4.2 (j) – (l). On the fractured surface of the joints, there is the presence of dimples of different sizes, micro-voids and cleavage facets [164,172-174]. The existence of river-like fractured surfaces was evident in Figure 4.4.2 (a), (b), (c), and (d). Teared facets were seen in Figure 4.4.2 (c), which show aluminium matrix at the interface [175]. Figures 4.4.2 (e), (f), (h), (l), (j), and (k) show the existence of micro-voids and dimples fractured surfaces. The presence of dimples indicates that the failure mode is ductile. The presence of cleavage fractured surfaces was also seen in Figure 4.4.2 (h). The existence of river-like fractured surfaces with ductile failure mechanism was observed in figure 4.2.2 (h), (j) and (l). The microstructural arrangement and tensile characteristics indicate inadequate material mixing, as seen by the river-like patterns on the surfaces of joint processed. The existence of river-like structures indicates inadequate material mixing or a joint that has been subjected to significant heat input, which is usually indicated by fracture at the stir zone [176-180].

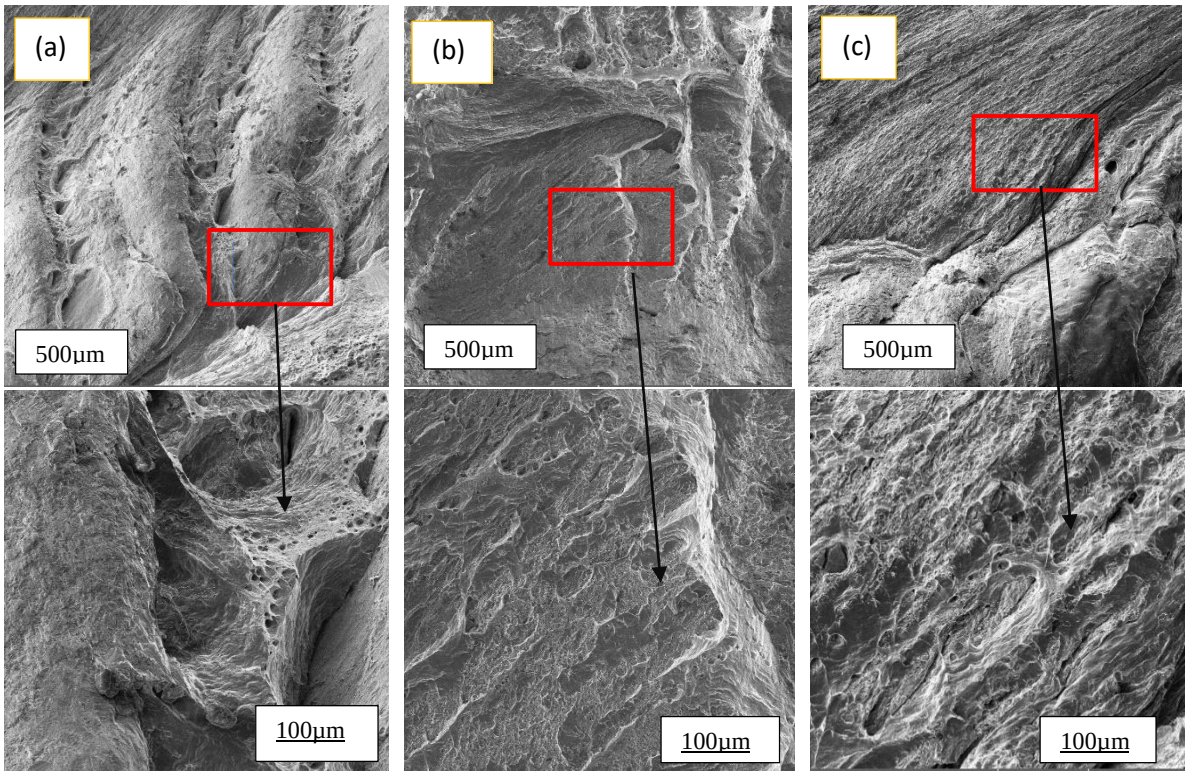

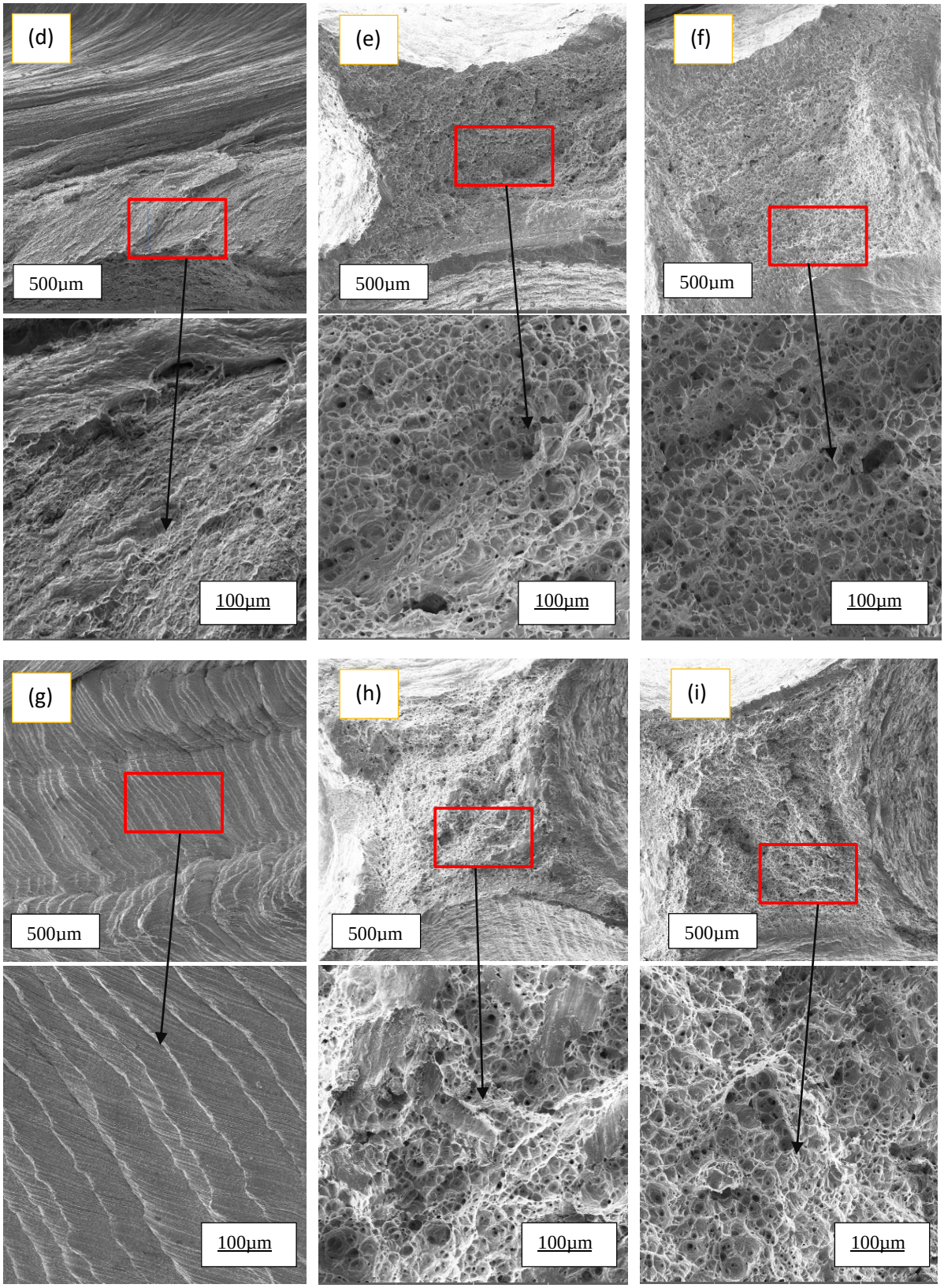
(d)
500µm
100µm
(e)
500µm
100µm
(f)
500µm
100µm
(g)
500µm
100µm
(h)
500µm
100µm
(i)
500µm
100µm

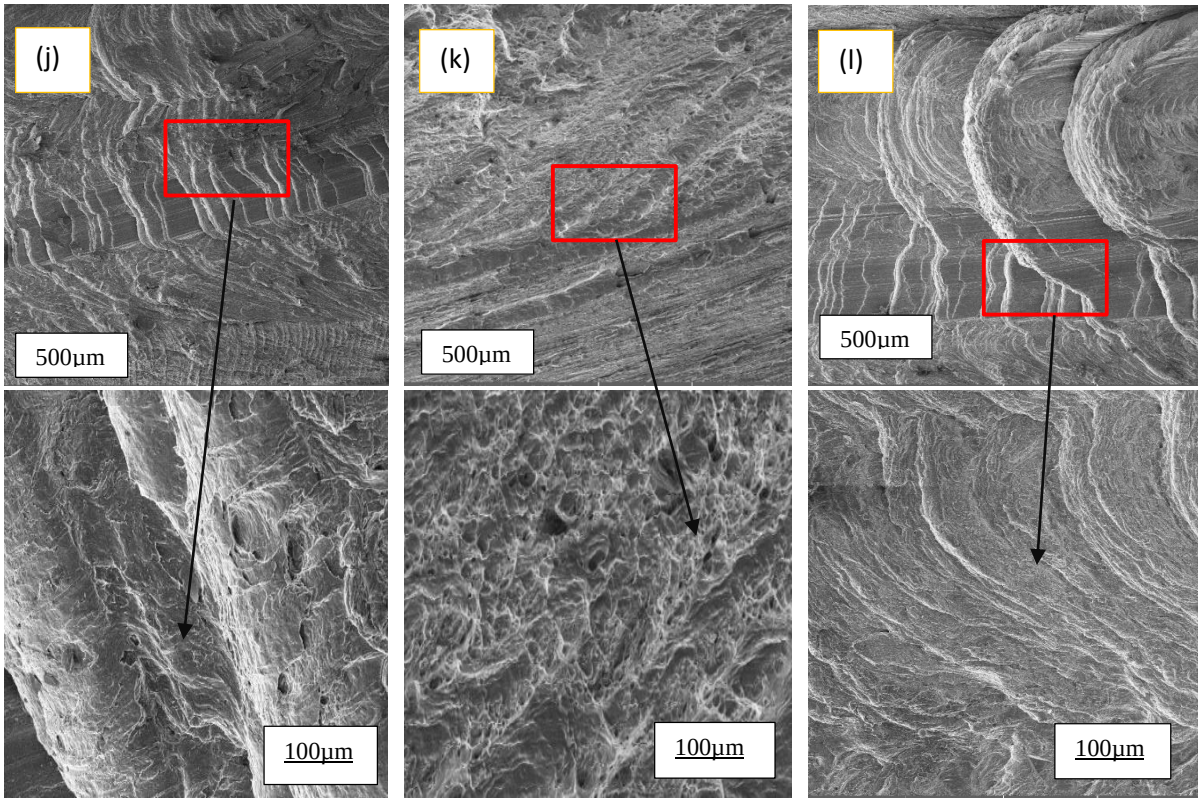

Figure 4.4.2: SEM tensile; 1P6082/1050 (a) S, (b) M. (c) E; 2P6082/1050 (d) S, (e) M, (f) E; 3P6082/1050 (g) S, (h) M, (i) E and 4P6082/1050 (j) S, (k) M, (l) E.

4.5 Microhardness Tests

The Vickers microhardness data acquired during the microhardness test are presented in this section. The Vickers microhardness data were examined further, with a focus on the stir zone (SZ).

4.5.1 AA1050/AA6082 FSPed joints results

Vickers microhardness values for the FSPed AA6082/AA1050 joints are shown in Figure 4.5.1. The microhardness profiles for specimens obtained at the S, M, and E of 1P up to 4P1050/6082 joint are shown in Figure 4.5.1 (a), (b), (c), and (d). The SZ vickers microhardness of the 1P joint ranged between 30.84 and 65.54 HV at the S, M, and E of the sampled specimen, with the maximum SZ vickers microhardness for the mentioned joint being 65.54 HV at the end of the sampled specimen of the 1P FSPed AA1050/AA6082 joint. From start to finish, the SZ vickers microhardness of the 2P FSPed joint varied between 23.85 and 60.37 HV, with the highest SZ microhardness of 60.37 HV measured towards the end of the specimen of the 2P1050/6082 joint. The SZ vickers microhardness of the 3P FSPed joint varied between 21.3 and 56.75 HV from start to finish, with the highest SZ microhardness of 56.75 HV recorded in the center of the specimen of the 3P1050/6082 joint. From start to finish, the SZ vickers microhardness of the 4P1050/6082 joint fluctuated between 23.33 and 57.14 HV, with the highest SZ microhardness of 57.14 HV measured on the specimen sample in the middle. The microhardness of the 1050/6082 1P, 2P, 3P, and 4P FSPed joint increased towards the AA6082. When AA1050 is on the advancing side in all passes for all FSPed joints, the microhardness in the TMAZ area of the advancing side is lower than that of the retreating

side. The retreating side of AA6082 has more highly elongated grains with fine cells than the advancing side, which accounts for the difference in microhardness in this region [181]. The increase in microhardness of this specimen can be linked to the precipitation and nucleation of thick intermetallic compounds caused by high temperature and high deformation rate [69,99,151].

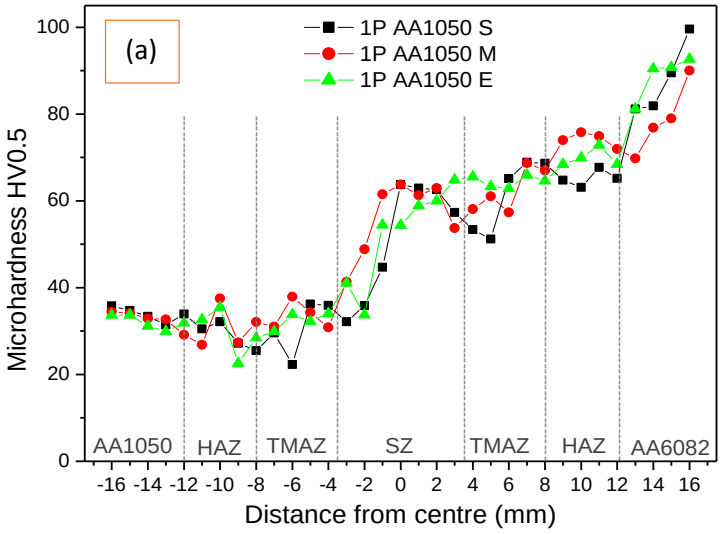

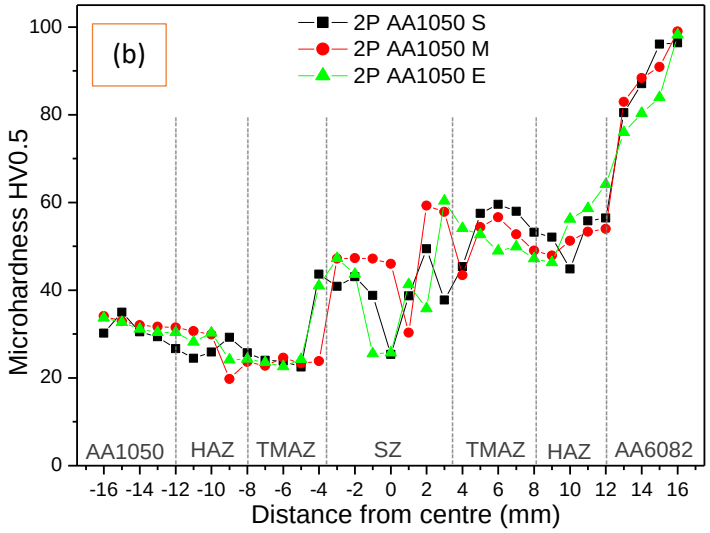

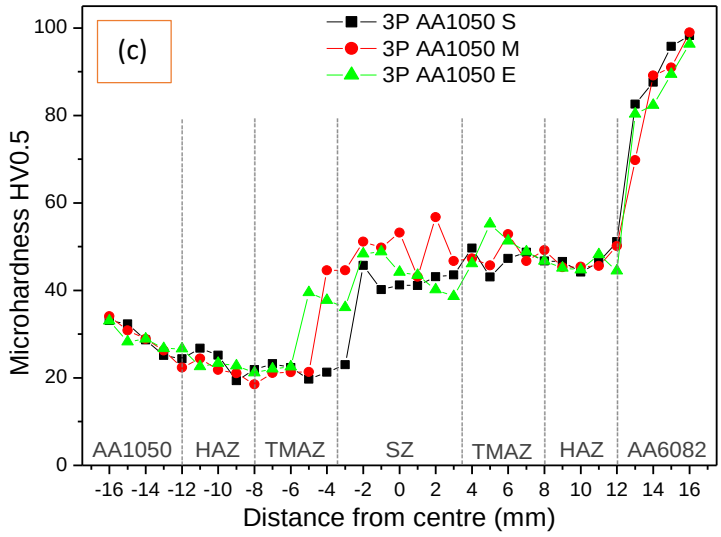

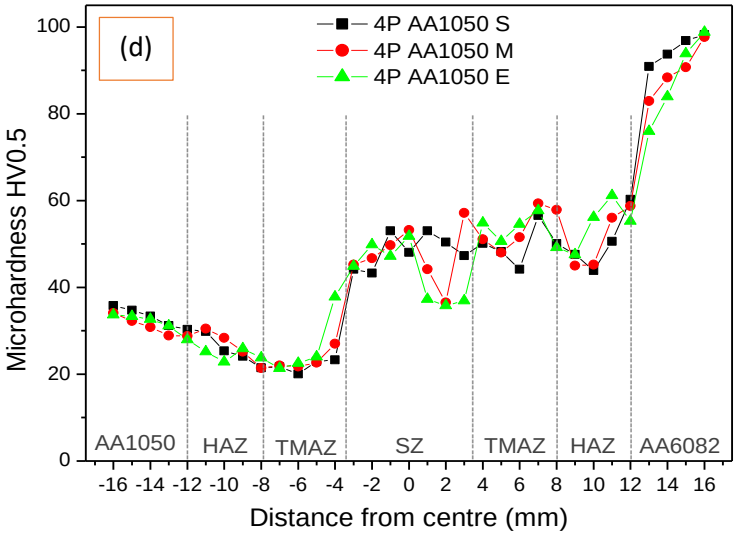

Figure 4.5.1: Vickers microhardness HV0.5; (FSPed) (a) 1P1050/6082; (b) 2P1050/6082; (c) 3P1050/6082 and (d) 4P1050/6082.

4.5.2 AA6082/AA1050 FSPed joints results

Vickers microhardness results for the FSPed 6082/1050 joints are shown in Figure 4.5.2. The vickers microhardness profiles for specimens obtained at the S, M, and E of 1P up to 4P 6082/1050 FSPed joint are shown in Figure 4.5.2 (a), (b), (c), and (d). From S to E, the microhardness of the SZ of the 1P joint fluctuated between 18.62 and 61.04 HV. At the middle of the sampled specimen of the 1P6082/1050 joint, the maximum SZ vickers microhardness for the above-mentioned joint was measured to be 61.06 HV. From S to E, the SZ microhardness of the 2P FSPed joint varied between 25.73 and 58.15 HV, with the maximum SZ microhardness measured in the center of the specimen of the 2P6082/1052 joint at 58.15 HV. From S to E, the microhardness of the SZ of the 3P FSPed joint varied between 22.99 and 59.25 HV, with the maximum SZ microhardness of 59.25 HV measured towards the E of the specimen of the 3P6082/1050 joint. From start to finish, the SZ vickers microhardness of the 4P FSPed joint fluctuated between 40 and 59.6 HV, with the highest microhardness of 59.6 HV recorded on a specimen sample from the center of the 4P6082/1052 joint. The vickers microhardness of the 6082/1050 1P, 2P, 3P, and 4P FSPed joints decreased as towards the AA1050. The decline in hardness is mostly caused by a thermal cycle in which the strengthening precipitates dissolve and coarsen [182]. The microhardness at the TMAZ area of the advancing side is greater than that of the retreating side when AA6082 is on the advancing side for all FSPed joints in all passes [183-184]. Microhardness decreases in the HAZ and TMAZ regions respectively due to coarsening caused by the high-temperature gradient, and the creation of overaged precipitates [181,184].

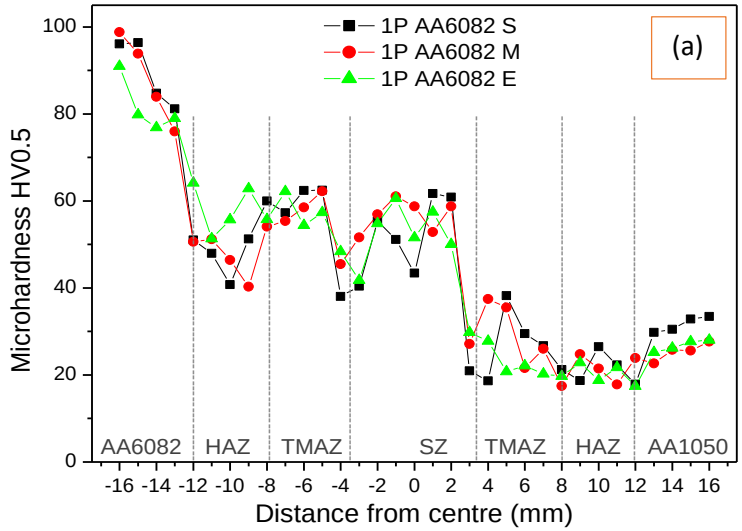
1P AA6082 S
1P AA6082 M
1P AA6082 E
(a)
Microhardness HV0.5
AA6082
HAZ
TMAZ
SZ
TMAZ
HAZ
AA1050
Distance from centre (mm)

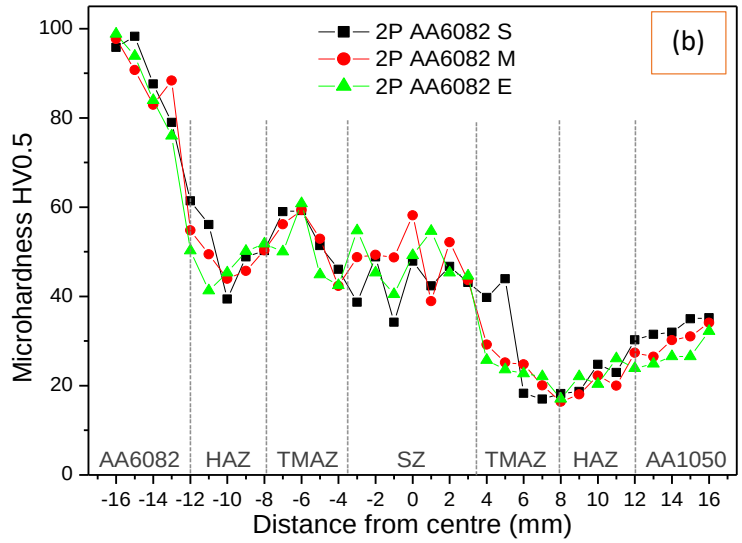
2P AA6082 S
2P AA6082 M
2P AA6082 E
(b)
Microhardness HV0.5
AA6082
HAZ
TMAZ
SZ
TMAZ
HAZ
AA1050
Distance from centre (mm)

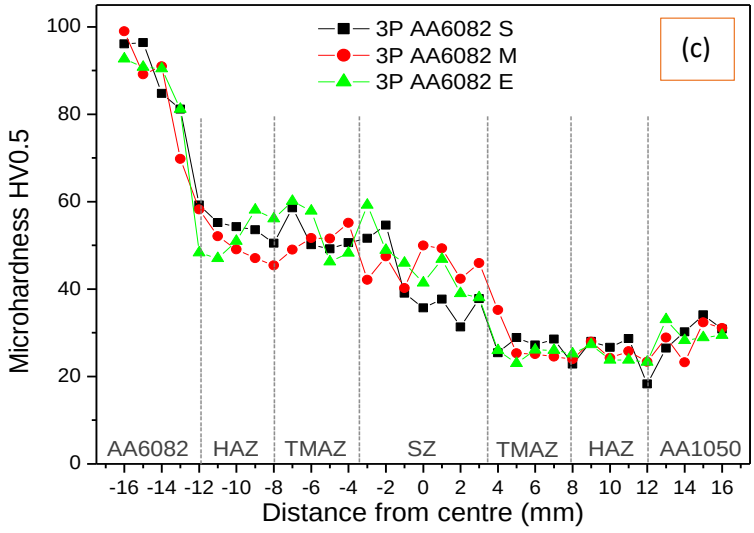
3P AA6082 S
3P AA6082 M
3P AA6082 E
(c)
Microhardness HV0.5
AA6082
HAZ
TMAZ
SZ
TMAZ
HAZ
AA1050
Distance from centre (mm)

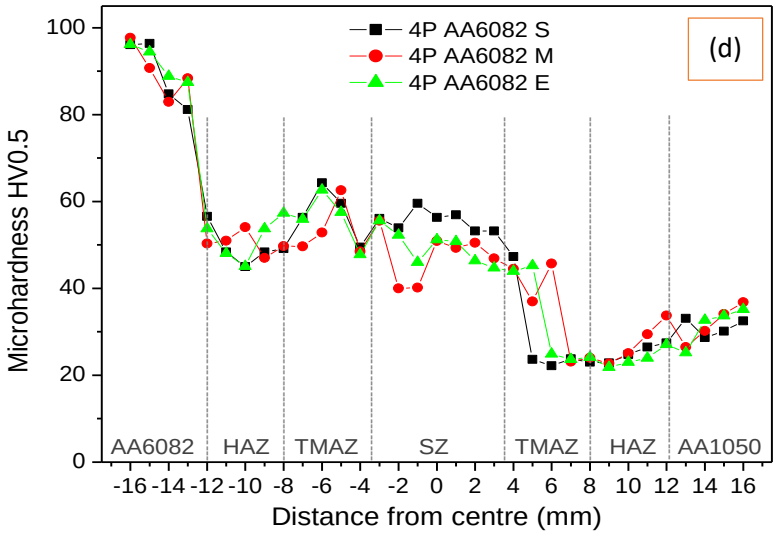

Figure 4.5.2: Vickers microhardness HV0.5; (FSPed) (a) 1P6082/1050; (b) 2P6082/1050; (c) 3P6082/1050and (d) 4P6082/1050.

4.5.3 Comparative between the multi-pass FSP AA1050/AA6082 and AA6082/AA1050 FSPed joints results.

When compared to the AA6082, the microhardness of the AA1050 base material is lower. The microhardness in the HAZ area of the advancing side is lower than that of the retreating side when AA1050 is on the advancing side for all FSPed joints in all passes. The microhardness in the HAZ area of the advancing side is greater than that of the retreating side when AA6082 is on the advancing side for all FSPed joints in all passes. The microhardness in the TMAZ area of the advancing side is lower than that of the retreating side when AA1050 is on the advancing side for all FSPed joints in all passes. The microhardness in the TMAZ area of the advancing side is greater than that of the retreating side when AA6082 is on the advancing side for all FSPed joints in all passes. It's worth noticing that the microhardness of the 1050/6082 1P, 2P, 3P, and 4P FSPed joint increased towards the AA6082, but the microhardness of the 6082/1050 1P, 2P, 3P, and 4P FSPed joint decreased towards the AA1050. Specimens with AA1050 on the advancing side increased in microhardness to the AA6082 side, while specimens with AA6082 decreased in microhardness to the AA1050 side.

4.6 Bending Tests

This section contains the data collected during a bending test, often known as a flexural test. The flexural test was carried out on both sides of the joints, that is, on the face and the root. The surface in contact with the processing tool is known as the face, whereas the area in contact with the back-base plate's is known as the root.

4.6.1 AA1050/AA6082 FSPed joints results

The post flexural test specimens for the 1050/6082 FSPed joints are shown in Figures 4.6.1 (a) – (h). Figure 4.6.1 shows the post-flexural test specimens for the roots: (a) for 1P1050/6082, (c) for 2P1050/6082, (e) for 3P1050/6082, and (g) for 4P1050/6082. Figure 4.6.1 shows the post

flexural test specimens for the face: (b) for 1P1050/6082, (d) for 2P1050/6082, (f) for 3P1050/6082, and (h) for 4P1050/6082. It was observed that the roots specimens didn't fail/break, reaction is the same in all of them while the faces of processed specimens failed in different locations. The roots specimen bent towards the soft materials. After a maximum deflection, some specimen's joints were free of cracks, while others showed evident cracks, as shown in figure 4.6.1.

Figure 4.6.1: Post flexural test specimens; (a) 1P1050/6082 (Root), (b) 1P1050/6082 (Face), (c) 2P1050/6082 (Root), (d) 2P1050/6082 (Face), (e) 3P1050/6082 (Root), (f) 3P1050/6082 (Face), (g) 4P1050/6082 (Root) and (h) 4P1050/6082 (Face).

The flexural stress and strain curves of friction stir processed joints with AA1050 on the advancing side are depicted in Figure 4.6.1 (i) – (p). Figure 4.6.1 shows the specimen's root stress and strain curves: (i) for the 1P1050/6082, (k) for the 2P1050/6082, (m) for the 3P1050/6082, and (o) for the 4P1050/6082. Figure 4.6.1 shows the specimen's stress and strain curves for the face: (j) for the 1P1050/6082, (l) for the 2P1050/6082, (n) for the 3P1050/6082, and (p) for the 4P1050/6082. Root and face flexural highest strengths were 298.5 MPa and 281.25 MPa, respectively. For the root, the highest flexural strength was recorded in the middle of the joint on the 2P, and for the face, it was observed in the middle of the joint on the 3P.

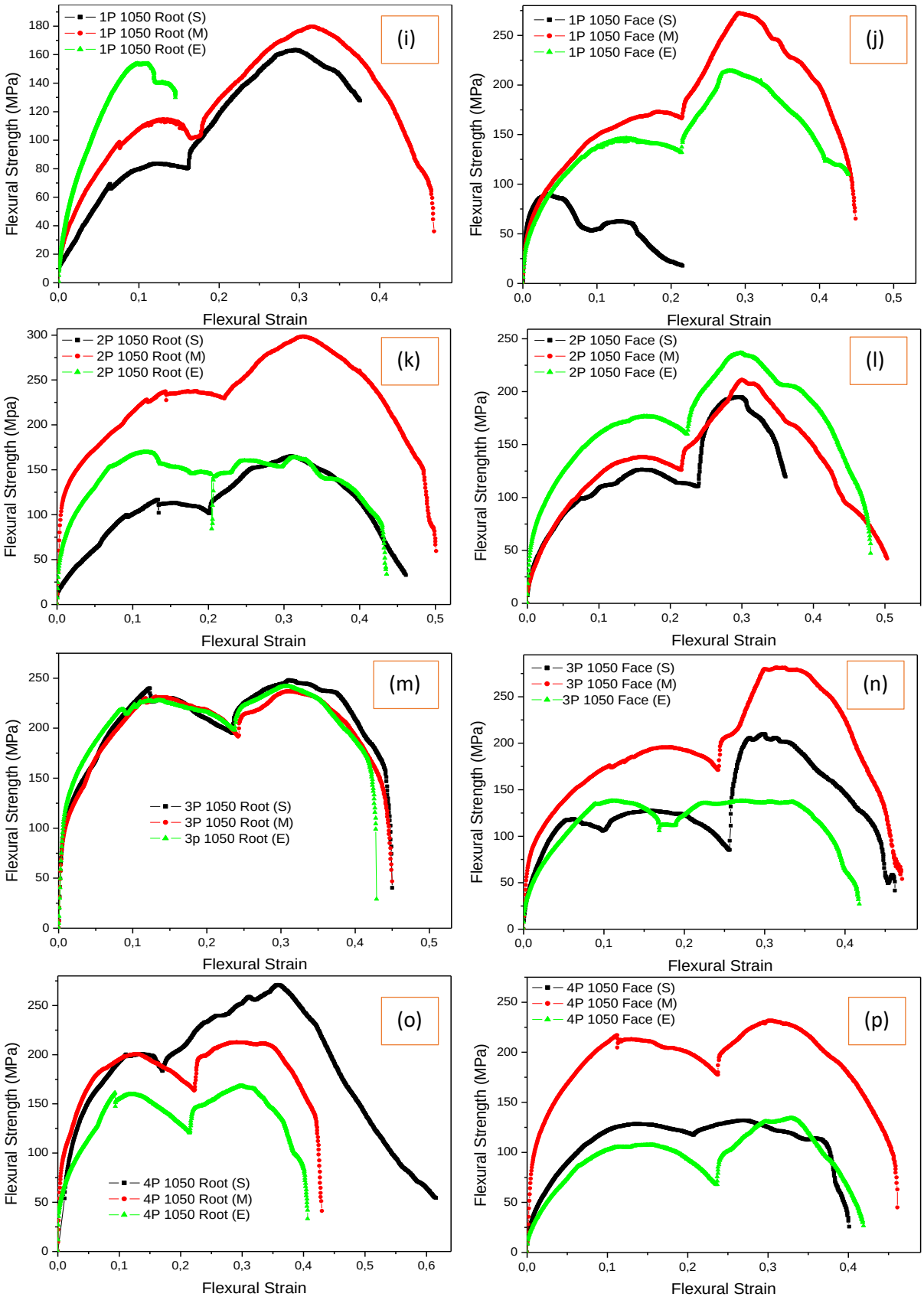

Figure 4.6.1: Flexural stress and strain curves with AA6082 on the AS; (i) 1P (Root), (j) 1P (Face), (k) 2P (Root), (l) 2P (Face), (m) 3P (Root), (n) 3P (Face), (o) 4P (Root) and (p) 4P (Face).

The ultimate flexural strength and maximum flexural strain for the post flexural test specimens depicted in figures 4.6.1 (i) – (p) are displayed in bar charts in figures 4.6.1 (q) and (r). The average UFS was found to be higher on the root side of the processed joint specimens than on the face side. The average MFS was found to be higher on the root side of the processed specimen's joints than on the face side. The grain refinement of the material has an impact on this type of behaviour [185]. The root UFS fluctuated from 1P - 4P FSPed joints. The face UFS of the 1P, 3P, and 4P fluctuated, whilst the UFS of the 2P was increasing. The root MFS was found to be fluctuating for the 1P, while decreasing for the 2P, 3P, and 4P. The face MFS ranged from 1P to 4P FSPed joints. The MFS and the UFS results had no clear relation.

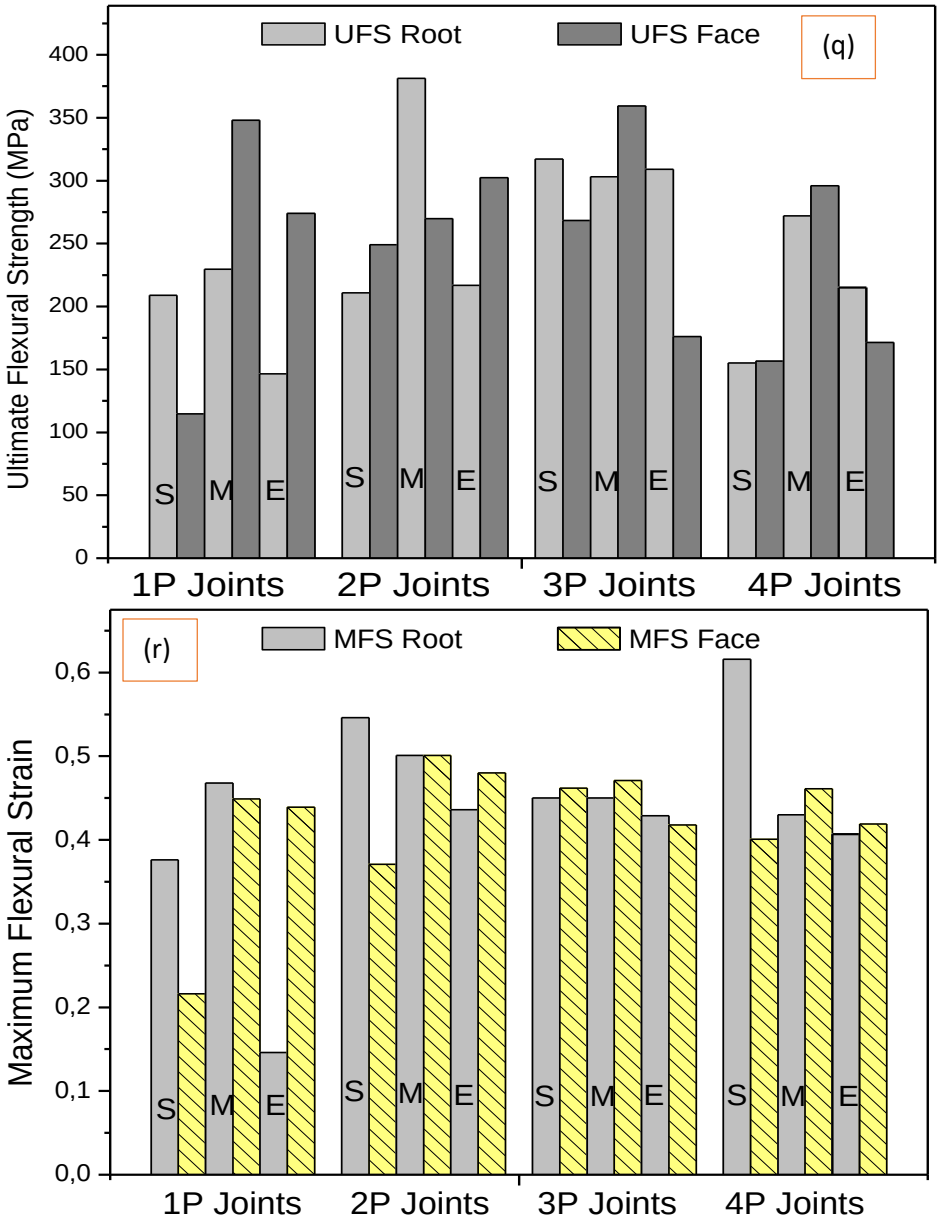

Figure 4.6.1: Bar charts for the FSPed joints; (q) Ultimate flexural strength (UFS) and (r) Maximum flexural strain (MFS).

4.6.2 AA6082/AA1050 FSPed joints results

The post flexural test specimens for the 6082/1050, FSPed joints are shown in Figures 4.6.2 (a) – (h). Figure 4.6.2 shows the roots post-flexural test specimens: (a) for the 1P6082/1050, (c) for the 2P6082/1050, (e) for the 3P6082/1050, and (g) for the 4P6082/1050. Figure 4.6.2 shows the face post-flexural test specimens: (b) for the 1P6082/1050, (d) for the 2P6082/1050, (f) for the 3P6082/1050, and (h) for the 4P6082/1050. It was discovered that the root and face processed specimens both failed in different locations. After a maximum deflection, some joints specimens were free of cracks, while others had visible cracks.

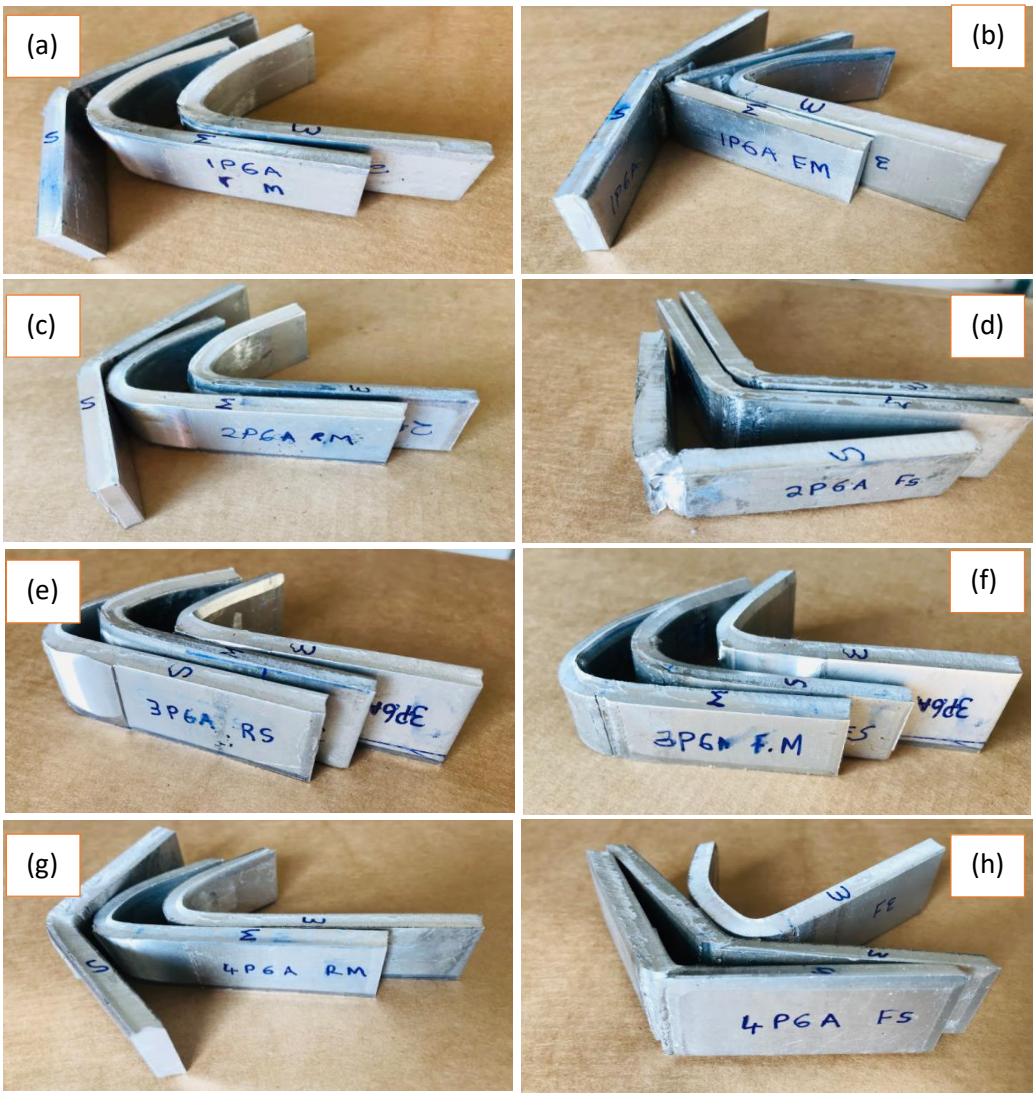

Figure 4.6.2: Post flexural test specimens; (a) 1P6082/1050 (Root), (b) 1P6082/1050 (Face), (c) 2P6082/1050 (Root), (d) 2P6082/1050 (Face), (e) 3P6082/1050 (Root), (f) 3P6082/1050 (Face), (g) 4P6082/1050 (Root) and (h) 4P6082/1050 (Face).

The flexural stress and strain curves of friction stir processed joints with AA6082 on the advancing side are shown in Figure 4.6.2 (i) – (p). Figure 4.6.2 shows the specimen's root stress and strain curves: (i) for the 1P6082/1050, (k) for the 2P6082/1050, (m) for the 3P6082/1050, and (o) for the 4P6082/1050. Figure 4.6.2 shows the specimen's stress and strain curves for the face: (j) for the 1P6082/1050, (l) for the 2P6082/1050, (n) for the 3P6082/1050, and (p) for the 4P6082/1050. The root and face highest flexural strengths were 276.94 MPa and 226.5 MPa, respectively. The 4P at the end of the joint had the highest flexural strength for the root, while the 2P at the middle of the joint had the highest flexural strength for the face.

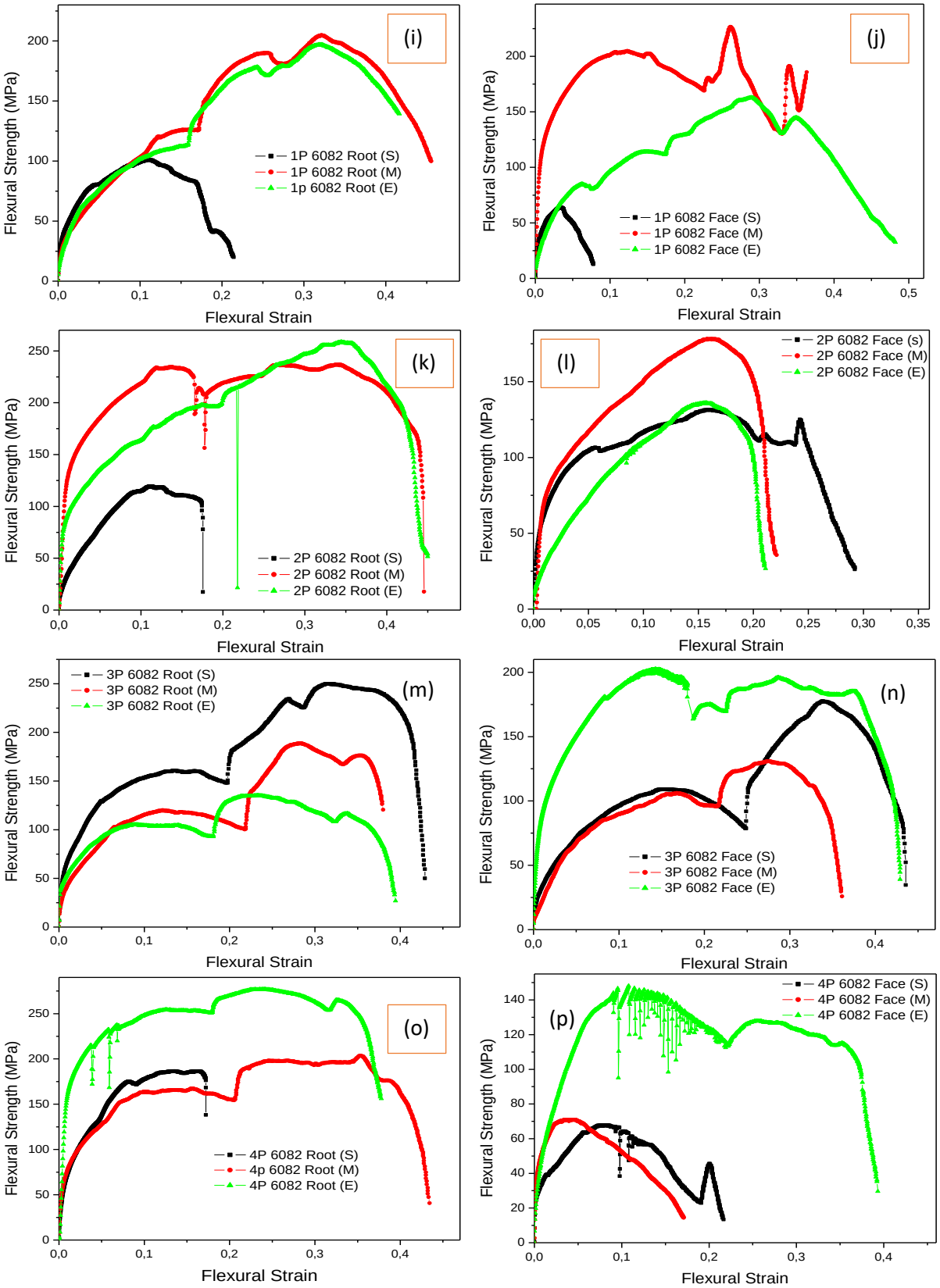

Figure 4.6.2: Flexural stress and strain curves with AA6082 on the AS; (i) 1P (Root), (j) 1P (Face), (k) 2P (Root), (l) 2P (Face), (m) 3P (Root), (n) 3P (Face), (o) 4P (Root) and (p) 4P (Face).

Figures 4.6.2 (q) and (r) show the ultimate flexural strength and maximum flexural strain for the post-flexural test specimens presented in figures 4.6.2 (i) – (p). The average UFS was found to be higher on the root side of the processed joint specimens than on the face side. The average MFS was found to be higher on the root side of the processed specimen's joints than on the face side. The grain refinement of the material has an impact on this type of behaviour as well [185]. The 1P's UFS for the root was fluctuating. The UFS for the 2P and 4P was increasing, whereas the UFS for the 3P was decreasing. For the 1P and 2P, the UFS for the face was fluctuating. The UFS was increasing in the 3P and 4P. The MFS for the root for the 1P, 3P, and 4P was fluctuating, but it was increasing for the 3P. The face's 1P MFS was increasing, while the 2P MFS was decreasing. The MFS for the 3P and 4P face appeared to be fluctuating. The average UFS and the average MFS results are directly proportional.

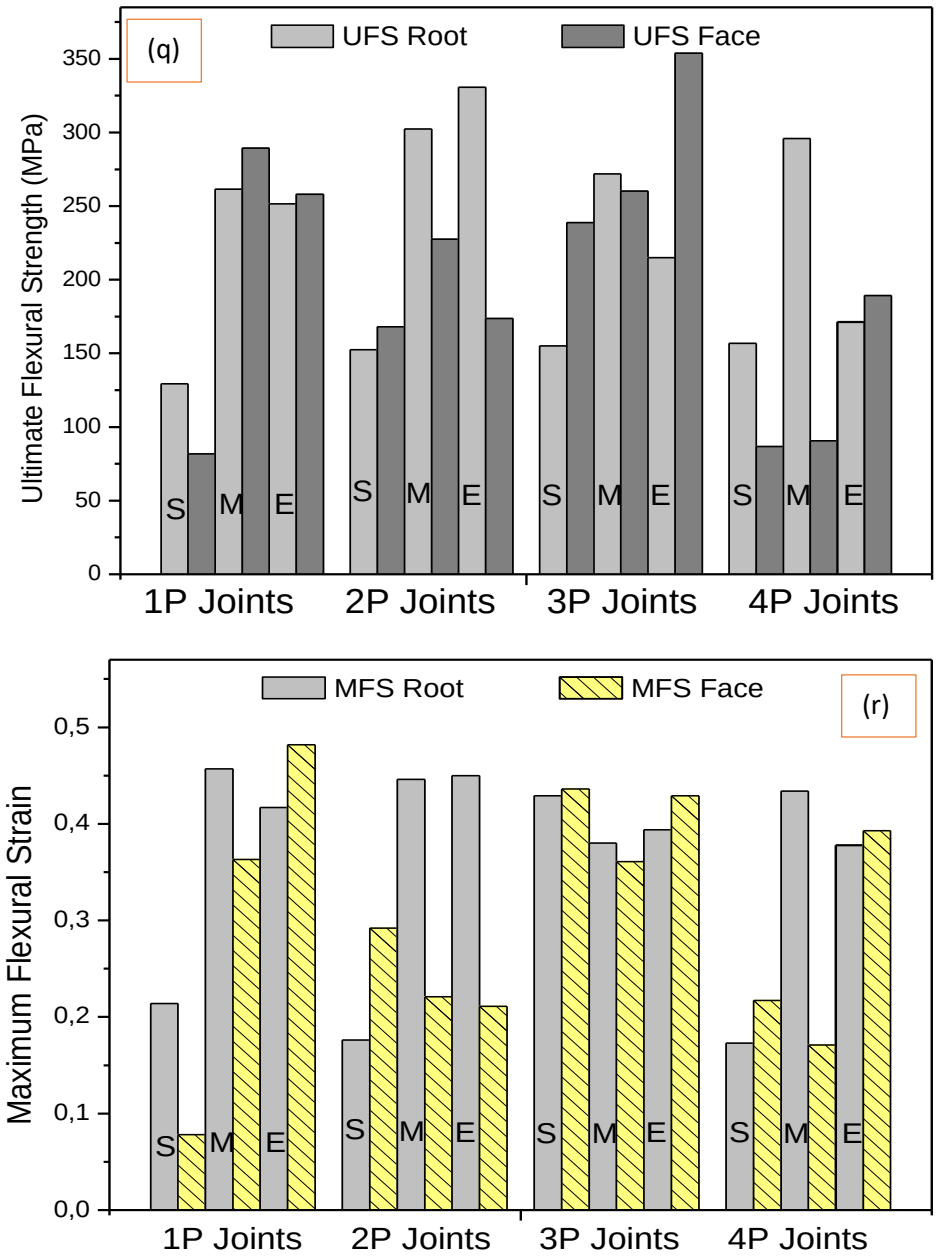

Figure 4.6.2: Bar charts for the FSPed joints; (q) Ultimate flexural strength (UFS) and (r) Maximum flexural strain (MFS).

CHAPTER 5
CONCLUSION AND RECOMMENDATION

The main points of this chapter are summarized in this chapter. It also highlights points of improvement when one wants to take the study forward.

5.1 Conclusion

This study was aimed to investigate the impact of the multi-pass FSPed joint between dissimilar aluminium alloys AA1050 as well as the AA6082. The aim was achieved through some set objectives. The objectives were to join the two dissimilar aluminium alloys using the FSW technique considering different material positioning before FSP, thereafter process the FSWed joints using a maximum of four FSP passes. After the completion of multi-pass FSP, the effect of material positioning and the impact of applying the FSP multi-passes on the mechanical properties was studied by performing tests on the processed plates. The test carried out were tensile test, bending test, microhardness test, fracture mechanism, and microstructural analysis.

The characterization of multi-pass friction stir processed AA1050 and AA6082 dissimilar joints was conducted successfully. Prior to the analysis, two aluminium alloys 1050 and 6082 were friction stir welded using friction stir welding technique to produce dissimilar joints (1050/6082 and 6082/1050). Using multi-pass friction stir processing procedure, the FSWed joints were friction stir processed to a maximum of four passes (1P FSP, 2P FSP, 3P FSP, and 4P FSP) for each material positioning. To better understand the nature of the joints, different specimens were prepared using the water jet cutting technology and different tests were then conducted on the prepared specimens. This includes tensile, bending, microhardness, fracture mechanism, macrostructure and microstructural analysis tests. The results obtained were studied and analysed comparatively. The following conclusions were drawn based on the findings:

The multi-pass FSP technique can be employed as an enhancement technique, according to the macroscopic and microscopic results. The SZ, HAZ, TMAZ, and non-affected BM (1050 and 6082) were observed on the macrostructure of the FSPed cross section on all joints. The stir zone region of all FSPed joints was characterized by the presence or the existence of onion rings pattern. Some macrostructures were observed to be free of defects, while others had defects. The cross section of multi-pass FSPed joints (1P, 2P, 3P, and 4P) were further analysed microstructurally. The dynamic recrystallization and plastic deformation experienced by the joints have shown that friction stir processing can break down coarse grain structure into fine equiaxed grain structure. The grain structure of the multi-pass friction stir processed 1050/6082 and 6082/1050 FSPed joints was refined from 19.84 µm to 5.381 µm for the 1050/6082 and from 13.12 µm to 1.744 µm for the 6082/1050 FSPed joints. The joint with 6082 on the advancing side exhibited significantly finer grains (1.744 µm) than the joint with AA1050 on the advancing side (5.381 µm). As the number of passes increased, the grain sizes decreased and the distribution of grain sizes became more uniform across the processed zone, regardless of material position.

The 1P, 2P, 3P, and 4P 1050/6082 FSPed joints were tested until they failed during tensile testing. When AA1050 was positioned on the advancing side due to grain refinement, an increase in the joint's tensile strength was noticed as the number of FSP passes increased. The maximum ultimate tensile strength was obtained at 86.1 MPa on the fourth pass. When compared to both base materials, the percentage elongation of all four joints was determined to be greater. The FSPed joints' tensile elongation range was determined to be between 18.65% and 22.22%. When the post-test specimen mode of fracture were analysed using SEM, the fracture surface morphology results correlated with the tensile results. The SEM fractographs of the fractured surface for the 1050/6082 FSPed joints indicated ductile trans-granular failure features. It was discovered that tensile strength and microhardness had a connection. The specimens with lower tensile strength had higher Vickers microhardness as compared to the ones with higher tensile strength. With AA1050 on the advancing side, the stir zone achieved a maximum hardness of 65.54 HV. The Vickers microhardness of 1050/6082 FSPed joints increased towards AA6082 regardless of the number of passes.

Tensile test was performed on the 1P, 2P, 3P, and 4P 6082/1050 FSPed joints until they fail. The results revealed that the ultimate tensile strength of the 6082/1050 did not depend on the number of FSP passes; rather, it varied between specimens taken from various FSPed joint locations. The percentage elongation was found to be greater than 100% when compared to both base materials for all the FSPed joints. The maximum ultimate tensile strength was obtained to be 79.3 MPa on the second pass. The FSPed joints' tensile elongation range was determined to be between 10.18 % and 24.95 %. The post-test tensile specimen were examined for fracrure mode using SEM. The SEM fractographs show ductile trans-granular failure and brittle failure features for the 6082/1050. The Vickers microhardness for the 6082/1050 was discovered to be slightly dependent on the number of FSP passes. With AA6082 on the advancing side, the stir zone achieved a maximum hardness of 61.06 HV. The Vickers microhardness of 6082/1050 FSPed joints decreased towards AA1050regardless of the number of passes.

The behaviour of FSPed joints when subjected to bending was also analyzed. There was no particular trend in flexural strength that was observed during analysis. For 1050/6082 FSPed joints, the average UFS of the root was found to be greater than that of the face, with the maximum UFS attained at 381.34 MPa for the root and 359.37 MPa for the face. For 6082/1050 processed joints, the average UFS of the root was higher than that of the face, with the maximum UFS obtained at 353.75 MPa for the root and 258.75 MPa for the face. For 1050/6082 processed joints, the average MFS of the root was higher than that of the face, with the maximum MFS of 0.616 for the root and 0.501 for the face. For 6082/1050 processed joints, the average MFS of the root was found to be higher than that of the face, with the maximum MFS of 0.457 for the root and 0.482 for the face. The deflection for the processed joints was detected in various regions of the joints, with some of the joints showing cracks and others being crack-free.

In conclusion, the findings have revealed that multi-pass friction stir processing has an impact on joint mechanical properties regardless of material positioning. This can be seen by the obtained results for the 1050/6082 and 6082/1050 FSPed dissimilar joints. As a result, it can be concluded that multi-pass friction stir processing improves mechanical properties significantly.

5.2 Recommendations

The aluminium alloys 1050 and 6082 were the focus of this thesis. According to the outcomes of this study, multi-pass FSP can be used to improve the mechanical properties of dissimilar materials. In the future, a comparison study of different grades of dissimilar aluminium alloys of the multi-pass FSP should be considered. During multi-pass, it would be advisable to consider the effects of using different tool geometries. The relationship between tool circulation and traverse velocities must be carefully considered to manage thermal energy and eliminate defects, which is the most critical element during processing.

REFERENCES

1.Chung, D.D. 2010. *Composite materials: science and applications*. Springer Science and Business Media.

2. Liu, H.J., Fujii, H., Maeda, M. and Nogi, K. 2003. Mechanical properties of friction stir welded joints of 1050–H24 aluminium alloy. *Science and technology of welding and joining*, *8*(6), pp.450-454. https://doi.org/10.1179/136217103225005598

3. Ilangovan, M., Boopathy, S.R. and Balasubramanian, V. 2015. Microstructure and tensile properties of friction stir welded dissimilar AA6061–AA5086 aluminium alloy joints. *Transactions of Nonferrous Metals Society of China*, *25*(4), pp.1080-1090.https://doi.org/10.1016/S1003-6326(15)63701-3.

4. Ashby, M.F. and Zones, D.R.H. 1998. Engineering Materials. Butterworth-Heinemann, vol. 2, 2nd edition.

5. Sampath, P., Parangodath, V.K., Udupa, K.R. and Kuruveri, U.B. 2015. Fabrication of friction stir processed Al-Ni particulate composite and its impression creep behaviour. *Journal of Composites,* 428630: pp.1-9. https://doi.org/10.1155/2015/428630.

6. Cam, G. and Kocak, M. 1998. Progress in joining of advanced materials. *Int. Mater. Rev,* 43(1): pp.–44.

7. Nicholas, E.D. 1998. Developments in the friction stir welding of metals. In Proceedings of the 6th International Conference on Aluminium Alloys, Toyohashi, Japan, 5–10: pp.139–151.

8. Patel, V., Li, W., Wang, G., Wang, F., Vairis, A. and Niu, P. 2019. Friction stir welding of dissimilar aluminium alloy combinations: State-of-the-art. *Metals, 9*: p.270.

9. Gupta, M.K. 2020. Friction stir process: a green fabrication technique for surface composites - a review paper. *SN Appl. Sci,* 2: p.532. https://doi.org/10.1007/s42452-020-2330-2.

10. Mabuwa, S. and Msomi, V. 2020. The effect of friction stir processing on the friction stir welded AA1050-H14 and AA6082-T6 joints. *Mater. Today: Proceedings, 26 (2)*: pp.193–199.

11. Seifiyan, H., Sohi, M.H., Ansari, M., Ahmadkhaniha, D., Saremi, M. 2019. Influence of friction stir processing conditions on corrosion behavior of AZ31B magnesium alloy. *Journal of Magnesium and Alloys, 7 (4):* pp.605–616.

12. Mishra, R.S., Mahoney, M.W., Mcfadden, S.X., Mara, N.A. & Mukherjee, A.K. 2000. *Scripta Mater, 42:* pp.163–168.

13. Berbon, P.B., Bingel, W.H., Mishra, R.S., Bampton, C.C. & Mahoney, M.W. 2001. *Scripta Mater, 44:* pp.61–66.

14. Ma, Z.Y., Mishra, R.S. and Mahoney, M.W. 2002. Superplastic deformation behaviour of friction stir processed 7075Al alloy. *Acta materialia*, *50*(17): pp.4419-4430.

15. Mishra, R.S., Ma, Z.Y. and Charit, I. 2003. Friction stir processing: a novel technique for fabrication of surface composite. *Materials Science and Engineering: A*, *341*(1-2): pp.307-310.

16. Kwon, Y.J., Shigematsu, I. and Saito, N. 2003. Grain refinement and mechanical property improvements in aluminium alloys using the friction stir process. *Nippon Kinzoku Gakkaishi (1952)*, *67*(10): pp.547-554.

17. Liu, H.J., Fujii, H. and Nogi, k. 2004. Mater. Sci. Tech, 20: pp.399–402.

18. Ma, Z.Y., Mishra, R.S. and Mahoney, M.W. 2004. Superplasticity in cast A356 induced via friction stir processing. *Scripta Materialia*, *50*(7): pp.931-935.

19. Sharma, S.R., Ma, Z.Y. and Mishra, R.S. 2004. Effect of friction stir processing on fatigue behavior of A356 alloy. *Scripta Materialia*, *51*(3): pp.237-241.

20. Santella, M.L., Engstrom, T., Storjohann, D. and Pan, T.Y. 2005. Effects of friction stir processing on mechanical properties of the cast aluminium alloys A319 and A356. *Scripta materialia*, *53*(2): pp.201-206. https://doi.org/10.1016/j.scriptamat.2005.03.040.

21. Charit, I. and Mishra, R.S. 2005. Low temperature superplasticity in a friction-stir-processed ultrafine grained Al–Zn–Mg–Sc alloy. *Acta Materialia*, *53*(15): pp.4211-4223.

22. Mishra, R.S. and Ma, Z.Y. 2005. Friction stir welding and processing. *Materials Science and Engineering: R,* 50, pp.1–78. https://doi.org/10.1016/j.mser.2005.07.001.

23. Su, J.Q., Nelson, T.W. and Sterling, C.J. 2005. *Mater. Sci. Eng: A, 405*. pp.277–286.

24. Thomas, W.M. 1991. International Patent Application No. PCT/GB92/02203 and GB Patent Application No. 9125978.8, 6, U.S. Patent No. 5,460,317.

25. Ma, Z.Y., Sharma, S.R., Mishra, R.S. and Mahoney, M.W. 2003, January. Microstructural modification of cast aluminium alloys via friction stir processing. In *Materials Science Forum*,Vol. 426, No. 4; pp. 2891-2896. Transtec Publications; 1999.

26. Spowart, J.E., Ma, Z.Y., Mishra, R.S., Jata K.V., Mahoney M.W. and Semiatin, S.L. 2003. Friction stir welding and processing II. Warrendale: TMS: pp. 243-252.

27. Jana, S., Mishra, R.S. and Grant, G. 2015. *Friction stir casting modification for enhanced structural efficiency: a volume in the friction stir welding and processing book series*. Butterworth-Heinemann.

28. Węglowski, M.S., Sędek, P. and Hamilton, C. 2016. The effect of process parameters on residual stress in a friction stir processed cast aluminium alloy AlSi9Mg. *Engineering Transactions*, *64*(3): pp.301-309.

29. Mahoney, M.W., Rhodes, C.G., Flintoff, J.G., Bingel, W.H. and Spurling, R.A. 1998. Properties of friction-stir-welded 7075 T651 aluminium. *Metallurgical and materials transactions A*, *29*(7): pp.1955-1964.

30.Mishra, R.S. and Mahoney, M.W. 2001. Friction stir processing: a new grain refinement technique to achieve high strain rate superplasticity in commercial alloys. In *Materials Science Forum;* Trans Tech Publications Ltd, 357: pp. 507-514

31. Benavides, S., Li, Y., Murr, L.E. and Mishra, R.S. 2000. Ultrafine Grained Materials. The Minerals, Metals and Materials Society; p. 155.

32. Saito, N., Shigematsu, I., Komaya, T., Tamaki, T., Yamauchi, G. and Nakamura, M. 2001. Grain refinement of 1050 aluminium alloy by friction stir processing. *Journal of materials science letters*, *20*(20): pp.1913-1915.

33.Kwon, Y.J., Saito, N. and Shigematsu, I. 2002. Friction stir process as a new manufacturing technique of ultrafine grained aluminium alloy. *Journal of materials science letters*, *21*(19): pp.1473-1476.

34. Ma, Z.Y. 2008. "Friction Stir Processing Technology: A Review," *Metallurgical and Materials Transactions A,* vol. 39: pp. 642-658. https://doi.org/10.1007/s11661-007-9459-0

35. Patel, V.V., Badheka, V. and Kumar, A. 2016. Friction stir processing as a novel technique to achieve superplasticity in aluminium alloys: process variables, variants, and applications. *Metallography, Microstructure, and Analysis*, *5*(4): pp.278-293.

36.Sun, N. and Apelian, D., 2011. Friction stir processing of aluminium cast alloys for high performance applications. *JOM*, *63*(11): pp.44-50.

37.Salih, O.S., Ou, H., Sun, W. and McCartney, D.G. 2015. A review of friction stir welding of aluminium matrix composites. *Materials & Design*, *86*: pp.61-71.

38. McNelley, T.R., Swaminathan, S. and Su, J.Q. 2008. Recrystallization mechanisms during friction stir welding/processing of aluminium alloys. *Scripta materialia*, *58*(5): pp.349-354.

39. Ma, Z.Y., Sharma, S.R. and Mishra, R.S. 2006. Effect of friction stir processing on the microstructure of cast A356 aluminium. *Materials Science and Engineering: A*, *433*(1-2): pp.269-278.

40. John Baruch, L., Raju, R., Balasubramanian, V., Rao, A.G. I. and Dinaharan. 2016. Influence of Multi-pass Friction Stir Processing on Microstructure and Mechanical Properties of Die Cast Al–7Si–3Cu Aluminium Alloy. Acta Metall. Sin. (Engl. Lett.), 29(5): pp.431–440, https://doi.org/10.1007/s40195-016-0405-2.

41. Andalucia, G. 2013. Aluminium Alloy 1050: 1050.

42. Birol, Y. 2015. Effect of extrusion press exit temperature and chromium on grain structure of EN AW 6082 alloy forgings. *Materials Science and Technology*, *31*(2): pp.207-211.

43. Chang, Y.L., Hung, F.Y. and Lui, T.S. 2019. Study of microstructure and tensile properties of infrared-heat-treated cast-forged 6082 aluminium alloy. *Journal of Materials Research and Technology*, *8*(1): pp.173-179.

44. Chen, X. 2017. Introduction. In: New Strategies for N-Heterocyclic Carbenes Catalyzed Annulations. *Springer Thesis (Recognizing Outstanding Ph.D. Research). Springer, Singapore.* pp.1–28. https://doi.org/10.1007/978-981-10-2899-1_1

45.Kubit, A., Wydrzynski, D. and Trzepiecinski, T. 2018. Refill friction stir spot welding of 7075-T6 aluminium alloy single-lap joints with polymer sealant interlayer. *Composite Structures*, *201*: pp.389-397.

46. Chandana, A., Lawrence, I.D. and Jayabal, S. 2018.Characterization of Particulate-Reinforced Aluminium 7075/TiB2 Composites. *Materials. Today Proc. 5*: pp. 4317–14326, https://doi.org/10.1016/j.matpr.2018.03.014.

47. Bhaskar, K.V., Sundarrajan, S., Rao, B.S. and Ravindra, K. 2018. Effect of reinforcement and wear parameters on dry sliding wear of aluminium composites-a review. *Materials today: proceedings*, *5*(2): pp.5891-5900. https://doi.org/10.1016/j.matpr.2017.12.188.

48. Kalaiselvan, K., Dinaharan, I. and Murugan, N. 2014. Characterization of friction stir welded boron carbide particulate reinforced AA6061 aluminium alloy stir cast composite. *Materials & Design 55:* pp.176-182. https://doi.org/10.1016/j.matdes.2013.09.067

49. Mishra, R., Johannes, L., Charit, I. and Dutta, A. 2005. Multi-pass friction stir superplasticity in aluminium alloys. In *Proceedings of NSF DMII Grantee Conference, Scottsdale, Arizona, DMI-0323725*.

50. Salem, H.G., Reynolds, A.P. and Lyons, J.S. 2002. Microstructure and retention of superplasticity of friction stir welded superplastic 2095 sheet. *Scripta materialia*, *46*(5): pp.337-342.

51. Charit, I. and Mishra, R.S. 2003. High strain rate superplasticity in a commercial 2024 Al alloy via friction stir processing. *Materials Science and Engineering: A*, *359*(1-2): pp. 290-296.

52. Dutta, A., Charit, I., Johannes, L.B. and Mishra, R.S. 2005. Deep cup forming by superplastic punch stretching of friction stir processed 7075 Al alloy. *Materials Science and Engineering: A*, *395*(1-2): pp.173-179.

53. Purcek, G., Saray, O., Karaman, I. and Kucukomeroglu, T. 2008. Effect of severe plastic deformation on tensile properties and impact toughness of two-phase Zn–40Al alloy. *Materials Science and Engineering: A*, *490*(1-2): pp.403-410.

54. Azushima, A., Kopp, R., Korhonen, A., Yang, D.Y., Micari, F., Lahoti, G.D., Groche, P., Yanagimoto, J., Tsuji, N., Rosochowski, A., Yanagida, A. 2008. *CIRP Ann-Manuf. Techn. 57*: pp.716-735.

55. Valiev, R.Z. and Langdon, T.G. 2006. Principles of equal-channel angular pressing as a processing tool for grain refinement. *Progress in materials science*, *51*(7): pp.881-981.

56. Johannes, L.B. and Mishra, R.S. 2007. Multiple passes of friction stir processing for the creation of superplastic 7075 aluminium. *Materials Science and Engineering: A*, *464*(1-2), pp.255-260. https://doi.org/10.1016/j.msea.2007.01.141.

57. Chuang, C.H., Huang, J.C. and Hsieh, P.J. 2005. Using friction stir processing to fabricate MgAlZn intermetallic alloys. *Scripta Materialia*, *53*(12): pp.1455-1460.

58. Xue, P., Xiao, B.L. and Ma, Z.Y. 2013. Achieving large-area bulk ultrafine grained Cu via submerged multiple-pass friction stir processing. *Journal of Materials Science & Technology*, *29*(12): pp.1111-1115.

59. Zheng, F.Y., Wu, Y.J., Peng, L.A., Li, X.W., Fu, P.H. and Ding, W.J. 2013. Microstructures and mechanical properties of friction stir processed Mg–2.0 Nd–0.3 Zn–1.0 Zr magnesium alloy. *journal of magnesium and alloys*, *1*(2): pp.122-127.

60. Ma, Z.Y., Sharma, S.R. and Mishra, R.S., 2006a. Effect of multiple-pass friction stir processing on microstructure and tensile properties of a cast aluminium–silicon alloy. *Scripta materialia*, *54*(9): pp.1623-1626.

61. Zhang, D., Suzuki, M. and Maruyama, K. 2005. Microstructural Evolution of a Heat Resistant Magnesium Alloy due to Friction Stir Welding. *Scripta Materialia, Vol. 52*: pp. 899-903.

62.Ma, Z.Y., Sharma, S.R. and Mishra, R.S. 2006. Microstructural modification of as-cast Al-Si-Mg alloy by friction stir processing. *Metallurgical and Materials Transactions A*, *37*(11): pp.3323-3336.

63. Ma, Z.Y., Pilchak, A.L., Juhas, M.C. and Williams, J.C. 2008. Microstructural refinement and property enhancement of cast light alloys via friction stir processing. *Scripta Materialia*, *58*(5): pp.361-366.

64. Kwon, Y.J., Shigematsu, I. and Saito, N. 2003. Mechanical properties of fine-grained aluminium alloy produced by friction stir process. *Scripta materialia*, *49*(8), pp.785-789.

65. Yadav, D. and Bauri, R. 2012. Effect of friction stir processing on microstructure and mechanical properties of aluminium. *Materials Science and Engineering: A*, *539*: pp.85-92. https://doi.org/10.1016/j.msea.2012.01.055.

66. Jana, S., Mishra, R.S., Baumannn, J.B. and Grant, G. 2009. Effect of stress ratio on the fatigue behavior of a friction stir processed cast Al–Si–Mg alloy. *Scripta Materialia,* 61: pp. 992–995, https://doi.org/10.1016/j.scriptamat.2009.08.011.

67. Akinlabi, E., Oyindamola, K., Olufayo, O. and Agarana, M. 2018. Effect of multi-pass friction stir processing on mechanical properties of AA6061-T6. IJMET, 9:6: pp.667–679.

68. Yang, R., Zhang, Z., Zhao, Y., Chen, G., Guo, Y., Liu, M. and Zhang, J. 2015. Effect of multi-pass friction stir processing on microstructure and mechanical properties of Al3Ti/A356 composites. *Materials Characterization*, vol. 106: pp. 62-69. DOI: 10.1016/j.matchar.2015.05.019.

69. El-Rayes, M.M. and El-Danaf, E.A. 2012. The influence of multi-pass friction stir processing on the microstructural and mechanical properties of Aluminium Alloy 6082. *Journal of Materials Processing Technology*, *212*(5): pp.1157-1168.
DOI: 10.1016/j.jmatprotec.2011.12.017

70. Gan, W.Y., Zheng, Z.H.O.U., Zhang, H. and Tao, P.E.N.G. 2014. Evolution of microstructure and hardness of aluminium after friction stir processing. *Transactions of Nonferrous Metals Society of China*, *24*(4): pp.975-981.https://doi.org/10.1016/S1003-6326(14)63151-4.

71. Węglowski, M.S., 2014. Microstructural characterisation of friction stir processed cast AlSi9Mg aluminium alloy. *Archives of Foundry Engineering*, *14*(3 spec.): pp.75-78.

72. Charit, I., Mishra, R.S. and Mahoney, M.W. 2002. Multi-sheet structures in 7475 aluminium by friction stir welding in concert with post-weld superplastic forming. *Scripta Materialia*, *47*(9): pp.631-636.

73.Johannes, L.B., Charit, I., Mishra, R.S. and Verma, R. 2007i. Enhanced superplasticity through friction stir processing in continuous cast AA5083 aluminium. *Materials Science and Engineering: A*, *464*(1-2): pp.351-357. https://doi.org/10.1016/j.msea.2007.02.012

74. Johannes, L.B. and Mishra, R.S. 2007ii. 'Multiple passes of friction stir processing for the creation of plastic 7050 aluminium'. *Materials Science and Engineering,A; 463*: pp.255- 260.

75. Liu, F.C. and Ma, Z.Y. 2008. Low-temperature superplasticity of friction stir processed Al–Zn–Mg–Cu alloy. *Scripta Materialia*, *58*(8): pp.667-670.

76. Paidar, M., Ojo, O.O., Ezatpour, H.R. and Heidarzadeh, A. 2019. Influence of multi-pass FSP on the microstructure, mechanical properties and tribological characterization of Al/B4C composite fabricated by accumulative roll bonding (ARB). *Surface and Coatings Technology*, *361*: pp.159-169. https://doi.org/10.1016/j.surfcoat.2019.01.043.

77. Krishna, V.V.M.G. and Satyanarayana, K. 2015. Microstructure and mechanical properties of multi-pass friction stir processed aluminium silicon carbide metal matrix. *International Journal of Scientific Engineering and Technology, vol. 42 (2)* pp. 88-90, DOI: 10.17950/ijset/v4s2/212.

78. Wais, A.M.H., Salman, J.M. and Al-Roubaiy, A.O., 2013. Effect of friction stir processing on mechanical properties and microstructure of the cast pure aluminum. *international journal of scientific & technology research*, *2*(12).

79. Tutunchilar, S., Besharati Givi, M.K., Haghpanahi, M. and Asad, P. 2012. Eutectic Al-Si Piston Alloy Surface Trandformed to Modified Hypereutectic Alloy via FSP. *Mater.Sci.Eng. A,534:* pp. 557–567.

80. Mahmoud, T.S and Mohamed S.S. 2012. Improvement of Microstructural, Mechanical and Tribological Characteristics of A413 Cast Al Alloys Using Friction Stir Processing. *Mater.Sci.Eng. A,558:* pp.502–509.

81. Chen, Y., Ding, H., Li, J., Cai, Z., Zhao, J. and Yang, W. 2016. Influence of multi-pass friction stir processing on the microstructure and mechanical properties of Al-5083 alloy. *Mater. Sci. Eng. A, 650*: pp.281–289. https://doi.org/10.1016/j.msea.2015.10.057.

82. Salman, J.M., 2014. Effect of Friction Stir Processing on Some Mechanical Properties and Microstructure of Cast (Al-Zn-/mg-Cu) Alloy. *Journal of University of Babylon*, *22*(2).

83. Hashim, F.A., Salim, R.K. and Khudair, B.H. 2015. Effect of friction stir processing on (2024-T3) aluminium alloy. *International Journal of Innovative Science Engineering and Technology*, *4*: pp.1822-1829. *DOI: 10.15680/ijirset.2015.0404003.*

84. Sun, N. and Apelian, D. 2009. Microstructural modification of A206 aluminium via friction stir processing. In *Materials Science Forum*; Trans Tech Publications Ltd, Vol. 618: pp. 361-364. DOI:10.4028/www.scientific.net/MSF.618-619.361.

85. Karthikeyan, L., Senthilkumar, V.S., Balasubramanian, V. and Natarajan, S. 2009. Mechanical property and microstructural changes during friction stir processing of cast *aluminium* 2285 alloy*. Materials & Design, 30(6):* pp.2237-2242.

86. Rahsepar, M. and Jarahimoghadam, H. 2016. The influence of multi-pass friction stir processing on the corrosion behavior and mechanical properties of zirconreinforced Al metal matrix composites. *Mater. Sci. Eng. 671*: pp. 214–220. https://doi.org/10.1016/j.msea.2016.05.0.

87. Barmouz, M. and Givi, M.K.B. 2011. Fabrication of in situ Cu/SiC composites using multi-pass friction stir processing: Evaluation of microstructural, porosity, mechanical and electrical behavior. *Composites Part A: Applied Science and Manufacturing*, *42*(10): pp.1445-1453. https://doi.org/10.1016/j.compositesa.2011.06.010.

88. Mahoney, M.W., Mishra, R.S., *Nelson, T., Flintoff, J., Islamgaliev, R. and Hovansky, Y.* 2001. High strain rate, Thick section superplasticity created via friction stir processing. *Friction Stir welding and Processing,* pp.183-194.

89. Ma, S.M., Zhang, P., Ji, G., Chen, Z., Sun, G.A., Zhong, S.Y., Ji, V. and Wang, H.W. 2014. Microstructure and mechanical properties of friction stir processed Al–Mg–Si alloys dispersion-strengthened by nanosized TiB2 particles. *Journal of alloys and compounds*, *616*: pp.128-136.

90. Guo, J.F., Liu, J., Sun, C.N., Maleksaeedi, S., Bi, G., Tan, M.J. and Wei, J. 2014. Effects of nano-Al2O3 particle addition on grain structure evolution and mechanical behaviour of friction-stir-processed Al. *Materials Science and Engineering: A*, *602*: pp.143-149.

91. Palani, K., Elanchezhian, C., Avinash, K., Karthik, C., Chaitanya, K., Sivanur, K. and Reddy, K.Y. 2018, July. Influence of Friction Stir Processing Parameters on Tensile properties and Microstructure of Dissimilar AA 8011-H24 and AA 6061-T6 aluminium alloy joints in Nugget Zone. In IOP Conference Series: *Materials Science and Engineering (Vol. 390)*, *No. 1:* p. 012108.

92. Palani, K., Elanchezhian, C., Saiprakash, K. H.V., Sreekanth, K., Dayanand, K., Kmar, D. Kumar. 2018. Effect of welding parameters on mechanical properties of dissimilar Friction Stir Processed AA 8011 and AA 5083-H321 aluminium alloys, *IOP Conf. Series: Materials Science and Engineering, 390: p.*012072.

93. Kumar, N., Mishra, R.S.and Huskamp, C.S. and Sankaran, K.K. 2011. Microstructure and mechanical behavior of friction stir processed ultrafine grained Al–Mg–Sc alloy. *Materials Science and Engineering: A*, *528*(18): pp.5883-5887.

94. Cui, G.R., Ni, D.R., Ma, Z.Y. and Li, S.X. 2014. Effects of friction stir processing parameters and in situ passes on microstructure and tensile properties of Al-Si-Mg casting. *Metallurgical and Materials Transactions A*, *45*(12): pp.5318-5331.

95. Rao, A.G., Katkar, V.A., Gunasekaran, G., Deshmukh, V.P., Prabhu, N. and Kashyap, B.P., 2014. Effect of multi-pass friction stir processing on corrosion resistance of hypereutectic Al–30Si alloy. *Corrosion Science*, *83*: pp.198-208.

96. Asadi, P., Faraji, G., Masoumi, A. and Givi, M.B. 2011. Experimental investigation of magnesium-base nanocomposite produced by friction stir processing: effects of particle types and number of friction stir processing passes. *Metallurgical and Materials Transactions A*, *42*(9): pp.2820-2832.

97. Nakata, K., Kim, Y.G., Fujii, H., Tsumura, T. and Komazaki, T. 2006. Improvement of mechanical properties of aluminium die casting alloy by multi-pass friction stir processing. *Materials Science and Engineering: A*, *437*(2): pp.274-280. https://doi.org/10.1016/j.msea.2006.07.150.

98. Surekha, K., Murty, B.S. and Rao, K.P. 2008. Microstructural characterization and corrosion behavior of multi-pass friction stir processed AA2219 aluminium alloy. *Surface and Coatings Technology*, *202*(17): pp.4057-4068. https://doi.org/10.1016/j.surfcoat.2008.02.001.

99. Al-Fadhalah, K.J., Almazrouee, A.I. and Aloraier, A.S. 2014. Microstructure and mechanical properties of multi-pass friction stir processed aluminium alloy 6063. *Materials & Design*, *53*: pp.550-560.

100. Pradeep, S. and Pancholi, V. 2013. Effect of microstructural inhomogeneity on superplastic behaviour of multi-pass friction stir processed aluminium alloy. *Materials Science and Engineering: A*, *561*: pp.78-87.

101. Mishra, R.S. and Mahoney, M.W. 2007. Friction Stir Welding and Processing. *ASM International*: 368.

102. Li, B., Shen, Y. and Hu, W. 2013. Surface nitriding on Ti–6Al–4V alloy via friction stir processing method under nitrogen atmosphere. *Applied surface science*, *274*: pp.356-364.

103. Su, J.-Q., Nelson, T.W. and Sterling, C.J. 2005. Friction stir processing of large-area bulk UFG aluminium alloys. *Scripta Materialia, 52(2)*: pp.135–140. https://doi.org/10.1016/j.scriptamat.2004.09.014.

104. Aktarer, S.M., Sekban, D.M., Saray, O., Kucukomeroglu, T., Ma, Z.Y. and Purcek, G. 2015. Effect of two-pass friction stir processing on the microstructure and mechanical properties of as-cast binary Al–12Si alloy. *Material science and Engineering: A, 636*: pp.311–319, https://doi.org/10.1016/j.msea.2015.03.111.

105. Nadammal, N., Kailas, S.V., Szpunar, J. and Suwas, S., 2017. Microstructure and texture evolution during single-and multiple-pass friction stir processing of heat-treatable aluminium alloy 2024. *Metallurgical and Materials Transactions A*, *48*(9), pp.4247-4261. https://doi.org/10.1007/s11661-017-4184-9

106. Ma, Z.Y., Mishra, R.S. and Liu, F.C. 2009. Superplastic behavior of micro-regions in two-pass friction stir processed 7075Al alloy. *Materials Science and Engineering: A*, *505*(1-2): pp.70-78.

107. Sinhmar, S., Dwivedi, D.K. and Pancholi, V. 2014, December. Friction stir processing of AA 7039 alloy. *In Int. Conf. Prod. Mech. Eng*, pp. 77-78. http://dx.doi.org/10.15242/IAE.IAE1214206.

108. Nascimento, Santos, F.T., Vilaça, P., Miranda, R.M., Quintino, L. 2009. Microstructural modification and ductility enhancement of surfaces modified by FSP in aluminium alloys, *Materials Science and Engineering: A,506(1)*: pp.16-22. Doi: https://doi.org/10.1016/j.msea.2009.01.008

109. Mabuwa, S. and Msomi, V. 2021. Analysis of mechanical properties between submerged and normal multiple-pass friction stir processing of the FSWed dissimilar aluminium joints. *Materials Today: Proceedings*. https://doi.org/10.1016/j.matpr.2021.02.101.

110. Mabuwa, S and Velaphi, M. 2020 Fatigue behaviour of the multi-pass friction stir processed AA8011-H14 and AA6082-T651 dissimilar joints*. Engineering Failure Analysis,118*, 104876,13506307. https://doi.org/10.1016/j.engfailanal.2020.104876.

111. Muribwathoho, O., Msomi, V., Mabuwa, S. and Motshwanedi, S.S. 2021. Impact of multi-pass friction stir processing on microhardness of AA1050/AA6082 dissimilar joints. *Materials Today: Proceedings*, pp2214-7853, Doi=https://doi.org/10.1016/j.matpr.2020.11.587.

112. Brown, R., Tang, W. and Reynolds, A.P. 2009. Multi-pass friction stir welding in alloy 7050-T7451: Effects on weld response variables and on weld properties. *Materials Science and Engineering: A*, *513*: pp.115-121. https://doi.org/10.1016/j.msea.2009.01.041.

113. Senthilkumar, R., Prakash, M., Arun, N. and Jeyakumar, A.A. 2019. The effect of the number of passes in friction stir processing of aluminium alloy (AA6082) and its failure analysis. *Applied Surface Science*, *491*: pp.420-431.

114. Shankar, M.R., Chandrasekar, S., Compton, W.D. and King, A.H. 2005. Characteristics of aluminium 6061-T6 deformed to large plastic strains by machining. *Materials Science and Engineering: A*, *410*: pp.364-368. DOI: 10.1016/j.msea.2005.08.137.

115. Ravikumar, E., Arunkumar, N. and Sunnapa, G.S. 2013, April. Characterization of mechanical properties of aluminium (AA 6061-T6) by friction welding. In *3rd International Conference on mechanical, automotive and materials engineering (ICMAME)*. Singapore, pp. 127 - 131.

116. Sato, Y.S., Urata, M., Kokawa, H. and Ikeda, K. 2003. Hall–Petch relationship in friction stir welds of equal channel angular-pressed aluminium alloys. *Materials Science and Engineering: A*, *354*(1-2): pp.298-305. DOI: 10.1016/s0921-5093(03)00008-x.

117. Meenia, S., Khan, F., Babu, S., Immanuel, R.J., Panigrahi, S.K. and Ram, G.J. 2016. Particle refinement and fine-grain formation leading to enhanced mechanical behaviour in a hypo-eutectic Al–Si alloy subjected to multi-pass friction stir processing. *Materials Characterization*, *113*: pp.134-143. https://doi.org/10.1016/j.matchar.2016.01.011.

118. Rao, A.G., Rao, B.R.K., Deshmukh, V.P., Shah, A.K. and Kashyap, B.P. 2009. Microstructural refinement of a cast hypereutectic Al–30Si alloy by friction stir processing. *Materials Letters*, *63*(30): pp.2628-2630. https://doi.org/10.1016/j.matlet.2009.09.022.

119. Pradeep, S., Sharma, S.K. and Pancholi, V. 2012. Microstructural and mechanical characterization of friction stir processed 5086 aluminium alloy. *In Materials Science Forum; Trans Tech Publications Ltd, Vol. 710:* pp. 253-257. https://doi.org/10.4028/www.scientific.net/msf.710.253

120. Ramesh, K.N., Pradeep, S. and Pancholi, V. 2012. Multi-pass friction-stir processing and its effect on mechanical properties of aluminium alloy 5086. *Metallurgical and Materials Transactions A*, *43*(11): pp.4311-4319. https://doi.org/10.1007/s11661-012-1232-3.

121. Mandal, P.K. 2021. Surface modification of Aluminium alloy (7xxx series) by multi-pass friction stir processing. *Global Journal of Engineering and Technology Advances*, *6*(2): pp.008-017. DOI: https://doi.org/10.30574/gjeta.2021.6.2.0127

122. Ghanbari, D., Asgarani, M.K., Amini, K. and Gharavi, F. 2017. Influence of heat treatment on mechanical properties and microstructure of the Al2024/SiC composite produced by multi–pass friction stir processing. *Measurement*, *104*: pp.151-158. https://doi.org/10.1016/j.measurement.2017.03.024.

123. Mirjavadi, S.S., Alipour, M., Hamouda, A.M.S., Matin, A., Kord, S., Afshari, B.M. and Koppad, P.G. 2017. Effect of multi-pass friction stir processing on the microstructure, mechanical and wear properties of AA5083/ZrO2 nanocomposites. *Journal of Alloys and Compounds*, *726*: pp.1262-1273. https://doi.org/10.1016/j.jallcom.2017.08.084.

124. Matsuda, Y., Itoh, G. and Motohashi, Y. 2012. Microstructure control and mechanical properties of 7075 aluminium alloy by means of multi-pass friction stir processing. *Advanced Materials Research, 409*: pp281–286. https://doi.org/10.4028/www.scientific.net/amr.409.281.

125. Rastabi, S.A. and Mosallaee, M. 2020. Effect of multi-pass friction stir processing and Mg addition on microstructure and tensile properties of Al-1050 alloy. *Int. J. Miner. Metall. Mater*, pp.1-24. https://doi.org/10.1007/s12613-020-2074-4.

126. Paidar, M., Asgari, A., Ojo, O.O. and Saberi, A. 2018. Mechanical properties and wear behavior of AA5182/WC nanocomposite fabricated by friction stir welding at different tool traverse speeds. *Journal of Materials Engineering and Performance*, *27*(4), pp.1714-1724. https://doi.org/10.1007/s11665-018-3297-7.

127. Chen, Y., Ding, H., Malopheyev, S., Kaibyshev, R., Cai, Z. and Yang, W. 2017. Influence of multi-pass friction stir processing on microstructure and mechanical properties of 7B04-O Al alloy. *Trans. Nonfer. Met. Soc. China, 27(4)*: pp.789–796. https://doi.org/10.1016/s1003-6326(17)60090-6.

128. Moharrami, A., Razaghian, A., Paidar, M., Šlapáková, M., Ojo, O.O. and Taghiabadi, R. 2020. Enhancing the mechanical and tribological properties of Mg2Si-rich aluminium alloys by multi-pass friction stir processing. *Materials Chemistry and Physics*, *250*: p.123066. https://doi.org/10.1016/j.matchemphys.2020.123066.

129. Mahmoud, T.S. 2013. Surface modification of A390 hypereutectic Al–Si cast alloys using friction stir processing. *Surface and Coatings Technology*, *228*: pp.209-220. https://doi.org/10.1016/j.surfcoat.2013.04.031.

130. Gandra, J., Miranda, R.M. and Vilaça, P. 2011. Effect of overlapping direction in multi-pass friction stir processing. *Materials Science and Engineering: A*, *528*(16-17): pp.5592-5599. https://doi.org/10.1016/j.msea.2011.03.105.

131. Moustafa, E. 2017. Effect of multi-pass friction stir processing on mechanical properties for AA2024/Al2O3 nanocomposites. *Materials*, *10*(9): p.1053. https://doi.org/10.3390/ma10091053.

132. Papantoniou, I.G., Markopoulos, A.P. and Manolakos, D.E. 2020. A new approach in surface modification and surface hardening of aluminium alloys using friction stir process: Cu-reinforced AA5083. *Materials*, *13*(6): p.1278. https://doi.org/10.3390/ma13061278.

133. Gangil, N., Maheshwari, S. and Siddiquee, A.N. 2018. Multi-pass FSP on AA6063-T6 Al: Strategy to fabricate surface composites. *Materials and manufacturing Processes*, *33*(7): pp.805-811. https://doi.org/10.1080/10426914.2017.1415448.

134. Satyanarayana, M.V.N.V. and Kumar, A. 2019, July. Effect of heat treatment on AA2014 alloy processed through multi-pass friction stir processing. In *Journal of Physics: Conference Series*, Vol. 1240, No.1: p.012077. IOP Publishing. https://doi.org/10.1088/1742-6596/1240/1/012077.

135. García-Vázquez, F., Vargas-Arista, B., Muñiz, R., Ortiz, J.C., García, H.H. and Acevedo, J. 2016. The role of friction stir processing (FSP) parameters on TiC reinforced surface Al7075-T651 aluminium alloy. Soldagem & Inspeção, 21(4): pp.508-516. http://dx.doi.org/10.1590/0104-9224/SI2104.10.

136. Lu, D.H., Wei, S.S., Zhou, M., Jiang, Y.H. and Zhou, R. 2011. Effects of the parameters of friction stir processing on silicon particles and hardness in hypereutectic Al-Si alloys. In *Advanced Materials Research*; Trans Tech Publications Ltd, Vol. 148: pp. 1689-1694.

137. Hajizamani, M. and Alizadeh, M. 2017. Modification of microstructure and mechanical properties of Al–Zn–Mg/3 wt.% Al2O3 composite through semi-solid thermomechanical processing using variable loads. *International Journal of Materials Research*, *108*(10): pp.840-847.

138. Handbook, A.S.M., 1989. Volume 16: machining. *ASM International Handbook Committee, ASM International, Electronic*.

139.Khojastehnezhad, V.M., Pourasl, H.H. and Vatankhah Barenji, R., 2019. Effect of tool pin profile on the microstructure and mechanical properties of friction stir processed Al6061/Al2O3—TiB2 surface hybrid composite layer. *Proceedings of the Institution of Mechanical Engineers, Part L: Journal of Materials: Design and Applications*, *233*(5), pp.900-912.

140. Khodir, S.A. and Shibayanagi, T. 2008. Friction stir welding of dissimilar AA2024 and AA7075 aluminium alloys. *Materials Science and Engineering: B*, *148*(1-3): pp.82-87.

141. Fuller, C.B., Mahoney, M.W., Calabrese, M. and Micona, L. 2010. Evolution of microstructure and mechanical properties in naturally aged 7050 and 7075 Al friction stir welds. *Materials Science and Engineering: A*, *527*(9): pp.2233-2240.

142. Olea, C.A.W., Roldo, L., Dos Santos, J.F. and Strohaecker, T.R. 2007. A sub-structural analysis of friction stir welded joints in an AA6056 Al-alloy in T4 and T6 temper conditions. *Materials Science and Engineering: A*, *454*: pp.52-62.

143. Chandran, R. and Santhanam, S.K.V. 2018. Submerged friction stir welding of 6061-T6 aluminium alloy under different water heads. *Materials Research*, *21*.

144. Vaira Vignesh, R., Padmanaban, R. and Datta, M.2018. Influence of FSP on the microstructure, microhardness, intergranular corrosion susceptibility and wear resistance of AA5083 alloy. *Tribology-Materials, Surfaces & Interfaces*, *12*(3), pp.157-169.

145. Baghdadi, A.H., Selamat, N.F.M. and Sajuri, Z. 2017, September. Effect of tool offsetting on microstructure and mechanical properties dissimilar friction stir welded Mg-Al alloys. In *IOP Conference Series: Materials Science and Engineering* (Vol. 238, No. 1, p. 012018). IOP Publishing.

146. Xiaoping, L.U.O., Daqing, F.A.N.G., Qiushu, L.I. and Yuesheng, C.H.A.I. 2016. Microstructure and mechanical properties of An Mg-4.0 Sm-1.0 Ca alloy during thermomechanical treatment. *Journal of Rare Earths*, *34*(11), pp.1134-1138.

147. Ramaiyan, S., Santhanam, S.K.V. and Muthuguru, P. 2018. Effect of scroll pin profile and tool rotational speed on mechanical properties of submerged friction stir processed AZ31B magnesium alloy. *Materials Research*, *21*.

148. Chai, F., Zhang, D., Li, Y. and Zhang, W. 2013. High strain rate superplasticity of a fine-grained AZ91 magnesium alloy prepared by submerged friction stir processing. *Materials Science and Engineering: A*, *568*, pp.40-48.

149. Huang, G., Wu, J., Hou, W. and Shen, Y., 2018. Microstructure, mechanical properties and strengthening mechanism of titanium particle reinforced aluminum matrix composites produced by submerged friction stir processing. *Materials Science and Engineering: A*, *734*, pp.353-363.

150. Feng, A.H., Chen, D.L. and Ma, Z.Y. 2010. Microstructure and cyclic deformation behavior of a friction-stir-welded 7075 Al alloy. *Metallurgical and Materials Transactions A*, *41*(4): pp.957-971.

151. Mabuwa, S. and Msomi, V. 2020. Comparative analysis between normal and submerged friction stir processed friction stir welded dissimilar aluminium alloy joints. *Journal of Materials Research and Technology*, *9*(5): pp.9632-9644.

152. Ceschini, L., Boromei, I., Minak, G., Morri, A. and Tarterini, F. 2007. Effect of friction stir welding on microstructure, tensile and fatigue properties of the AA7005/10 vol.% Al2O3p composite. *Composites science and technology*, *67*(3-4): pp.605-615.

153. Dialami, N., Cervera, M. and Chiumenti, M. 2020. Defect formation and material flow in friction stir welding. *European Journal of Mechanics-A/Solids*, *80*, p.103912.

154. Netto NG. The Effect of Friction Stir Processing on the Microstructure and Tensile Behavior of Aluminium Alloys. 2018. UNF Graduate Thesis and Dissertations;790.

155. Mishra, R.S., De, P.S. and Kumar, N. 2014. Friction stir processing. In Friction stir welding and processing. *Springer International Publishing, Switzerland*, pp. 259-296.

156. Porter, D.A. and Easterling, K.E. 2009. Phase transformations in metals and alloys (revised reprint). *CRC press*.

157. Kianezhad, M. and Raouf, A.H. 2019. Effect of nano-Al2O3 particles and friction stir processing on 5083 TIG welding properties. *Journal of Materials Processing Technology*, *263*, pp.356-365.

158. Cavaliere, P. and Panella, F. 2008. Effect of tool position on the fatigue properties of dissimilar 2024-7075 sheets joined by friction stir welding. *Journal of materials processing technology*, *206*(1-3), pp.249-255.

159. Guo, J.F., Chen, H.C., Sun, C.N., Bi, G., Sun, Z. and Wei, J. 2014. Friction stir welding of dissimilar materials between AA6061 and AA7075 Al alloys effects of process parameters. *Materials & Design (1980-2015)*, *56*: pp.185-192.

160. Sadeesh, P., Kannan, M.V., Rajkumar, V., Avinash, P., Arivazhagan, N., Ramkumar, K.D. and Narayanan, S., 2014. Studies on friction stir welding of AA 2024 and AA 6061 dissimilar metals. *Procedia Engineering*, *75*, pp.145-149.

161. Mabuwa, S. and Msomi, V., 2019. Effect of friction stir processing on gas tungsten arc-welded and friction stir-welded 5083-H111 aluminium alloy joints. *Advances in Materials Science and Engineering*, pp1-15.

162. Ilangovan, M., Boopathy, S.R. & Balasubramanian, V. 2015. ScienceDirect Effect of tool pin profile on microstructure and tensile properties of friction stir welded dissimilar AA 6061 e AA 5086 aluminium alloy joints. *Defence Technology*, 11(2): 174–184. http://dx.doi.org/10.1016/j.dt.2015.01.004.

163.Silva, A.A.M., Arruti, E., Janeiro, G., Aldanondo, E., Alvarez, P. & Echeverria, A. 2011. Material flow and mechanical behaviour of dissimilar AA2024-T3 and AA7075-T6 aluminium alloys friction stir welds. *Materials and Design*, 32(4): 2021–2027. http://dx.doi.org/10.1016/j.matdes.2010.11.059.

164. Sameer, M.D. and Birru, A.K. 2019. Mechanical and metallurgical properties of friction stir welded dissimilar joints of AZ91 magnesium alloy and AA 6082-T6 aluminium alloy. *Journal of Magnesium and Alloys*, *7*(2): pp.264-271.

165. Lee, W.B., Yeon, Y.M. and Jung, S.B. 2003. The joint properties of dissimilar formed Al alloys by friction stir welding according to the fixed location of materials. *Scripta materialia*, *49*(5): pp.423-428.

166. Selvaraj, G., Karthikeyan, T., Mohanadass, R. and Indhumath, S., 2015. Investigation on mechanical properties of welded aluminium joints of aa 8011 using friction stir welding. *International journal of applied engineering research*, *10*(13), pp.11095-11100.

167. Braga, D.F.O., de Sousa, L.M.C., Infante, V, da Silva, L.F.M and Moreira, P.M.G. 2016 Aluminium Friction Stir Weld-bonded Joints. *The Journal of Adhesion,* 92: pp.665–78

168. Sathiskumar, R., Murugan, N., Dinaharan, I. and Vijay, S.J. 2013. Characterization of boron carbide particulate reinforced in situ copper surface composites synthesized using friction stir processing. *Materials characterization*, *84*: pp.16-27.

169. Khodabakhshi, F., Gerlich, A.P. and Švec, P. 2017. Fabrication of a high strength ultra-fine-grained Al-Mg-SiC nanocomposite by multi-step friction-stir processing. *Materials Science and Engineering: A*, *698*: pp.313-325.

170. Orłowska, M., Brynk, T., Hütter, A., Goliński, J., Enzinger, N., Olejnik, L. and Lewandowska, M. 2020. Similar and dissimilar welds of ultrafine grained aluminium obtained by friction stir welding. *Materials Science and Engineering: A*, *777*: p.139076.

171. Shunmugasundaram, M., Kumar, A.P., Sankar, L.P. and Sivasankar, S. 2020. Optimization of process parameters of friction stir welded dissimilar AA6063 and AA5052 aluminium alloys by Taguchi technique. *Materials Today: Proceedings*, *27 (2)*: pp.871-876.

172. Dieter, G.E. 1988. Mechanical Metallurgy; McGraw Hill: New York.

173. Peng, G., Ma, Y., Hu, J., Jiang, W., Huan, Y., Chen, Z. and Zhang, T. 2018. Nanoindentation hardness distribution and strain field and fracture evolution in dissimilar friction stir-welded AA 6061-AA 5A06 aluminium alloy joints. *Advances in Materials Science and Engineering*, pp.1-11.

174. Pantazopoulos, G.A. 2019. A short review on fracture mechanisms of mechanical components operated under industrial process conditions: fractographic analysis and selected prevention strategies. Metals, 9 (2): p.148.

175. Derazkola, H.A., Eyvazian, A. and Simchi, A. 2020. Submerged friction stir welding of dissimilar joints between an Al-Mg alloy and low carbon steel: thermo-mechanical modeling, microstructural features, and mechanical properties. *Journal of Manufacturing Processes*, *50*: pp.68-79.

176. John J., Shanmughanatan S.P., Kiran M.B.2018. Effect of tool geometry on microstructure and mechanical Properties of friction stir processed AA2024-T351 aluminium alloy*. Materials Today: Proceedings.* 5(1): 2965-2979

177. Paidar M., Vignesh R.V., Khorram A., Ojo O.O., Rasoulpouraghdam A., Pustokhina I.2020. Dissimilar modified friction stir clinching of AA2024-AA6061 aluminum alloys: Effects of materials positioning. Journal of Materials Research and Technology. 9(3): 6037-6047

178. Peng, G., Ma, Y., Hu, J., Jiang, W., Huan, Y., Chen, Z. and Zhang, T., 2018. Nanoindentation hardness distribution and strain field and fracture evolution in dissimilar friction stir-welded AA 6061-AA 5A06 aluminum alloy joints. *Advances in Materials Science and Engineering*, *2018*.

179. Khodabakhshi, F., Simchi, A., Kokabi, A.H. and Gerlich, A.P. 2015. Friction stir processing of an aluminum-magnesium alloy with pre-placing elemental titanium powder: in-situ formation of an Al3Ti-reinforced nanocomposite and materials characterization. *Materials Characterization*, *108*, pp.102-114.

180. Muribwathoho, O., Msomi, V., Mabuwa, S. and Merdji, A., 2021. The mechanical properties of AA6082/AA1050 dissimilar joints subjected to multi-pass friction stir processing. *Engineering Research Express*, *3*(3), p.035012.

181. Cabibbo, M., McQueen, H.J., Evangelista, E., Spigarelli, S., Di Paola, M. and Falchero, A. 2007. Microstructure and mechanical property studies of AA6056 friction stir welded plate. *Materials Science and Engineering: A*, *460 (461)*: pp.86-94.

182. Chen, Y.C., Feng, J.C. and Liu, H.J. 2009. Precipitate evolution in friction stir welding of 2219-T6 aluminium alloys. *Materials characterization*, *60* (6): pp.476-481.

183. Msomi, V. and Mabuwa, S. 2020. Analysis of material positioning towards microstructure of the friction stir processed AA1050/AA6082 dissimilar joint. *Advances in Industrial and Manufacturing Engineering*, *1*: p.100002. https://doi.org/10.1016/j.aime.2020.100002.

184. Cavaliere, P., De Santis, A., Panella, F. and Squillace, A. 2009. Effect of welding parameters on mechanical and microstructural properties of dissimilar AA6082–AA2024 joints produced by friction stir welding. *Mater. Des, 30 (3):* pp. 609–616.

185. Kurt, A., Uygur, I. and Cete, E., 2011. Surface modification of aluminium by friction stir processing. *Journal of materials processing technology, 211(3)*, pp.313-317.

APPENDIX

APPENDIX A

FSW/ FSP tool pin

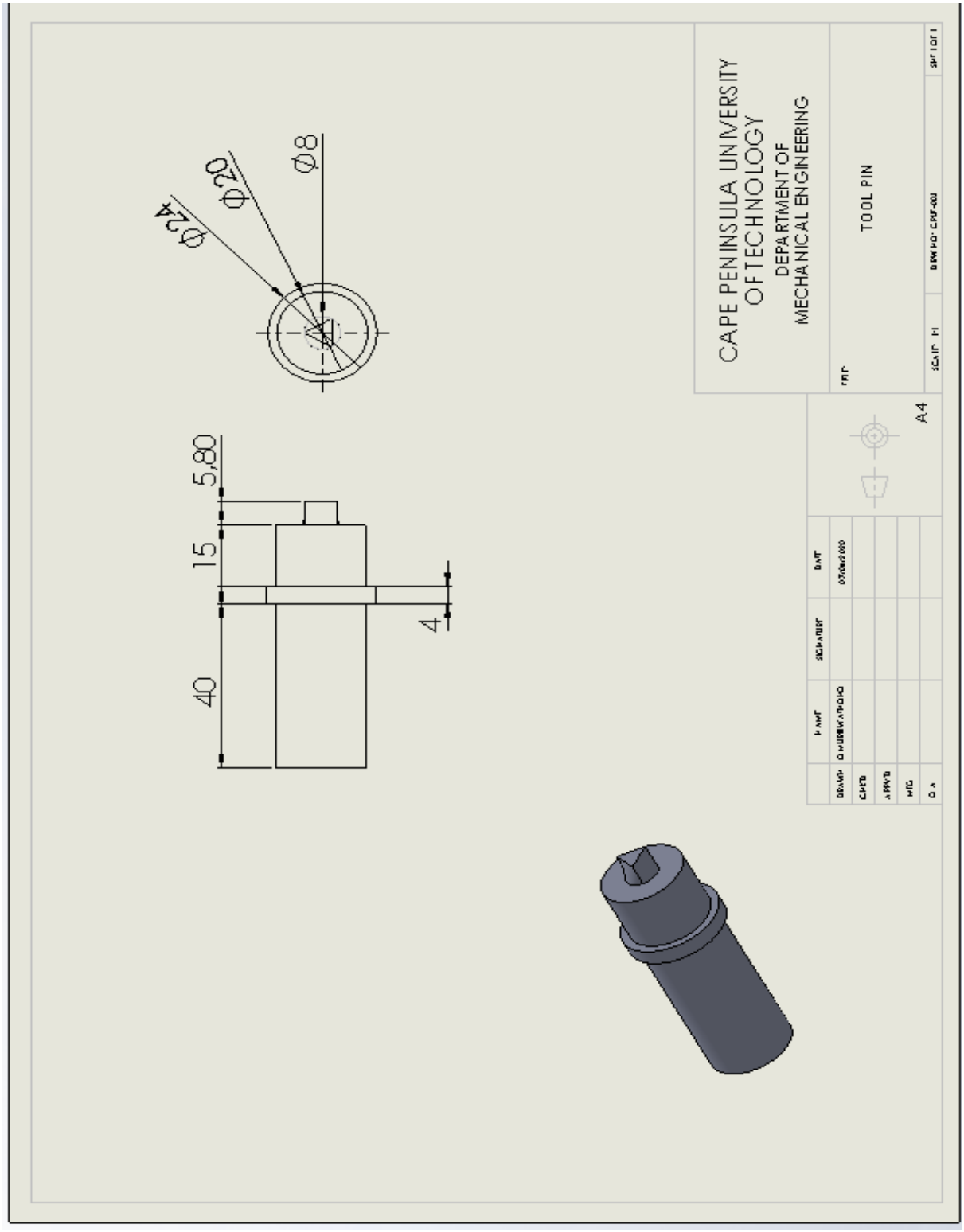

Figure A1: Tool pin drawing.

APPENDIX B

Tensile Test Specimen

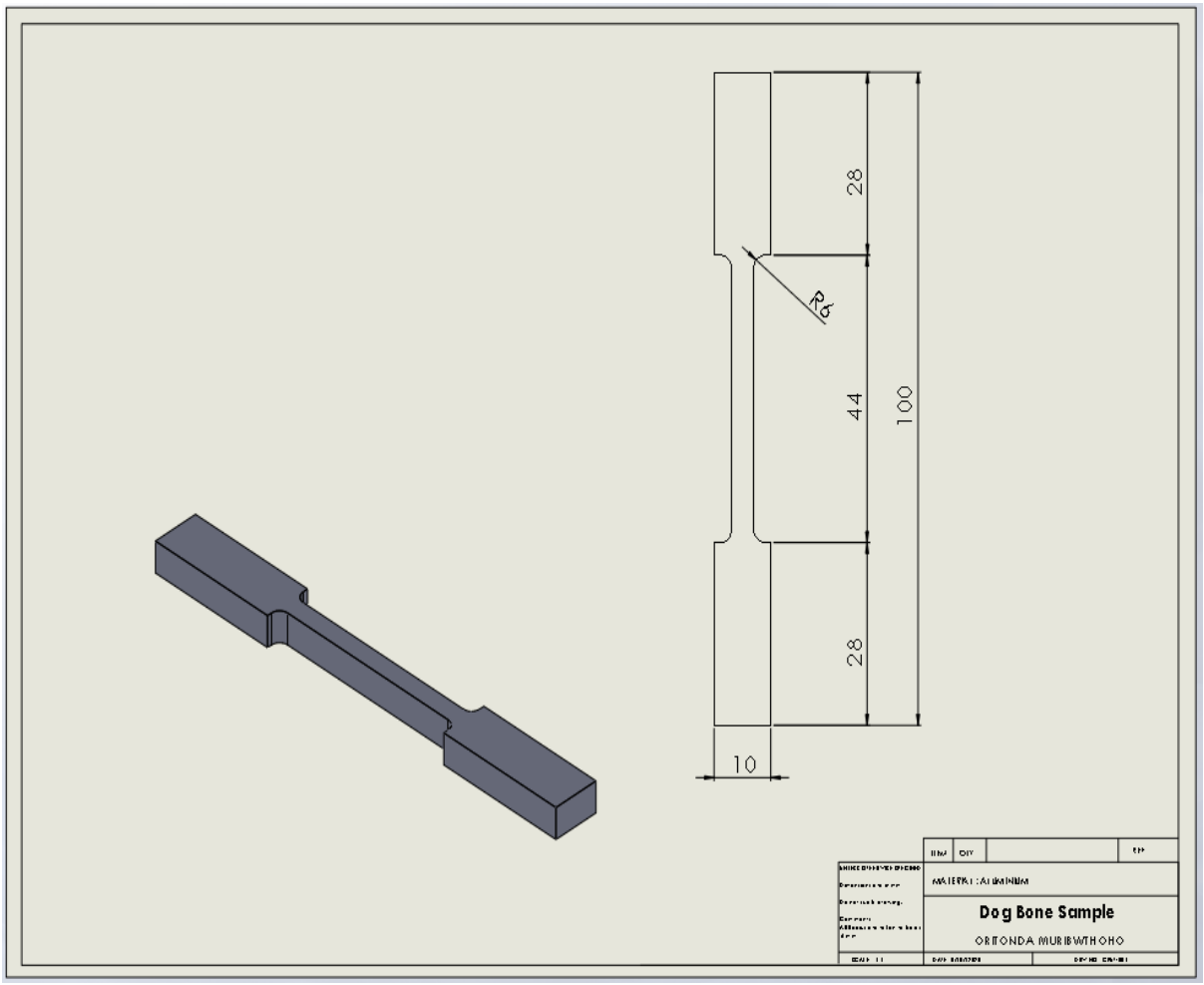

Figure B1: Dog bone sample

APPENDIX C

Microstructure and microhardness specimen

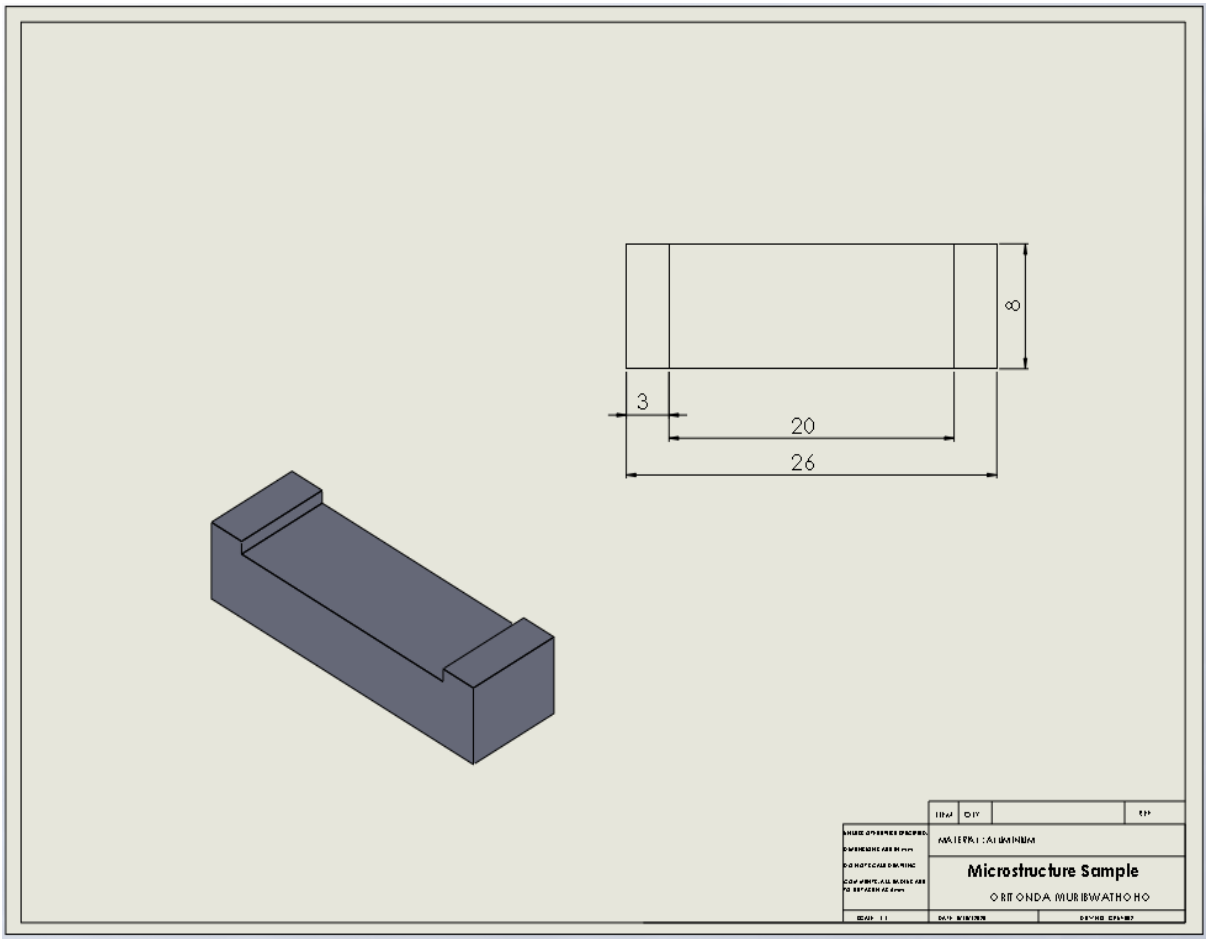

Figure C1: Microstructure and microhardness sample

APPENDIX D

Bending test specimen

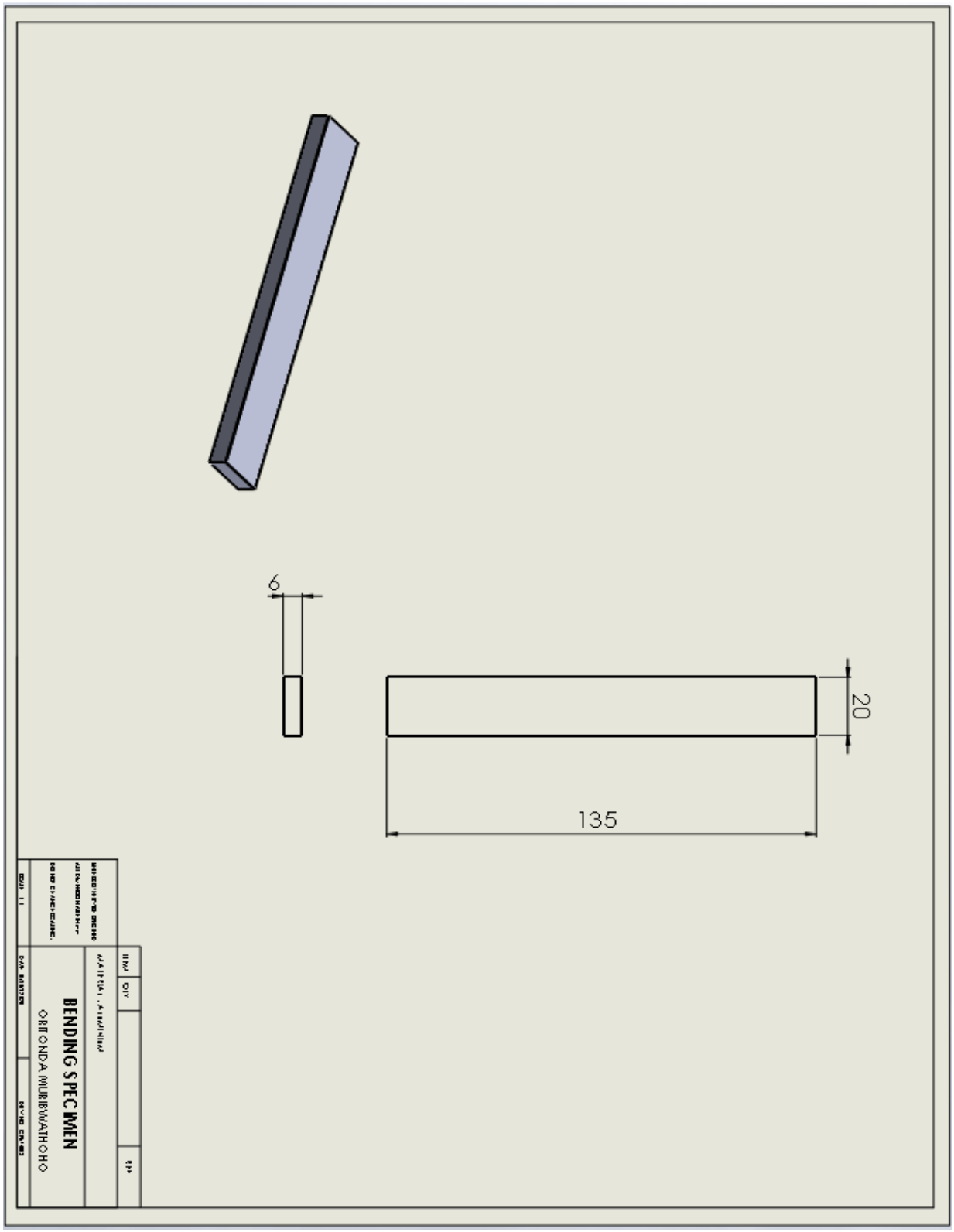

Figure D1: Bending specimen sample.

APPENDIX E

Sample Calculations

Tensile test calculations

(a) F =0N, A =36mm^2

$$\sigma = \frac{F}{A} = \frac{0}{0.000036}$$
= 0 MPa

$$\varepsilon = \frac{\Delta L}{L_o} = \frac{0}{35.06}$$
= 0

$$\%\ Elongation = \frac{\Delta L}{L_o} \times 100 = \frac{0}{35.06} \times 100$$
= 0 %

(b) F=45N, A=36mm^2

$$\sigma = \frac{F}{A} = \frac{45}{0.000036}$$
= 1.25 MPa

$$\varepsilon = \frac{\Delta L}{L_o} = \frac{0.038}{35.06}$$
= 0.0011

$$\%\ Elongation = \frac{\Delta L}{L_o} \times 100 = \frac{0.038}{35.06} \times 100$$
= 0.11 %

(c) F=2529N, A=36mm^2

$$\sigma = \frac{F}{A} = \frac{2529}{0.000036}$$
= 70.25 MPa

$$\varepsilon = \frac{\Delta L}{L_o} = \frac{3.967}{35.06}$$
= 0.1131

$$\%\ Elongation = \frac{\Delta L}{L_o} \times 100 = \frac{3.967}{35.06} \times 100$$
= 11.31 %

(d) F=250N, A=36mm^2

$$\sigma = \frac{F}{A} = \frac{250}{0.000036}$$
= 6.94 MPa

$$\varepsilon = \frac{\Delta L}{L_o} = \frac{7.921}{35.06}$$
= 0.2259

$$\% \, Elongation = \frac{\Delta L}{L_o} \times 100 = \frac{7.921}{35.06} \times 100$$

= 22.59 %

Bending test calculations

(a) F =0N, L=90mm, b=20mm, d=6mm

$$\sigma_F = \frac{3FL}{2bd^2} = \frac{3 \times 0 \times 0.09}{2 \times 0.02 \times 0.006^2}$$

= 0 MPa

$$\varepsilon_F = \frac{\Delta L}{L_o} = \frac{0}{90}$$

= 0

(b) F =921N, L=90mm, b=20mm, d=6mm

$$\sigma_F = \frac{3FL}{2bd^2} = \frac{3 \times 921 \times 0.09}{2 \times 0.02 \times 0.006^2}$$

= 172.6875 MPa

$$\varepsilon_F = \frac{\Delta L}{L_o} = \frac{16.6}{90}$$

= 0.184

(c) F =1325N, L=90mm, b=20mm, d=6mm

$$\sigma_F = \frac{3FL}{2bd^2} = \frac{3 \times 1325 \times 0.09}{2 \times 0.02 \times 0.006^2}$$

= 248.437 MPa

$$\varepsilon_F = \frac{\Delta L}{L_o} = \frac{24.2}{90}$$

= 0.269

(d) F =348N, L=90mm, b=20mm, d=6mm

$$\sigma_F = \frac{3FL}{2bd^2} = \frac{3 \times 348 \times 0.09}{2 \times 0.02 \times 0.006^2}$$

= 65.25 MPa

$$\varepsilon_F = \frac{\Delta L}{L_o} = \frac{40.4}{90}$$

= 0.449